KTH Engineering Sciences

Optical Parametric Amplification with Periodically Poled $KTiOPO_4$

Anna Fragemann

Doctoral Thesis

Department of Physics
Royal Institute of Technology
Stockholm, Sweden 2005

Optical Parametric Amplification with Periodically Poled $KTiOPO_4$

Anna Fragemann
ISBN 91-7178-201-X

Doktorsavhandling vid Kungliga Tekniska Högskolan
TRITA-FYS 2005:62
ISSN 0280-316X
ISRN KTH/FYS/--05:62--SE

Akademisk avhandling som med tillstånd av Kungliga Tekniska Högskolan framlägges till offentlig granskning for avläggande av teknisk doktorsexamen i fysik, fredag den 9 december 2005, kl 10, Sal FD 5, AlbaNova, Roslagstullsbacken 21.
Avhandlingen kommer att försvaras på engelska.

Laser Physics
Department of Physics
Royal Institute of Technology
S-106 91 Stockholm, Sweden

Cover: Broadband optical parametric generation in periodically poled $KTiOPO_4$
Photo: Carlota Canalias

Printed by Universitetsservice US-AB, Tryck & Media Stockholm, 2005.

Fragemann, Anna
Optical Parametric Amplification with Periodically Poled $KTiOPO_4$
Laser Physics, Department of Physics, Royal Institute of Technology, S-106 91 Stockholm, Sweden
ISBN 91-7178-201-X, TRITA-FYS 2005:62, ISSN 0280-316X, ISRN KTH/FYS/--05:62--SE

Abstract

This thesis explores the use of engineered nonlinear crystals from the $KTiOPO_4$ (KTP) family as the gain material in optical parametric amplifiers (OPAs), with the aim to achieve more knowledge about the benefits and limitations of these devices. The work aims further at extending the possible applications of OPAs by constructing and investigating several efficient and well performing amplifiers.

An OPA consists of a strong pump source, which transfers its energy to a weak seed beam while propagating through a nonlinear crystal. The crystals employed in this work are members of the KTP family, which are attractive due to their large nonlinear coefficients, high resistance to damage and wide transparency range. The flexibility of OPAs with respect to different wavelength regions and pulse regimes was examined by employing various dissimilar seed and pump sources.

The possibility to adapt an OPA to a specific pump and seed wavelength and achieve efficient energy conversion between the beams, originates from quasi-phasematching, which is achieved in periodically poled (PP) nonlinear crystals. Quasi-phasematched samples can be obtained by changing the position of certain atoms in a ferroelectric crystal and thereby reversing the spontaneous polarisation.

In this thesis several material properties of PP crystals from the KTP family were examined. The wavelength and temperature dispersion of the refractive index were determined for PP $RbTiOPO_4$, which is essential for future use of this material. Another experiment helped to increase the insight into the volumes close to domain walls in PP crystals

Further, several OPAs were built and their ability to efficiently amplify the seed beam without changing its spectral or spatial properties was studied. Small signal gains of up to 55 dB and conversion efficiencies of more than 35 % were achieved for single pass arrangements employing 8 mm long PPKTP crystals. Apart from constructing three setups, which generated powerful nanosecond, picosecond and femtosecond pulses, the possibility to amplify broadband signals was investigated. An increase of the OPA bandwidth by a factor of approximately three was achieved in a noncollinear configuration.

Keywords: nonlinear optics, optical parametric amplification, optical parametric generation, optical parametric oscillation, broadband amplification, optical parametric chirped pulse amplification, $KTiOPO_4$, quasi-phasematching, $RbTiOPO_4$, electric field poling.

Preface

The work resulting in this thesis was performed in the Laser Physics group, Department of Physics, at the Royal Institute of Technology.

This project was made possible thanks to the decision of KTH to offer me an "Excellenstjänst" and thereby providing my salary. Additional generous funding has been obtained from the Göran Gustafsson Foundation, the Carl Trygger Foundation and the Swedish Research Council.

The collaboration with Dr. V. Petrov's group at the Max-Born Institute in Berlin, Germany, was possible due to sponsoring from the EU programme Cluster of Large Scale Laser Installations (LIMANS).

The thesis consists of an introductory part, where a general background to nonlinear optics and this work is given. Both theoretical and experimental characteristics are introduced and the most important results from the experiments are presented. This section is followed by the reprints of the publications listed below.

List of Publications

The thesis is based upon the following articles, which will be referred to by their respective number:

I A. Fragemann, V. Pasiskevicius, and F. Laurell
Broadband nondegenerate optical parametric amplification in the mid infrared with periodically poled $KTiOPO_4$
Opt. Lett. **30**, 2296 (2005).

II A. Fragemann, V. Pasiskevicius, and F. Laurell
Optical parametric amplification of a gain-switched picosecond laser diode
Opt. Expr. **13**, 6482 (2005).

III A. Fragemann, V. Pasiskevicius, G. Karlsson, and F. Laurell
High-peak power nanosecond optical parametric amplifier with periodically poled KTP
Opt. Expr. **11**, 1297 (2003).

IV A. Fragemann, V. Pasiskevicius, and F. Laurell
Second-order nonlinearities in the domain walls of periodically poled $KTiOPO_4$
Appl. Phys. Lett. **85**, 375 (2004).

V A. Fragemann, V. Pasiskevicius, J. Nordborg, J. Hellström, H. Karlsson, and F. Laurell
Frequency converters from visible to mid-infrared with periodically poled $RbTiOPO_4$
Appl. Phys. Lett. **83**, 3090 (2003).

VI V. Petrov, F. Noack, F. Rotermund, V. Pasiskevicius, A. Fragemann, F. Laurell, H. Hundertmark, P. Adel, and C. Fallnich
Efficient All-Diode-Pumped Double Stage Femtosecond Optical Parametric Chirped Pulse Amplification at 1-kHz with Periodically Poled $KTiOPO_4$
Jpn. J. Appl. Phys. **42**, L 1327 (2003).

VII V. Pasiskevicius, A. Fragemann, F. Laurell, R. Butkus, V. Smilgevicius, and A. Piskarskas
Enhanced stimulated Raman scattering in optical parametric oscillators from periodically poled $KTiOPO_4$
Appl. Phys. Lett. **82**, 325 (2003).

Other journal publications by the author related to the subject but not included in this thesis:

A1 C. Canalias, V. Pasiskevicius, A. Fragemann, and F. Laurell
High resolution domain imaging on the nonpolar y-face of periodically poled $KTiOPO_4$ by means of atomic force microscopy
Appl. Phys. Lett. ***83****, 734, (2003).*

A2 G. Karlsson, V. Pasiskevicius, A. Fragemann, J. Hellström, and F. Laurell
Generation of 100 kW-level pulses at 1.53 μm in the diode-pumped Er-Yb:glass laser – PPKTP optical parametric amplifier system
Proc. SPIE ***5137****, 37 (2003).*

A3 M. Pelton, P. Marsden, D. Ljunggren, M. Tengner, A. Karlsson, A. Fragemann, C. Canalias, and F.Laurell
Bright, single-spatial-mode source of frequency non-degenerate, polarization-entangled photon pairs using periodically poled KTP
Opt. Expr. ***12****, 3573 (2004).*

In the text these publications will be referred to according to the notification used here.

Acknowledgements

This thesis is the result of several years of work and has only been possible thanks to the help and support from many different people.

First of all, I would like to thank Professor Fredrik Laurell for accepting me as a PhD student in his group. Despite your tight time schedule you have always had the time to encourage and support me when problems seemed to be overwhelming. Your positive and optimistic attitude has often helped me to go back to the lab or computer and continue with my work.

Secondly, but not less important, Dr. Valdas Pasiskevicius deserves very much of my gratitude for investing such enormous amounts of time and energy in helping and explaining physics to me. I will never forget all the evenings and weekends that we spent in the lab trying to get the best possible results before important deadlines. Thanks for your enthusiasm and interest in my work and for always believing in me!

Further, I was very fortunate to receive the opportunity to become a member of the Laser Physics group with all its wonderful people. Especially, I would like to thank Carlota Canalias, Shunhua Wang, Mikael Tiihonen, and Stefan Holmgren with whom I have shared the office during long or short periods. Sometimes it had maybe been easier for me to concentrate on my work if I had been on my own, but by sharing the office with you, I always had somebody to ask for help and it would also have been extremely boring without you. I also would like to thank all former and present members of the group with whom I have not had the pleasure to share a room: Marcus Alm for always taking his time to listen to me and encourage me; Jonas Hellström, Björn Jacobsson, Junji Hirohashi, Sandra Johansson, Stefan Bjurshagen, Pär Jelger, Assoc. Prof. Jens A. Tellefsen, Dr. Gunnar Karlsson, Dr. Stefan Spiekermann and Lars-Gunnar Andersson for all the help, the discussions about topics related to physics and other parts of life, for interesting and fun lunches, coffee breaks, parties and other events.

Also, I do not want to miss the chance to thank all the people at Cobolt AB with whom I have worked or had contact for some other reason, especially Dr. Håkan Karlsson, Dr. Jonas Hellström, Dr. Jenni Nordborg, Holger Maas and Mats Hede.

I am also very glad for all the help I received from David Koch for cutting and polishing my crystals and from Rune Persson for the Al-evaporations. Thanks also to Agneta Falk for handling the administrative work so perfectly.

In addition I am very grateful to KTH for placing their trust in me and financing my studies, by offering me an “Excellenstjänst”.

One of the biggest “Thanks” goes to my parents and my brother for their unconditional and endless support. Without your encouragement and love I would never have been where I am today. Thanks also to my friends outside of KTH for making me understand that there is more to life than just physics and my friends inside of KTH for making me understand that there is more to physics than just lasers.

Finally, thank you, Mattias, for always being there for me and never letting me down. For reminding me of what is important in life and making sure that I do not loose perspective. For being interested in my work and supporting me whenever possible. For trying even when it was impossible. For choosing to be such an important part of my life.

Table of Contents

Chapter 1

Introduction

In August 1961, only one year after Maiman's article on the first laser was published,[1] a paper was printed reporting the first observation of an optical nonlinear phenomenon. Franken *et al.*[2] had observed the generation of second harmonic radiation when light emitted by a ruby laser was focussed into crystalline quartz. This publication initiated a new research field, covering phenomena where the optical properties of a material are changed due to intense electromagnetic radiation. Since powerful light sources are necessary to observe nonlinear effects, the research on nonlinear optics and on lasers are intimately entwined and have developed in parallel during the last decades.

1.1 Properties and Applications of Nonlinear Crystals

Since the development of the laser, it has entered many different areas of application. Lasers are used for industrial and astronomical measurements, analysis of chemicals, treatment of diseases, micro-machining, as transmitters in fibre communication and in a variety of other applications. A drawback of most laser materials is, however, their limited ability to generate radiation in a wide spectral region. For some purposes an energetic beam at a wavelength where no laser material operates would be needed. In yet other applications appropriate laser sources exist, however, the emitted power is restricted by thermal properties of the laser crystal. A solution to both these problems is given by nonlinear optics, since one of the primary applications of a nonlinear material is to efficiently transfer energy from one wavelength to another wavelength. Nonlinear crystals can therefore be employed both for the generation of beams at wavelengths not available with laser materials, but also to amplify weak lasers. Apart from the wavelength, the output from a nonlinear device has basically the same properties as those of a laser. Hence the possible applications for nonlinear optics are identical to all areas where lasers are used.

For many applications a general desire is to employ more and more powerful laser radiation. However, instead of attempting to scale up the laser itself, a wiser strategy is generally to amplify a well performing laser in a second stage. Thus, the overall task is split into two,

where the generator will focus only on the generation of a high quality signal, while the amplifier specialises on boosting the signal without adding too much noise. This drive for high powers is, however, not a new phenomenon. Basically as soon as the laser was invented, ideas came up of how to amplify this coherent radiation and one suggestion was to employ nonlinear crystals as the gain material.

Amplifiers based on nonlinear crystals are called optical parametric amplifiers (OPAs) and consist essentially of three main components: a powerful pump laser, a nonlinear gain material and a seed source, which operates at a different wavelength than the pump and emits radiation that is considerably weaker than the pump beam. When the pump and the seed interact inside the nonlinear crystal, power is extracted from the strong pump and converted to the seed wavelength resulting in its amplification. At the same time a completely new beam, the idler, is generated at a wavelength, which will ensure the conservation of energy. One of the main advantages of employing nonlinear crystals instead of laser crystals in amplifiers is that the thermal load is reduced considerably, which allows the generation of energetic pulses at high repetitions rates. Another beneficial property is the large gain that can be achieved for parametric amplification when employing material with large nonlinear coefficients. Instead of having to construct the multi-pass setups commonly used for laser amplifiers, single or double pass arrangements, which are more easily controlled, will lead to comparable amplifications. Finally, nonlinear crystals are generally very flexible in the sense that they can operate efficiently in a large spectral region.

The nonlinear crystals, which were employed as the gain material in the OPAs constructed in this work, were all made of $KTiOPO_4$. Samples from this family can be used to amplify any wavelength in the spectral region spanning from the UV (350 nm) into the mid-infrared (~ 4.5 µm). In order to obtain efficient power conversion, apart from the energy also the momentum of the interaction has to be conserved. By employing a technique called quasi-phasematching, this can be achieved for any combination of pump and seed wavelengths, which turns optical parametric amplification into a very flexible process. In ferroelectric crystals quasi-phasematching can be achieved by a technique called electric field poling. If electric pulses are applied to a ferroelectric sample, the position of certain atoms can be changed. This can lead to a reversion of the spontaneous polarisation. If this modification is produced in a periodic manner over the whole crystal's length, the amplification process can reach gains of up to 55 dB in a 8 mm long sample.

1.2 Development of the Work

All in all, the aim of this thesis was to further explore the nonlinear processes, which are possible employing periodically poled crystals from the $KTiOPO_4$ (KTP) family. Although crystals from this family have become frequently used samples for nonlinear applications, the experiments performed during this work involved the attempt of increasing the already vast field of possible applications.

The main part of the experimental work was devoted to the investigation of OPAs based on periodically poled $KTiOPO_4$ (PPKTP). Several OPAs operating at various wavelengths with various pulse durations were constructed and studied. One of the first experiments explored the possibility to scale nanosecond OPAs based on PPKTP to the millijoule level. [III] The goal was achieved by designing an efficient double stage setup and the knowledge obtained during this work was employed extensively in the following experiments. The next OPA was built to amplify femtosecond pulses and employed a technique called optical parametric chirped pulse amplification (OPCPA). [VI] Here the femtosecond pulses were stretched to picosecond durations before reaching the nonlinear crystal. Although a gain of 60 dB was reached, the experiment had a weak point: the amplified signal was spectrally narrowed by the limited gain bandwidth of the PPKTP crystals, which increased the duration of the compressed pulses. This effect and the prospect of improving the results were the main inspiration for the next study: an OPA that would yield broadband amplification. [I] The approach that was chosen was to investigate and employ noncollinear signal and pump configurations in PPKTP, which has the potential to give large bandwidths. Finally, the last OPA experiment was motivated by the desire to construct a compact and simple, yet powerful picosecond source. [II] By seeding an OPA with a gain-switched laser diode, 1 µJ pulses with durations of 20 ps could be generated.

Parallel with the OPA experiments also some investigations were performed on the material properties of the KTP family. By studying the behaviour of periodically poled $RbTiOPO_4$ in several nonlinear processes the dependence of the refractive index on the wavelength and the temperature could be characterised. [V] Further a thorough investigation of nonlinear processes close to the domain walls in periodically poled KTP was carried out. [IV] It could be concluded that the domain inversion process causes the appearance of some nonlinear coefficients, which are not present in single domain KTP. Finally, an analysis of several PPKTP optical parametric oscillators resulted in the conclusion that stimulated Raman scattering is enhanced for certain spectral ranges in the mid IR. [VII] This result led to the demonstration of simultaneous optical parametric oscillation and Raman oscillation in crystals with certain domain inversion periods.

1.3 Thesis Outline

The thesis is built up as follows. Chapter 2 is intended to establish a general knowledge of the subject of nonlinear optics. Some important equations, which explain nonlinear phenomena, are derived and several devices, which employ nonlinear processes, are introduced and explained. Chapter 3 is covering the two main techniques used for phasematching nonlinear processes. Phasematching is a central requirement for achieving efficient nonlinear interaction in practical devices. Chapter 4 is devoted to the material $KTiOPO_4$ and its isomorphs, which was used for the nonlinear crystals in all the experiments. A brief, general introduction into crystal properties is given, and KTP's structure and its nonlinear characteristics are explained. The technique to periodically pole crystals by applying an electric field is treated in Chapter 5. This method is used to achieve the essential phasematching condition, by employing the principle of quasi-phasematching. Chapter 6 gives the general background to

optical parametric amplifiers. Their specific properties are discussed and two central OPA experiments performed during this work are described. Chapter 7 focuses on broadband parametric amplification employing periodically poled KTP. The goal is to both theoretically and experimentally explore the possibility to amplify femtosecond pulses without narrowing them spectrally.

Chapter 2

Second Order Nonlinear Processes

After the generation of the second harmonic was observed for the first time in 1961, it did not take long until the experimental observations of other nonlinear processes were reported. The existence of these nonlinear optical effects had earlier been predicted in theoretical articles, however, the experimental confirmation of these theories had to await the invention of the laser.

2.1 Nonlinear Polarisation

When an electromagnetic field, like a beam of light, is incident on a dielectric material, the atoms inside react by starting to oscillate. The electrons of each atom move in the opposite direction of the field, whereas the positive ions are displaced in the same direction as the applied field. Thus, dipoles are formed in which the electron cloud oscillates around the nucleus and the material becomes polarised. If the amplitude of the incident field is moderate, the electrons can follow the oscillating movement of the field to such a degree that the induced polarisation $\boldsymbol{P}$ can be approximated to be linearly dependent on the applied electric field $\boldsymbol{E}$. Therefore

$$\boldsymbol{P} = \boldsymbol{P}^{L} = \varepsilon_0 \chi^{(1)} \boldsymbol{E}\,, \tag{2.1}$$

where ε_0 is the permittivity of free space and $\chi^{(1)}$ denotes the linear susceptibility tensor. However, as the amplitude of the applied field increases, the electrons will not reproduce the oscillations accurately. When the electric field becomes large enough to modify the binding potential of the electrons, the electron – ion system in the material will exhibit a nonlinear response. Thus, the oscillation can no longer be described by one pure sinusoidal wave, since it has become deformed and the linear approximation does not hold any longer. Hence, the polarisation $\boldsymbol{P}$ has to be expanded

$$\boldsymbol{P} = \varepsilon_0\left(\boldsymbol{\chi}^{(1)}\boldsymbol{E} + \boldsymbol{\chi}^{(2)}\boldsymbol{E}^2 + \boldsymbol{\chi}^{(3)}\boldsymbol{E}^3 + ...\right) = \boldsymbol{P}^L + \boldsymbol{P}^{NL} \tag{2.2}$$

where $\boldsymbol{\chi}^{(2)}, \boldsymbol{\chi}^{(3)}$, etc. are the second order, third order, etc. nonlinear susceptibility tensors, which rapidly decrease in magnitude.[3,4,5,6] In a later section it will be shown that the nonlinear polarisation will contain components oscillating at frequencies different from the incident wave, for example at the second harmonic. Since oscillating electrons emit light corresponding to the frequency they are oscillating with, the nonlinear polarisation will generate electromagnetic waves at new frequencies.

According to (2.2) the generated polarisation for second order nonlinear processes is given by $\boldsymbol{P}^{(2)} = \varepsilon_0 \boldsymbol{\chi}^{(2)} \boldsymbol{E}^2$, where $\boldsymbol{\chi}^{(2)}$ is a 3 × 3 × 3 tensor. However, due to intrinsic permutation symmetries the $\boldsymbol{\chi}^{(2)}$ tensor can be replaced by a 3 × 6 matrix, called the nonlinear *d* matrix, where $2d_{ij} = \chi^{(2)}_{ikl}$. This simplifies further calculations and the polarisation for second order nonlinear processes is then given by

$$\begin{pmatrix} \left(P^{(2)}_{\omega_3}\right)_x \\ \left(P^{(2)}_{\omega_3}\right)_y \\ \left(P^{(2)}_{\omega_3}\right)_z \end{pmatrix} = 2\varepsilon_0 K \begin{pmatrix} d_{11} & d_{12} & d_{13} & d_{14} & d_{15} & d_{16} \\ d_{21} & d_{22} & d_{23} & d_{24} & d_{25} & d_{26} \\ d_{31} & d_{32} & d_{33} & d_{34} & d_{35} & d_{36} \end{pmatrix} \begin{pmatrix} \left(E_{\omega_1}\right)_x\left(E_{\omega_2}\right)_x \\ \left(E_{\omega_1}\right)_y\left(E_{\omega_2}\right)_y \\ \left(E_{\omega_1}\right)_z\left(E_{\omega_2}\right)_z \\ \left(E_{\omega_1}\right)_y\left(E_{\omega_2}\right)_z + \left(E_{\omega_1}\right)_z\left(E_{\omega_2}\right)_y \\ \left(E_{\omega_1}\right)_x\left(E_{\omega_2}\right)_z + \left(E_{\omega_1}\right)_z\left(E_{\omega_2}\right)_x \\ \left(E_{\omega_1}\right)_x\left(E_{\omega_2}\right)_y + \left(E_{\omega_1}\right)_y\left(E_{\omega_2}\right)_x \end{pmatrix} \tag{2.3}$$

Here *K* is a degeneracy factor, which is equal to ½ for second harmonic generation and optical rectification and equal to 1 for all other second order processes.

For most crystals the *d* matrix can be simplified due to spatial symmetries of the material, resulting in some elements to take the same value as others and some to be zero. Even further simplifications can be made if Kleinman symmetry holds, which means that all the interacting waves, the generating as well as the generated, are far from any resonances in the nonlinear material.

2.2 The Coupled Wave Equations

In order to understand the interaction of the involved electromagnetic fields in a nonlinear medium, a coupled set of wave equations would be useful. The starting point for this derivation is the set of Maxwell's equations. Assuming that the interaction takes place in a nonlinear, dielectric material, the following wave equation can be derived:

$$\nabla^2 \boldsymbol{E} - \mu_0\sigma\frac{\partial \boldsymbol{E}}{\partial t} - \mu_0\varepsilon_0\frac{\partial^2 \boldsymbol{E}}{\partial t^2} = \mu_0\frac{\partial^2 \boldsymbol{P}}{\partial t^2}, \tag{2.4}$$

where μ_0 is the permeability of vacuum and σ represents the material's conductivity. This equation describes the electric field in a nonlinear dielectric, where the polarization acts as a

source of radiation at new frequencies. It is common to express the wave equation using the Fourier components of $\boldsymbol{E}$ and $\boldsymbol{P}$ instead of the instantaneous fields. Assuming $\boldsymbol{E}$ and $\boldsymbol{P}$ to be plane and quasi-monochromatic waves propagating in the x-direction, they can be written in the following form:

$$\begin{aligned}\boldsymbol{E}(r,t) &= \frac{1}{2}\sum_{\omega}\left[\boldsymbol{E}_{\omega}(x,t)\exp(i(kx-\omega t))+c.c.\right]\\ \boldsymbol{P}(r,t) &= \frac{1}{2}\sum_{\omega}\left[\boldsymbol{P}_{\omega}(x,t)\exp(i(kx-\omega t))+c.c.\right]\end{aligned} \tag{2.5}$$

Here ω is the angular frequency of the wave and the wavenumber k is given by $k=\frac{n_{\omega}\omega}{c}$, n_{ω} being the refractive index at the angular frequency ω and c being the speed of light in vacuum. The complex conjugate *c.c.* has to be added, because the electric field and the polarisation are real functions.

The wave envelopes $\boldsymbol{E}_{\omega}(x,t)$ and $\boldsymbol{P}_{\omega}(x,t)$ vary when propagating through the medium. However, if their variations are slow as a function of distance and time, it is possible to neglect their second order derivatives with respect to x and t, respectively, (2.6). In nonlinear optics this is almost always a valid approximation and is called the slowly varying envelope approximation (SVEA).

$$\begin{aligned}\left|\frac{\partial^2\boldsymbol{E}_{\omega}(x,t)}{\partial x^2}\right| &<< \left|k\frac{\partial\boldsymbol{E}_{\omega}(x,t)}{\partial x}\right|\\ \left|\frac{\partial^2\boldsymbol{E}_{\omega}(x,t)}{\partial t^2}\right| &<< \left|\omega\frac{\partial\boldsymbol{E}_{\omega}(x,t)}{\partial t}\right|\\ \left|\frac{\partial^2\boldsymbol{P}_{\omega}(x,t)}{\partial t^2}\right| &<< \left|\omega\frac{\partial\boldsymbol{P}_{\omega}(x,t)}{\partial t}\right| << \left|\omega^2\boldsymbol{P}_{\omega}(x,t)\right|\end{aligned} \tag{2.6}$$

Inserting (2.5) in (2.4) and using SVEA, reduces the second-order differential wave equation to the following first-order equation:

$$\frac{\partial\boldsymbol{E}}{\partial x}+\alpha\boldsymbol{E}=\frac{i\mu_0 c\omega}{2n}\boldsymbol{P}^{NL} \tag{2.7}$$

where $\alpha=\frac{\mu_0\sigma c}{2}$ is the electric field loss coefficient and $c^2=\frac{1}{\mu_0\varepsilon_0}$.

In second order nonlinear processes three waves mix. All three waves are coupled to each other through the polarisations given by (2.3). Substituting (2.3) into (2.7) leads to the final set of coupled equations, describing one electromagnetic field's propagation through the nonlinear material in relation to the other present fields:

$$\begin{aligned}
\frac{\partial E_1}{\partial x} &= -\alpha_1 E_1 + \frac{i\omega_1^2}{k_1 c^2} K d_{eff} E_3 E_2^* \exp(i\Delta k x) \\
\frac{\partial E_2}{\partial x} &= -\alpha_2 E_2 + \frac{i\omega_2^2}{k_2 c^2} K d_{eff} E_3 E_1^* \exp(i\Delta k x) \\
\frac{\partial E_3}{\partial x} &= -\alpha_3 E_3 + \frac{i\omega_3^2}{k_3 c^2} K d_{eff} E_1 E_2 \exp(-i\Delta k x)
\end{aligned} \tag{2.8}$$

where $\Delta \boldsymbol{k} = \boldsymbol{k}_3 - \boldsymbol{k}_1 - \boldsymbol{k}_2$ is the phase mismatch between the interacting waves and $\omega_3 = \omega_1 + \omega_2$. The effective nonlinear coefficient d_{eff} can be derived from the matrix in (2.3), taking the polarisations of the interacting fields into account, and modifying it with a factor depending on the phasematching conditions.

In (2.8) we now have the set of desired coupled wave equations, which describes the interconnection between the three involved electric fields in second order nonlinear processes.

2.3 Second Order Nonlinear Processes

The second order nonlinear susceptibility is responsible for several processes: second harmonic generation (SHG), sum frequency generation (SFG), difference frequency generation (DFG), optical rectification (OR), optical parametric generation (OPG), optical parametric oscillation (OPO), optical parametric amplification (OPA) and the electro-optic effect. These processes can be divided into two main groups. SHG, SFG, DFG, OPA, OR and the electro-optic effect belong to the first group, where two fields are incident on the nonlinear material. Employing the photon picture, the first cases can be described as two incident photons interacting and generating a photon at a new frequency. The electro-optic effect results in a change of the refractive index for an incident photon under the influence of an applied low-frequency electrical field. OPG together with OPO form the second group, having the characteristics that only one electromagnetic field is incident on the nonlinear material, which causes a single photon to be split into two photons with lower frequencies.

2.3.1 Second Harmonic Generation

Second harmonic generation is one of the basic and most important effects of the first group. It is also the nonlinear process that was experimentally observed first. Two identical photons from a single pump beam are added and result in a photon having twice the frequency, $\omega_{SH} = 2 \cdot \omega$. This process can also be explained by employing the wave picture where an incident electric field, $E \sim \cos\omega$, will create a polarisation at the second harmonic, $P^{(2)} \sim \cos(2\omega)$, since $P^{(2)} \sim E^2$. This polarisation can lead to the generation of radiation at the second harmonic. If two beams with different frequencies ω_1 and ω_2 are incident on the crystal, the sum frequency $\omega_{SF} = \omega_1 + \omega_2$ and the difference frequency $\omega_{DF} = \omega_1 - \omega_2$ can be generated, see Fig. 2.1.

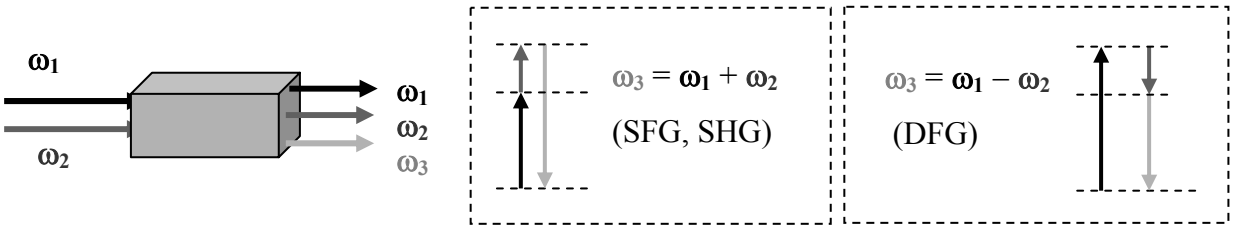

Figure 2.1. Schematic of the beams and photons involved in second harmonic generation, sum frequency generation and difference frequency generation.

For second harmonic generation the three coupled wave equations in (2.8) are reduced to two equations because $\omega_1 = \omega_2 = \omega$ and $\omega_3 = 2\omega$.

$$\begin{aligned}\frac{\partial E_\omega}{\partial x} &= \frac{i\omega}{n_\omega c} d_{eff} E_{2\omega} E_\omega^* \exp(i\Delta k x) \\ \frac{\partial E_{2\omega}}{\partial x} &= \frac{i\omega}{n_{2\omega} c} d_{eff} E_\omega E_\omega \exp(-i\Delta k x)\end{aligned} \tag{2.9}$$

where $\Delta k = k_{2\omega} - 2k_\omega$ and the material is assumed to be loss-less.

This set of equations can be solved analytically and the solution can be simplified, if it is reasonable to assume that the conversion is small. This means that if the pump is not depleted, $E_\omega(x) \cong E_\omega(0)$, the first equation can be integrated over the crystal length, *L*, and the intensity of the second harmonic at the end of the crystal can be derived to be

$$I_{2\omega} = \frac{n_{2\omega} c \varepsilon_0}{2} |E_{2\omega}|^2 = \frac{2\omega^2 d_{eff}^2 L^2 I_\omega^2}{n_\omega^2 n_{2\omega} c^3 \varepsilon_0} sinc^2\left(\frac{\Delta k L}{2}\right). \tag{2.10}$$

Here $sinc(x) = \frac{\sin(x)}{x}$, I_ω is the pump intensity, n_ω and $n_{2\omega}$ are the refractive index for the pump and the second harmonic, respectively. From this equation it can be seen that the intensity of the second harmonic decreases if the process is not phasematched, meaning that $\Delta k \neq 0$. However, if $\Delta k = 0$ the intensity increases as a function of the crystal length squared and the nonlinear coefficient squared. This derivation is only valid for loosely focussed beams, where the waves still can be assumed to be plane. For depleted pump and gaussian beam profiles see [7] and [8].

2.3.2 Optical Parametric Generation

The basic device of the second group, which consists of OPO and OPG, is the optical parametric generator. It has one incident pump beam and generates two new beams with different wavelengths – both longer than the pump. The first time, efficient and tuneable optical parametric generation was observed, was in 1967 by Harris *et al.*[9] This process had

however been predicted by various authors several years before.[10,11,12] Employing the photon picture, each pump photon is split into two photons, the signal and the idler photon. The commonly used definition is to denote the one having larger energy the signal. The generation of the signal and the idler starts from quantum noise and is called parametric fluorescence if the process is spontaneous and not phasematched. If it, however, is phasematched, which can lead to stimulated and amplified signal and idler fields, the process is denoted superfluorescence.

2.3.3 Optical Parametric Oscillation

In order to improve the conversion efficiency of an OPG, the crystal can be placed in a resonator, usually consisting of two partially reflecting mirrors, and the resulting device is then called an optical parametric oscillator, see Fig. 2.2. The first OPO was demonstrated in 1965 by Giordmaine and Miller and operated around 1 μm.[13] Depending on the choice of mirrors, different types of OPOs can be constructed. The pump can either pass once through the crystal (single pass OPO) or twice by back-reflection (double pass OPO). It is also possible to let one, two or all three waves be resonated in the OPO, resulting in singly resonant, doubly resonant or triply resonant OPOs. The most frequently used setup during this work was the single pass OPO, which only resonated the signal. Thus, the input and output coupler were only reflective at the signal wavelength and highly transmitting at both the pump and idler wavelengths.

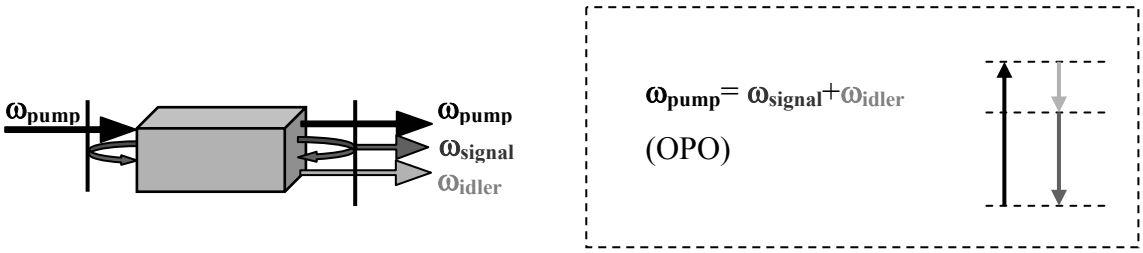

Figure 2.2. Schematic of the beams and photons involved in a singly resonant optical parametric oscillator.

OPOs are in a way comparable to lasers because they both have a cavity with resonator conditions, a gain medium and a threshold, below which no oscillation occurs. If the pump intensity is increased beyond the threshold point, the OPO starts to convert the energy of the pump efficiently to the signal and idler.

A measure of a nonlinear process' ability to convert energy from the incident wave to the generated waves is given by the conversion efficiency. The energy of the generated waves is divided by the energy of the incident wave; therefore the conversion efficiency for OPOs is given by:

$$\eta = \frac{\mathcal{E}_s(L) + \mathcal{E}_i(L)}{\mathcal{E}_p(0)} \tag{2.11}$$

where $\mathcal{E}_s(L)$ and $\mathcal{E}_i(L)$ are the energies of the signal and idler, respectively and $\mathcal{E}_p(0)$ is the energy of the incident pump.

In theory it is possible to achieve conversion efficiencies of 100 % for plane waves in a singly resonant OPO. In general, however, the intensity profiles of the beams are gaussian instead because focussing is needed in order to increase the intensities of the interacting beams. In this case the conversion efficiencies are commonly limited to values below 70 %.

Sometimes it is not possible to measure the energy of the generated idler because the nonlinear material is strongly absorbing at this wavelength. For these occasions the Manley-Rowe equation is useful, which was originally derived for nonlinear inductors and capacitors.[14]

$$-\frac{1}{\omega_p}\left(\frac{dI_p}{dx}\right)=\frac{1}{\omega_s}\left(\frac{dI_s}{dx}\right)=\frac{1}{\omega_i}\left(\frac{dI_i}{dx}\right) \tag{2.12}$$

Here I_p, I_s and I_i denote the intensity of the pump, signal and idler and ω_p, ω_s and ω_i are the corresponding frequencies. Thus, the power of the idler can easily be derived if the signal's power is known. Equation (2.12) describes the fact that each pump photon is converted into one signal and one idler photon, which illustrates the photon splitting taking place in OPOs.

2.3.4 Optical Parametric Amplification

Another way of developing the OPG into a more controllable device is to seed it, which results in an optical parametric amplifier, see Fig. 2.3. This means that apart from the powerful pump a comparably weak beam, having the signal's or the idler's wavelength, is incident on the crystal as well. In the former case the idler is then generated by difference frequency generation of the pump and the signal. At the same time the signal is coherently amplified, and by the coupling of these three beams both the signal and the idler can grow while propagating through the nonlinear crystal.

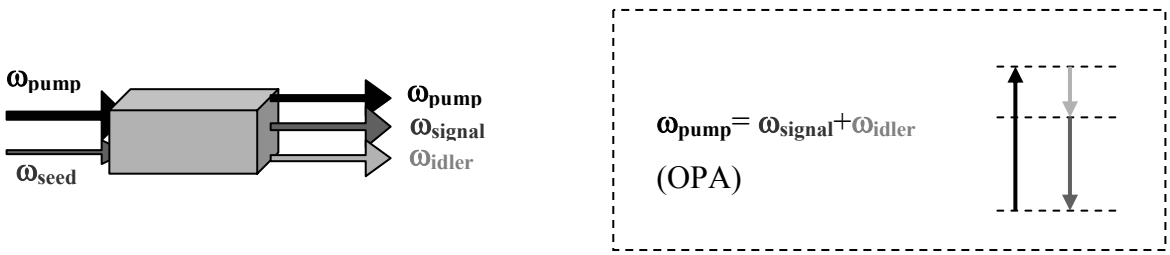

Figure 2.3. Schematic of the beams and photons involved in optical parametric amplification.

The principle for the OPA is thus comparable to a DFG. One main difference between them being that the power of the seed in an OPA is much lower than that of the pump, whereas the powers of the two incident beams in a DFG are of comparable magnitude. This large difference in input powers for the OPA generally leads to a signal energy growth that is

initially exponential. Another difference is that, usually, the wavelength of interest in OPAs is the seeded signal, whereas in the latter case the difference (the idler) is the main goal.

The analytical solution of the coupled wave equations (2.8) for parametric amplification, assuming no phase mismatch, is given by[5,15]

$$\eta_s = \frac{P_s(L)}{P_s(0)} = 1 - sn^2\left[i\frac{L}{L_{NL}}, i\gamma \right], \tag{2.13}$$

where $L_{NL} = \frac{1}{4\pi d_{eff}}\sqrt{\frac{2\varepsilon_0 n_p n_s n_i c\lambda_s\lambda_i}{I_p(0)}}$, $\gamma^2 = \frac{\lambda_s P_s(0)}{\lambda_p P_p(0)}$

and $sn(u,\gamma)$ is the Jacobi elliptic sine function. If the pump power is much larger than the seed power, which means if $\gamma < 0.1$, the Jacobi elliptic function can be approximated to a sine function. An imaginary first parameter leads to a hyperbolic function, resulting in the approximation $sn(iu, i\gamma) \cong i\,sinh(u)$. In case of negligible pump depletion ($\gamma << 0.1$), but permitting phase mismatch, the gain experienced by the seed can be approximated to

$$\frac{I_s(L)}{I_s(0)} = 1 + G = 1 + (gL)^2 \frac{\sinh^2\left(\sqrt{(gL)^2 - \left(\Delta kL/2\right)^2}\right)}{(gL)^2 - \left(\Delta kL/2\right)^2} \tag{2.14}$$

where $g^2 = \frac{2\omega_s\omega_i d_{eff}^2 I_p}{\varepsilon_0 c^3 n_p n_s n_i} = \frac{8\pi^2 d_{eff}^2 I_p}{\varepsilon_0 c n_p n_s n_i \lambda_s \lambda_i}$. (2.15)

Here g is the gain coefficient and a typical value for PPKTP is: $g^2 \approx I_p \cdot 10^{-7}$ / W.

Equation (2.14) can be simplified depending on whether the gain is small or large compared to the phase mismatch Δk. If $gL << \Delta kL/2$ the sinh(ξ) can be approximated to a sin(ξ) and the gain becomes

$$G = (gL)^2 \operatorname{sinc}^2\left(\frac{\Delta kL}{2}\right) \tag{2.16}$$

In case of the other extreme, if the gain is very strong, $gL >> \Delta kL/2$, the amplification of the seed will be exponential instead.

$$\begin{aligned} I_s(L) &= I_s(0)\cosh^2(gL) \\ I_i(L) &= \frac{\omega_i}{\omega_s} I_s(0)\sinh^2(gL) \end{aligned} \tag{2.17}$$

Thus, both the signal and the idler intensities increase exponentially as a function of the crystal length, describing the photon splitting of the pump into the signal and idler photons.

Since all the approximated equations given above assume plane waves, the gain will change for gaussian beams.[5] Instead

$$g^2 = \frac{16\pi^2 d_{eff}^2}{\varepsilon_0 c n_0^2 \lambda_0^2} P_p \left(1-\delta^2\right) \frac{\bar{h}_m(B,\xi)}{\lambda_0 L}, \tag{2.18}$$

where $n_0 \cong n_s \cong n_i$ is assumed, $\lambda_0 = 2\lambda_p$, $\lambda_s = \frac{2\lambda_p}{1+\delta}$, $\lambda_i = \frac{2\lambda_p}{1-\delta}$ and $\bar{h}_m(B,\xi)$ is the gain reduction factor derived by Boyd and Kleinman.[7] The double refraction parameter B takes walk-off into account and ξ depends on the focussing conditions inside the crystal.

2.4 Third Order Nonlinear Processes

Although both this chapter and the thesis focus on second order nonlinear interaction, some of the higher order processes have to be mentioned as well. Since the third order susceptibility, $\chi^{(3)}$, usually is much smaller than the second order susceptibility, $\chi^{(2)}$, third order effects are in general less efficient and concealed by the strong second order effects. However, in certain materials, e.g. in fibres, the second order susceptibility is zero because the material is isotropic and therefore centrosymmetric. This facilitates the observation of higher order phenomena, but it is still necessary to let intense waves interact to generate efficient third order processes, since $P^{(3)} = \varepsilon_0 \chi^{(3)} E^3$. These conditions can be fulfilled e.g. in single mode fibres, where high intensities are achieved, because the beams are confined to the very small area of the core that has a typical radius of a few micrometres. Even tighter confinement can be obtained in the recently developed photonic crystal fibres, which results in nonlinear processes with still larger efficiencies. However, under certain favourable conditions third order phenomena can be observed in non-centrosymmetric crystals like KTP as well.

Self-phase modulation, stimulated Raman scattering and four-wave mixing are the most important third order processes – at least considering the scope of this work.

2.4.1 Self-Phase Modulation

Self-phase modulation (SPM) originates from the fact that the refractive index is dependent on the intensity of a beam. Generally, the intensity of incident radiation varies in time and space, which will cause the refractive index to vary as well, according to[4]

$$n(\omega) = n_0(\omega) + n_2(\omega)|E|^2, \tag{2.19}$$

where $n_2(\omega) = \frac{3 \cdot \mathrm{Re}\left\{\chi^{(3)}(-\omega;\omega,-\omega,\omega)\right\}}{8 n_0(\omega)}$.

Spatial variation leads to self-focusing or self-defocusing depending on the sign of n_2. Temporal variation, however, causes phase changes in the wave. Different parts of the wave undergo different phase shifts. If the intensity is high enough, this effect will be clearly visible in the beam's spectrum, since different phase shifts lead to frequency changes in the different parts of the pulse and results in a chirped pulse, thus broadening the spectrum of the incident beam.

2.4.2 Stimulated Raman Scattering

Raman scattering, which is described more closely in Chapter 4, is an inelastic scattering process, where an incident photon is split into one so-called Stokes photon, which has lower energy than the incident one, and one phonon, which causes vibration of atomic groups in the medium. This results in an additional peak in the spectrum, which is situated at a longer wavelength than the incident wavelength. The shift is further a multiple of the vibrational frequency of the interacting atomic group.

In general the Raman process is spontaneous, but under certain conditions stimulated Raman scattering (SRS) can occur. A Stokes photon, which is incident together with a pump photon, stimulates the creation of a second Stokes photon, which is coherent with the first one, as can be seen in Fig. 2.4. The polarisation, which drives the stimulated generation of the Stokes photons, is induced by the interaction of the pump beam and the Stokes beam.

In the presence of a strong pump, the Stokes field will experience gain and if the Raman active medium is placed between two mirrors and the gain is strong enough to overcome the cavity's losses, oscillation at ω_S will occur. This was observed in Paper [VII].

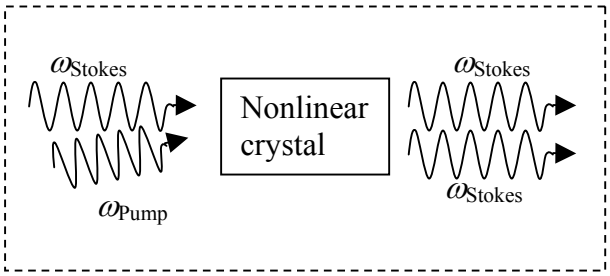

.

Figure 2.4. The principle of stimulated Raman scattering.

2.4.3 Four-Wave Mixing

Another important third order nonlinear process is four-wave mixing (FWM), which generates new frequencies by mixing present frequencies $\omega_4 = \omega_1 \pm \omega_2 \pm \omega_3$. This can lead to transferring energy from initially more efficient processes to less efficient ones, if the four-wave mixing process is phasematched.

2.5 The Dominant Nonlinear Process in a Crystal

In general, all the processes mentioned in the previous sections take place in a nonlinear crystal, because they are all permitted according to the law of energy conservation. If we only consider second order processes for a while, the energy conservation is given by $\hbar\omega_1 + \hbar\omega_2 = \hbar\omega_3$. However, also the conservation of momentum $\hbar k_1 + \hbar k_2 = \hbar k_3$, where k_i are the wave vectors, has to be fulfilled in order to achieve efficient energy conversion. This law can be rewritten as $n_1\omega_1 + n_2\omega_2 = n_3\omega_3$ using $k_i = n_i\omega_i/c$, where n_i is the refractive index of the wave having the frequency ω_i. This condition is not trivial due to dispersion in nonlinear materials. In general the index of refraction is not constant but dependent on the wavelength and the angle of propagation. In the biaxial crystal $KTiOPO_4$ the refractive index for wavelengths inside the transparency range between 350 nm and 3 μm increases with increasing frequency.

However, two main techniques are available to satisfy the momentum conservation condition. These are birefringent phasematching and quasi-phasematching, which will be treated in detail in Chapter 3.

Clearly, not all of the possible processes can fulfil the conservation of momentum at the same time, thus only the one fulfilling both laws will grow in strength while passing through the nonlinear crystal.

Chapter 3

Phasematching

A factor complicating nonlinear processes is that electric fields with different frequencies in general propagate with different phase velocities due to dispersion. In SHG for instance, the fundamental radiation moves with the phase velocity c/n_{ω} and so does the driving polarisation. The generated field, the second harmonic, however, propagates with a phase velocity of $c/n_{2\omega}$. Thus the driving polarisation and the generated wave drift out of phase. The direction of the power flow from one wave to the other is determined by the relative phase between the interacting waves. Therefore, an alternating phase shift results in power flowing back and forth between the fundamental and the second harmonic instead of solely converting power from the fundamental radiation to the second harmonic.

The distance, after which back-conversion starts, is typically only a few micrometres. If nothing is done to prevent the back-conversion, the maximum generated power will therefore be limited to the power that is obtained within this short region. Efficient conversion requires, however, significantly longer crystals, having typically sizes of several millimetres. Hence it is essential to employ techniques, which prevent the phases of the waves to drift apart, namely to achieve phasematching.

Two important methods to achieve phasematching between the different components exist: birefringent phasematching and quasi-phasematching. The first time a nonlinear process showed efficient frequency conversion was birefringence phasematched second harmonic generation.[16,17] Only shortly afterwards quasi-phasematching was suggested independently by Armstrong *et. al.*[8] and Franken *et al.*[18] This technique was demonstrated for the first time by the latter group employing a stack of thin plates of quartz, where every second piece was rotated by 180°. Another idea suggested at the same time, was to adjust the phase mismatch between the interacting waves by internal reflections in quartz.

3.1 Birefringent Phasematching

The most commonly used method to achieve the momentum conservation $\hbar k_1 + \hbar k_2 = \hbar k_3$, which also can be written as

$$n_1\omega_1 + n_2\omega_2 = n_3\omega_3 \tag{3.1}$$

is, to employ birefringent phasematching (BPM). BPM utilizes the fact that the three principal axes in biaxial materials have different indices of refraction. By letting the beams enter at different angles and/or be polarised in different directions, the needed relationship between n_1, n_2 and n_3 can be fulfilled. Fig. 3.1 shows BPM for SHG in a uniaxial, negative ($n_o > n_e$) crystal.

The fundamental wave is launched at an angle θ relative to the optical z axis. It is polarised in the x-y plane, which results in an ordinary beam. Thus, it propagates with a phase velocity of c/n_o^{ω}, and so does the driving polarisation. The second harmonic is then generated as an extraordinary beam. Therefore, its index of refraction is dependent on the angle θ and given by:

$$\frac{1}{\left(n_e^{2\omega}(\theta)\right)^2} = \frac{\sin^2\theta}{(n_e)^2} + \frac{\cos^2\theta}{(n_o)^2} \tag{3.2}$$

This relation describes an ellipse as can be seen in Fig. 3.1. If it is possible to match these two velocities by achieving $n_o^{\omega} = n_e^{2\omega}(\theta)$ the two beams will propagate through the crystal in phase and the energy will flow from the fundamental wave to the second harmonic.

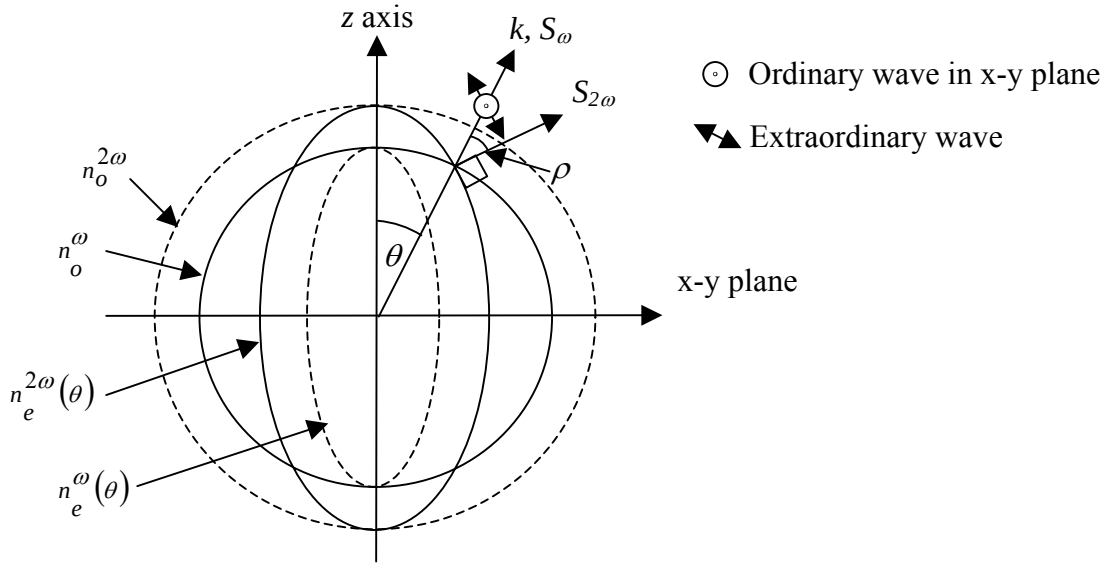

Figure 3.1. Birefringent phasematching in a negative uniaxial crystal.

The angle of the beam propagation in relation to the optic axis, θ, does not only control the phasematching condition, but also whether the interaction is denoted critical or noncritical. The ideal case is noncritical phasematching and can in uniaxial crystals only be achieved for $\theta = 90°$. All other angles ($\theta \neq 90°$) result in critical phasematching. The drawback with critical phasematching is a phenomenon called walk-off, which complicates the phasematching

process. For the extraordinary wave the wavevector direction and the direction of the power flow, which is determined by the Poynting vector $S_{2\omega}$, differ by the walk-off angle ρ, given by

$$\tan\rho = \frac{1}{2}\left[n_e(\theta)\right]^2\left(\frac{1}{(n_e)^2} - \frac{1}{(n_o)^2}\right)\sin 2\theta\,. \tag{3.3}$$

Thus, for critical interaction the ordinary and the extraordinary beam do not overlap after a certain distance any longer. This, obviously, prevents further energy conversion and reduces the useful crystal length. Another consequence of the Poynting vector walk-off is that it limits the ability to focus tightly, because narrow beams separate quicker than large ones. However, tight focussing is sometimes necessary in order to increase the intensity.

Due to these limitations in the interaction distance, noncritical phasematching is preferred, where energy can flow between the tightly focused beams while propagating through a longer crystal. However, in order to achieve noncritical phasematching in uniaxial BPM crystals $n_o^{\omega} = n_e^{2\omega}(\theta = 90°)$ has to be fulfilled in addition to the energy conservation. This limits the possible wavelengths for which phasematching is achievable in a particular material.

3.2 Quasi-Phasematching

In quasi-phasematching (QPM) a perfect matching of the phase velocities is not possible. Instead the phase mismatch between the generating polarisation and the generated radiation, which is accumulated while propagating through the nonlinear medium, is reset to its optimal value at certain distances. At the beginning of the crystal the phases for the nonlinear processes adjust themselves to give maximum conversion from the incident field to the generated field, for example the second harmonic. While propagating deeper into the crystal, the phases drift apart and the conversion decreases. After a certain distance, called the coherence length, L_c, the accumulated phase shift is π, and the power starts to flow back from the second harmonic into the pump. However, if it is possible to adjust the phase shift back to its optimal value after each coherence length, the power will flow from the pump to the second harmonic over the whole crystal length. This principle is called quasi-phasematching. Although the power conversion to the second harmonic will not be as fast for QPM crystals as for perfect phasematching, which can be seen in Fig. 3.2, this technique has other important advantages.

Adjustment of the phase shift after each coherence length can be achieved by reversing the sign of the appropriate nonlinear coefficient for every second coherence length. The change of the sign results in an additional phase shift of π to the accumulated phase mismatch, thus avoiding the occurrence of destructive interference.

The effect of QPM can also be explained by using a mathematical approach involving Fourier transformations: The wave vectors associated with the interacting beams, k_{ω} and $k_{2\omega}$, and the wave vector associated with the domain structure of the material, K_m, are added. For SHG this results in

$$\Delta k = k_{2\omega} - 2k_{\omega} - K_m \tag{3.4}$$

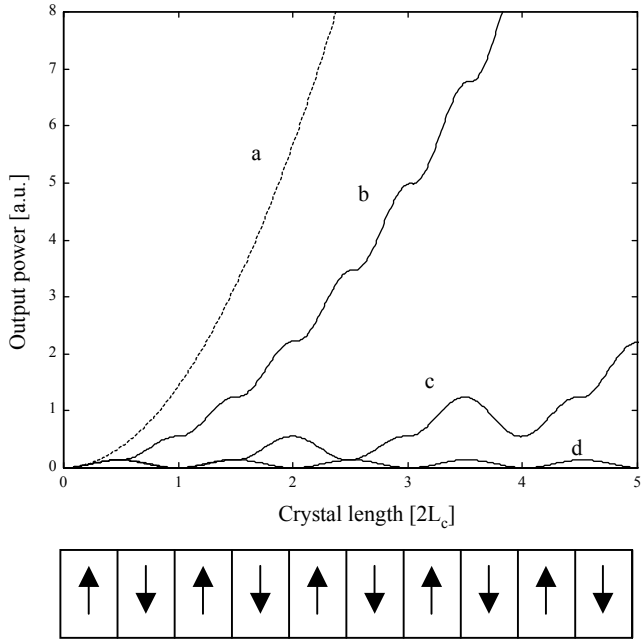

Figure 3.2. The output power of SHG for perfect phasematching (a) and quasi-phasematching versus the crystal length.[19] Curve (b) is for first order QPM, curve (c) for third order and (d) is no phasematching at all. A schematic of a crystal for first order QPM is also shown.

where the m*th*-harmonic grating vector is given by $K_m = \frac{2\pi m}{\Lambda}$ and $\Lambda = 2L_c$ is the period of the structure. If the domain inversion structure is perfect, the nonlinear coefficient can be assumed to be a square function taking the values $\pm d_{ij}$. For simplicity a function

$$g(x) \equiv d(x)/d_{ij} \tag{3.5}$$

is defined taking the values ±1.[20] If *g(x)* is a periodic function, having the period Λ, it can be expanded into a Fourier series

$$g(x) = \sum_{m=-\infty}^{m=\infty} G_m e^{iK_m x} \tag{3.6}$$

If (3.5) and (3.6) are inserted into (2.9) for SHG, this results in the electric field for the harmonic being:

$$E_{2\omega}(L) = \frac{i\omega E_\omega^2}{n_{2\omega} c} d_{ij} \int_0^L \sum_{-\infty}^{\infty} G_m \exp[i(K_m - \Delta k')x]dx \tag{3.7}$$

where $\Delta k' = k_{2\omega} - 2k_{\omega}$. The only considerable contribution in this sum is given by the grating vector K_m, which is approximately equal to $\Delta k'$, leading to $\Delta k = \Delta k' - K_m \approx 0$.

Hence, the behaviour of QPM is similar to ordinary phasematching, except for substituting the nonlinear coefficient d_{ij} by the effective nonlinear coefficient $d_{eff} = d_{ij}G_m$, which was introduced in section 2.2. An idea about the value for G_m can be achieved by rewriting it as the standard Fourier coefficient:

$$G_m = \frac{2}{\pi m}\sin(\pi m D), \tag{3.8}$$

where D is the duty cycle given by the ratio between the sections having positive nonlinear coefficients and the period of the structure. The most efficient QPM structure is therefore given by $m = 1$ with $D = 0.5$, leading to $d_{eff} = \frac{2}{\pi} d_{ij}$. Thus, the possibility to engineer crystals for the desired application leads to a small reduction of the nonlinear coefficient and the subsequent reduction in the second harmonic power compared to perfect phasematching. However, this is a small price to pay for the possibility to noncritically phasematch any interaction within the transparency range of the nonlinear crystal.

3.3 Birefringent Phasematching versus Quasi-Phasematching

Both birefringent and quasi-phasematching have advantages and disadvantages. The main advantage of BPM is the absence of the poling process, which is described in Chapter 5. The electric field poling technique, which is used to obtain QPM crystals, involves the application of high voltage pulses to reverse the spontaneous polarisation in ferroelectric material. Not only does this add several processing steps before obtaining a functioning crystal, but it also limits the thickness of the crystals. For BPM crystals, however, the size of the sample is only restricted by the growth technique. This makes BPM crystals the first choice for high power applications, since a large aperture allows the beams to interact without the risk of reaching the crystal's damage threshold. Despite this limitation to the intermediate power regime, many applications exist which favour the usage of QPM crystals.

One of the most important advantages with QPM is the possibility to engineer the crystals and make them suitable for any process, i.e. achieving more flexible nonlinear crystals. Any nonlinear process can be phasematched as long as the interacting wavelengths are in the material's transparency range. However, for BPM samples the exploitable wavelength range of a material is determined by the phasematching conditions for the particular crystal and is therefore limited.

Another positive consequence of producing QPM crystals is the possibility to utilise the largest nonlinear coefficient of the material and not, as in BPM, the one leading to the suitable birefringence. Although the nonlinear coefficient, which in KTP isomorphs' case is d_{33}, has to be replaced with the effective nonlinear coefficient d_{eff}, in general it still has a substantially larger magnitude than the suitable nonlinear coefficients for BPM.

Another disadvantage of BPM is the restricted possibility to employ noncritical phasematching. Instead walk-off has to be taken into consideration, which leads to a limited interaction length for the nonlinear processes as mentioned above, decreasing the conversion efficiency.

Finally, the nonlinear coefficient is dependent on the angles at which the interacting waves propagate through a BPM crystal. Since different wavelengths need different phasematching angles, the nonlinear coefficient varies also as a function of the wavelengths. The fact that the coefficient is not a constant can be detrimental in experiments where large bandwidths are used or angle tuning is employed, since the gain will differ.

Thus, even though the dimensions of QPM crystals are limited, the possibility to obtain noncritical phasematching with large nonlinear coefficients, instead of having to find a material, which has the proper behaviour for the optical process in mind, is extremely practical and powerful.

3.4 Čerenkov Phasematching

A less commonly employed technique to achieve phasematching for a nonlinear interaction is Čerenkov phasematching. This method has mainly been employed in waveguides and is analogous to Čerenkov radiation in particle physics. If particles are travelling in a material at a speed, which is faster than light in this particular medium, they emit coherent radiation in a direction dependent on the material's refractive index. This phenomenon was observed for the first time in 1934 by P. Čerenkov.[21]

A. Zembrod *et al.* were the first to observe SH radiation emitted in a Čerenkov cone by a $LiNbO_3$ crystal when irradiated with a Nd:YAG laser.[22] Shortly afterwards Tien *et al*. demonstrated efficient SHG, which was emitted in the Čerenkov direction as a collimated beam, by guiding a beam from a Nd:YAG laser in a ZnS waveguide on a ZnO substrate.[23] The situation for achieving Čerenkov phasematching is the following: As mentioned in the introduction of this chapter, the forced wave of SH polarisation propagates with a velocity of $v_F = c/n_F$, whereas the second harmonic radiation travels with a phase velocity of $v_{SH} = c/n_{SH}$. If $v_F > v_{SH}$ phasematching can be achieved in specific directions, which are called Čerenkov angles, and given by

$$\sin\theta = \frac{v_{SH}}{v_F} \quad . \tag{3.9}$$

In general this situation can occur in waveguides, where different regions have different refractive indices resulting in the nonlinear polarisation in the waveguide being faster than the free wave at the second harmonic in the substrate. Emission of the SH in the Čerenkov angles ensures conservation of the momentum component parallel to the interface, see Fig. 3.3 (a). In the same graph a schematic picture of this situation is shown. Only if the SH wave generated by the nonlinear polarisation at a specific point, A, is in phase with the SH wave generated at a point B, the interaction will be constructive, resulting in efficient SHG.

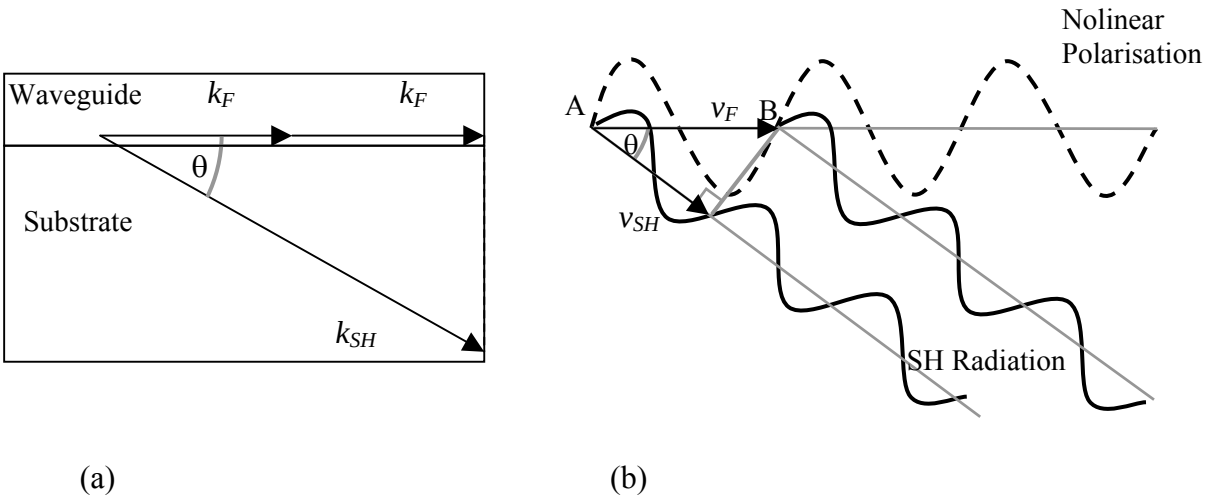

(a) (b)

Figure 3.3. (a) Phasematching of the wave vector components parallel to the interface of a waveguide. (b) Schematic illustration of Čerenkov phasematching.

Chapter 4

Properties of $KTiOPO_4$ Isomorphs

Over 100 years ago, in 1890, an article was published reporting the first synthesis of a $KTiOPO_4$ (KTP) crystal.[24] For several decades the material did not seem to have any valuable characteristics and the first detailed analysis of the crystal structure was not performed until 1974.[25] However, shortly afterwards KTP's large nonlinear susceptibility was discovered[26] and since then KTP has been intensively employed for various nonlinear processes.

Apart from the already mentioned large nonlinear susceptibility, the main advantages with KTP are its high resistance to optical and mechanical damage and its wide transparency range. Moreover, KTP's birefringence is large enough to permit its utilisation for BPM and since KTP is ferroelectric it can also be employed for QPM.

4.1 Crystal Structure of $KTiOPO_4$ Isomorphs

The two materials used for nonlinear processes during this work were KTP and $RbTiOPO_4$ (RTP). They both belong to the KTP family, where all members are denoted by $MTiOXO_4$. Here M represents K, Rb, Tl or NH_4 and X either P or As.[27] Apart from KTP and RTP two further members of the KTP family are commonly used in nonlinear optical experiments: $KTiOAsO_4$ (KTA) and $RbTiOAsO_4$ (RTA).

Both KTP and RTP are orthorhombic and belong to the acentric mm2 symmetry group. They are also members of the space group $Pna2_1$, which implies that the crystallographic directions *a*, *b*, *c* correspond to the optic axes *x*, *y*, *z* with *c* being the polar axis.

KTP's structure consists of distorted TiO_6 octahedra, which are linked at two corners to form chains. The Ti atom is displaced from the centre of the octahedron, leading to one long, one short and four medium Ti-O bonds in the structure. These alternating lengths of the Ti-O bonds cause a net *c*-directed polarisation in KTP. The TiO_6 chains are separated by slightly distorted PO_4 tetrahedra, see Fig. 4.1. The K^+ ions are weakly bonded to both the tetrahedra and octahedra and can occupy two different sites – either an eight-fold or nine-fold coordinated. Further, the cations can by diffusion mechanism travel through channels, which exist along the *c* direction. They diffuse by a vacancy hopping mechanism that causes the

ionic conductivity along the *c* axis to be several orders of magnitude higher than in the other directions.[28]

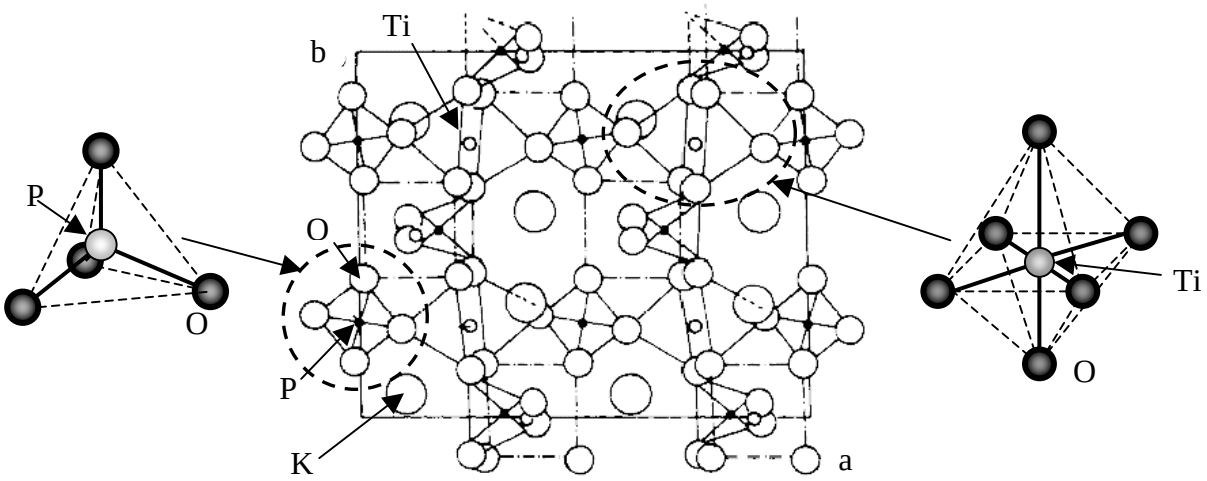

Figure 4.1. The structure of KTP seen along the *z* axis[29] together with the structures of the PO_4 tetrahedron and the TiO_6 octahedron.

A technique frequently employed to examine a crystal's structure more closely, is by detecting the Raman scattering that is emitted by the material, when it is irradiated by an intense laser beam. As mentioned in Chapter 2, a molecule (or an atomic group) can absorb a photon with a non-resonant frequency, ω_L. It will then be excited to a virtual state from where it quickly relaxes. It is, however, possible that the molecule does not return to the ground state, but instead to a vibrational state lying above the ground state. Thus, instead of emitting a photon with the same energy as the absorbed one, it emits a Stokes photon having less energy than the incoming photon $\omega_S = \omega_L - \omega_V$ and a phonon ω_V, which is schematically shown in Fig. 4.2 (a).

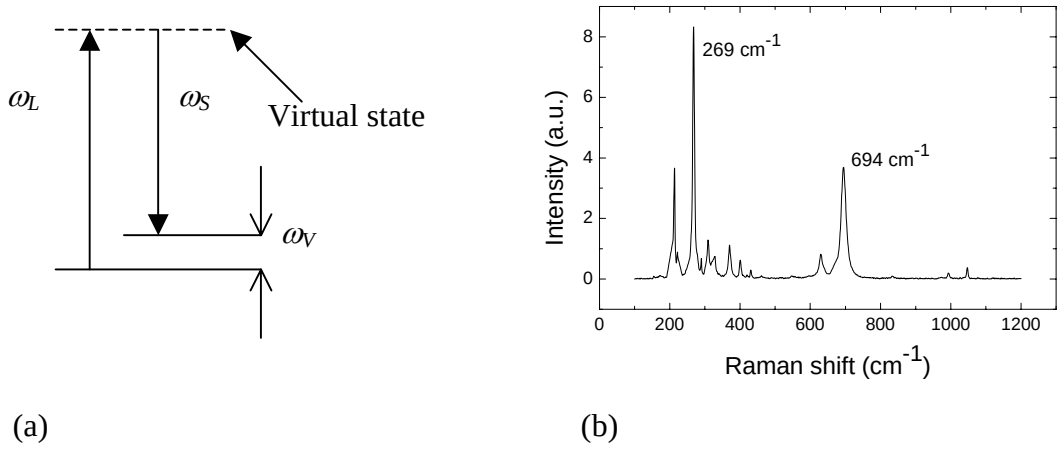

(a) (b)

Figure 4.2. (a) A schematic of the photons and the phonon involved in a Raman scattering process. (b) The spectrum of the Raman scattered light generated in KTP when irradiated at 1064 nm.

By analysing the Raman shift of the scattered light it is not only possible to deduce which atomic groups are present in the material, but also how these groups are connected to each other. The spectrum shown in Fig 4.2 (b) was obtained as a part of the initial studies in Paper [VII]. A *z*-polarised beam was generated by a cw Nd:YAG laser operating at 1064 nm and propagated through a KTP crystal in the *x*-direction. The backscattered Stokes lines polarised along the *z* axis were detected and the Raman shift was derived.

The spectrum can be divided into three regions. The first section between 200 and 400 cm^{-1} is associated with vibrational modes of TiO_6.[29] In this part, at 269 cm^{-1}, the strongest peak of the whole spectrum can be found. It is related to the interbond angle bending vibration of TiO_6, which is schematically drawn in Fig. 4.3 (a). The second region between 600 and 850 cm^{-1} is also associated with vibrational modes of TiO_6. The second strongest peak of the spectrum at 694 cm^{-1} is due to the pure bond stretching vibrational mode of TiO_6, which is shown in Fig. 4.3 (b). Finally, the last region between 1000-1100 cm^{-1} is associated with three degenerate modes of PO_4, see Fig. 4.3 (c)-(e).

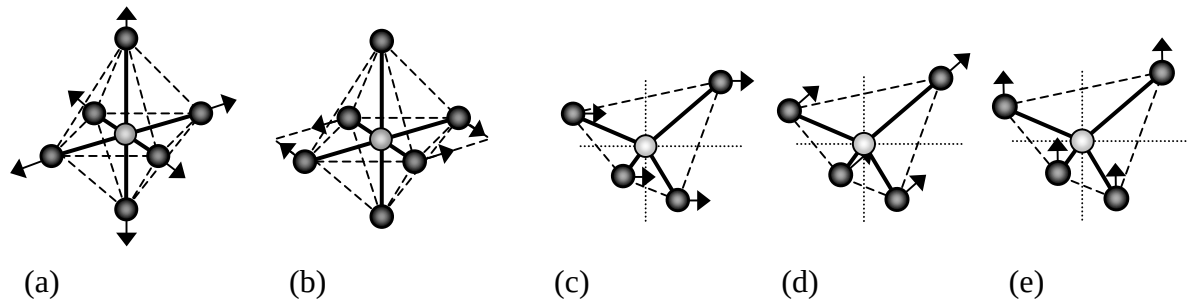

Figure 4.3. The dominant vibrational modes of TiO_6 and three fundamental degenerate vibrational modes of PO_4.

The origin of the high nonlinearity found in KTP crystals is still ambiguous. According to early experiments performed by Zumsteg *et al*.[26] the short bonds in the TiO_6 groups are considered to be the main cause for the high nonlinear coefficients. Some years later Xue and Zhang[30] came to another conclusion, which claimed that the K-O bonds and the PO_4 tetrahedra are responsible for the nonlinearity. However, recently Pasiskevicius *et al*. published an article, which supports the older opinion that the nonlinearity originates from the Ti-O bonds.[31]

In RTP it is the Rb^+ ion that replaces the K^+ ion, which is weakly bonded to the tetrahedra and the octahedra. Also this ion can diffuse more easily along the *c* axis than along any other axis. However, since Rb atoms have a larger atomic radius than K atoms, their transportation is slower. Hence, RTP has a typical ionic conductivity in the *c*-direction (~10^{-9} S/cm) that is several orders of magnitude lower than the conductivity in KTP (10^{-6} - 10^{-7} S/cm).[32]

The ionic conductivity of KTP crystals is found to vary by four to five orders of magnitude and depends on the employed growth technique and the conditions of the growth.[33] There are mainly two different methods: hydrothermal growth and flux growth. The hydrothermal growth process takes place in a high temperature (400 – 500 °C), high-pressure (1-2 kbar) container and takes usually ~ 3 weeks.[34]

Flux grown KTP is grown at higher temperatures (700 – 1000 °C) than hydrothermally grown KTP, but at atmospheric pressure. The crystals are grown from a composition,

consisting of the crystal's components, which are dissolved in a solvent, called the flux. If only the crystal's constituents are present in the flux, the growth technique is denoted self-flux growth. The growth of the crystals starts in a supersaturated melt and continues while the temperature is constantly decreased.[35] It is of utmost importance that the temperature is uniform and accurately controllable during this process, since flux inclusions and growth striations can occur otherwise.[27]

Flux growth is more critical, since the growth temperature is close to the Curie temperature, which for KTP is 936 °C. At this temperature the material undergoes a phase transition and becomes paraelectric. On the other hand, the two main advantages of flux compared to hydrothermal growth are the reduced growth times and the possibility to grow larger wafers. These benefits result in a better availability of flux grown KTP and a lower price compared to hydrothermal KTP. All crystals used in this work were produced by self-flux growth.

4.2 Ferroelectric Properties

KTP is a dielectric, which means that it has no free electrons at room temperature. In general, dipoles are formed if an electric field is applied to dielectrics, which causes the material to become polarised. However, some dielectrics, among them KTP, also possess a so-called spontaneous polarisation, P_s, if no external field is applied. These materials form the pyroelectric group.

If the spontaneous polarisation has two or more states of orientation in the absence of an electric field and the polarisation can be reversed, by applying an external field to the crystal, it belongs to the ferroelectric group. Ferroelectricity indicates that the centre of the positive charges inside the crystal does not coincide with the centre of the negative charges, as can be seen in Fig. 4.4. However, in general this spontaneous polarisation is temperature dependent according to the Curie-Weiss law, $P_s \sim \sqrt{T_C - T}$, and above the so-called Curie temperature T_C, the crystals undergo a phase transition. For KTP this temperature is as aforementioned 936 °C and above this value the material becomes paraelectric and has a centrosymmetric structure.

Most ferroelectric crystals consist of domains, which are regions where the spontaneous polarisation is directed along the same direction. The neighbouring areas, however, can have their polarisation facing the opposite direction, resulting in multi-domain crystals. In KTP the spontaneous polarisation is aligned along the *c* axis. All wafers used in this work were initially single domain, having the spontaneous polarisation vector pointing from the c^- surface to the c^+ surface. Whether a crystal is single- or multi-domain depends on several factors, most important are the growth and the cooling conditions and the seed quality.

By applying an electric field to the crystal, the polarisation can be reversed; meaning that the domains, which have dipole moments pointing in the same direction as the field will grow and those with opposite signs will decrease in size. The graph of KTP's spontaneous polarisation versus the applied electric field describes a hysteresis loop.[36] In order to achieve permanent inversion, the external field applied to the crystal has to be larger than the coercive field.

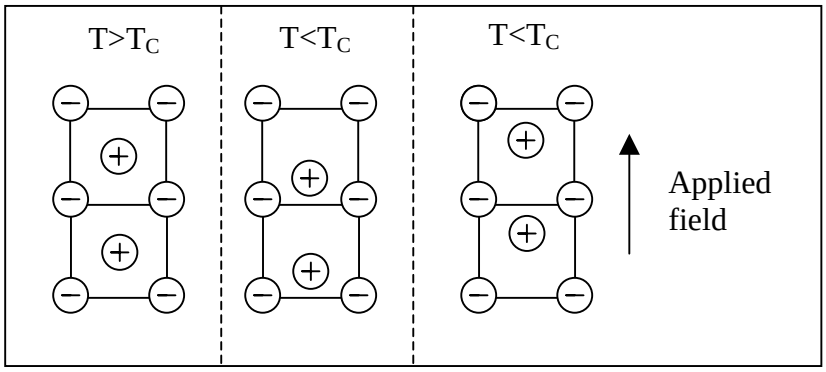

Figure 4.4. A schematic representation of a ferroelectric crystal's phases depending on external conditions, such as temperature and applied electric field.

4.3 Optical Properties of $KTiOPO_4$ and $RbTiOPO_4$

4.3.1 Refractive Index

The ability to determine precise QPM periods for specific parametric processes depends to a large degree on the accurate knowledge of the nonlinear material's refractive indices. Since all the members of the KTP family are biaxial, all axes have different indices of refraction. Nonlinear parametric processes involve the propagation of electromagnetic waves with different wavelengths through a material. Thus, for the determination of the refractive index for a specific beam in KTP, not only the direction of polarisation but also the dispersive character of the crystals has to be taken into consideration.

The Sellmeier equations are commonly used to calculate the refractive index and the general form is given by

$$n^2(\lambda) = A + \frac{B}{1-\frac{C}{\lambda^2}} + \frac{D}{1-\frac{E}{\lambda^2}} - F\lambda^2 \qquad (4.1)$$

where the wavelength λ has to be in µm.

Several sets of Sellmeier coefficients have been published both for KTP[37] and for RTP. Experiments have shown that the Sellmeier coefficients for KTP published by Fradkin *et al.*[38] show best correspondence for wavelengths longer than 1 µm, whereas the coefficients published by Fan *et al.*[39] give best results for wavelengths shorter than 1 µm. The accuracy of these coefficients is very important as mentioned above. For example, in order to fabricate a periodically poled crystal for SHG of a fundamental beam at 1 µm, with an accuracy of 0.1 nm, the uncertainty of the refractive index $\delta n/n$ has to be of the order $\sim 10^{-3}$.

All the experiments performed during this work employed *z*-polarised waves that were propagating along the *x*-direction. Therefore only the Sellmeier coefficient for the *z* indices of refraction are presented in Table 4.1.

	A	**B**	**C [μm^2]**	**D**	**E [μm^2]**	**F [μm^{-2}]**
KTP[38] (λ > 1μm)	2.12725	1.18431	0.0514852	0.6603	100.00507	0.00968956
KTP[39] (λ < 1μm)	2.25411	1.06543	0.05486	0	0	0.0214
RTP [V]	2.229382	1.230476	0.052475	2.40099	159.4113	0.00131914

Table 4.1. The Sellmeier coefficients of KTP and RTP for electric fields polarised along the *z* axis.

For RTP two sets of Sellmeier coefficients had been published, one by Dmitriev *et al.*[40] and one by Guillien *et al.*[41] Since a few RTP samples had been periodically poled, we compared the experimental data achieved when employing them in nonlinear processes with the results calculated using the two Sellmeier sets. The PPRTP samples were suitable for generating blue light by second harmonic processes and for optical parametric oscillation generating signal and idler wavelengths in the IR. Large discrepancies were observed between the experimental wavelengths and the calculated values using the Sellmeier equations. Thus, a systematic measurement was performed to obtain a new set of Sellmeier coefficients, which would enable the precise prediction of QPM periods in RTP. All in all six OPO crystals and nine SHG crystals were analysed.

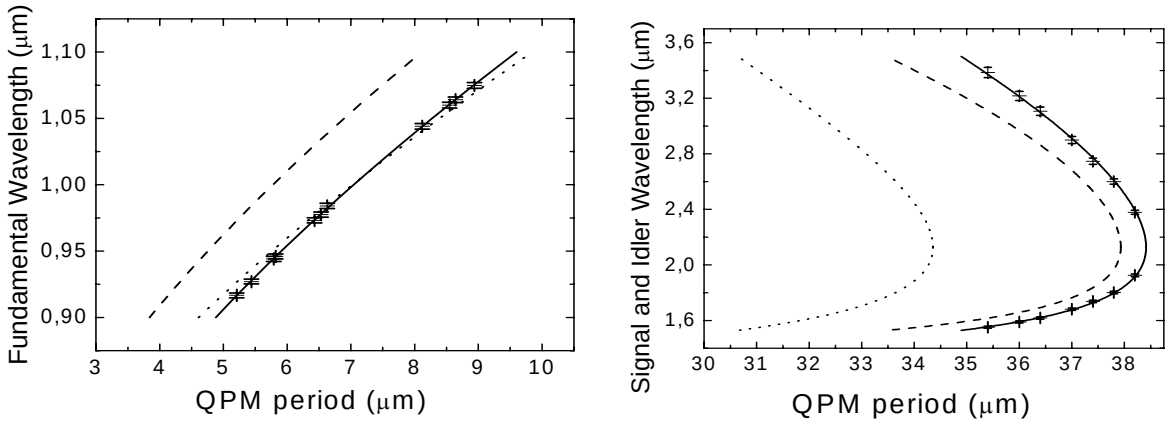

Figure 4.5. (a) Experimental and theoretical fundamental wavelengths for SHG as a function of the quasi-phasematching period. (b) Experimental and theoretical signal and idler wavelengths versus the QPM period. The solid curves used the newly derived RTP Sellmeier coefficients to determine the wavelengths, whereas the dotted curves used the coefficients from Dmitriev *et al.*[40] and the dashed curves used the coefficients from Guillien *et al.*[41]

This experiment resulted in a set of Sellmeier coefficients, which was much more accurate and allowed the determination of phasematching periods, which was not possible earlier. The

newly derived coefficients are given in Table 4.1 and a comparison between the two old sets and the new one can be seen Fig. 4.5.

4.3.2 Thermal Dispersion

The index of refraction is not only a function of wavelength and direction of polarisation; it is also dependent on the temperature of the crystal due to the thermo-optic effect. Thus by changing the temperature it is possible to tune the wavelength of the nonlinear process. In order to be able to do this systematically, the change of the refractive index as a function of the temperature has to be known. The temperature dispersion is approximated by a Laurent series of the form

$$\frac{dn_z}{dT} = \frac{p_1}{\lambda^3} + \frac{p_2}{\lambda^2} + \frac{p_3}{\lambda} + p_4 \tag{4.2}$$

where λ again has to be in µm.

	$p_1\times10^6$ [µm^3]	$p_2\times10^6$ [µm^2]	$p_3\times10^6$ [µm]	$p_4\times10^6$
KTP[42] (λ < 1µm)	12.415	-44.414	59.129	-12.101
RTP [V]	12.4126	-51.5705	59.0696	-12.0918

Table 4.2. The temperature dispersion coefficients for KTP and RTP.

Once again a set of coefficients giving reasonable correspondence between theory and experiments was available for KTP. The set of p_1, p_2, p_3 and p_4 published by Wiechmann *et al.*[42] can be found in Table 4.2. However, it seemed that no data had been published on the thermal dispersion of RTP. Therefore the OPO samples were temperature tuned from 20 to 150 °C and the signal and idler wavelengths were measured. From this data a set of temperature dispersion coefficients was derived, which also is presented in Table 4.2.

Except for wavelengths close to degeneracy the agreement between the theoretical and the experimental values was generally very good, as can be seen in Fig. 4.6. The discrepancy observed close to degeneracy is due to the broad parametric gain bandwidth of the crystal at these wavelengths, which decreased the accuracy of the experimental data.

4.3.3 Absorption and Nonlinear Properties

Another important optical property of KTP and RTP is their transmission as a function of the wavelength. Hansson *et al.*[43] performed accurate measurements for several members of the KTP family and their results are reproduced in Fig. 4.7. The data was taken for *z*-polarised electric waves propagating along the *x* axis of the crystals, which were approximately 10 mm long. As can be seen, both KTP and RTP are highly transmitting from 0.35 µm to 3 µm. Apart

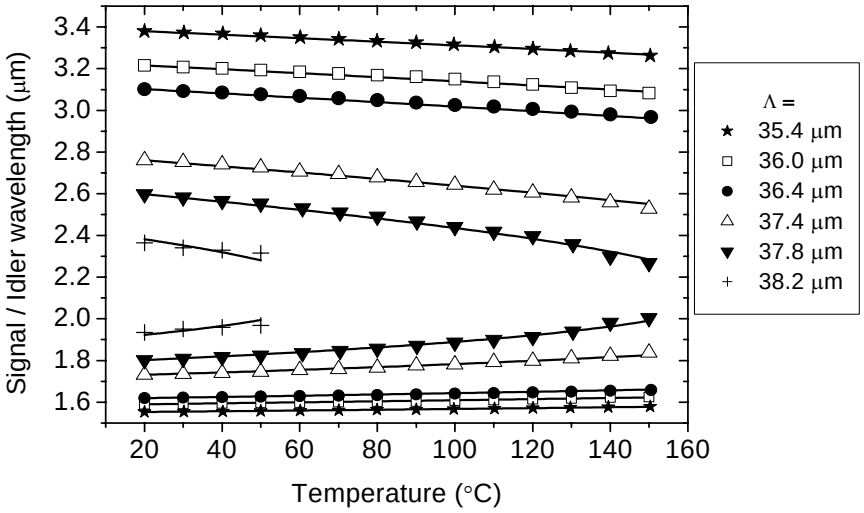

Figure 4.6. The signal and idler wavelengths as a function of temperature for six different OPOs. The solid curves are the theoretical fits using (4.2).

from the strong dip at 2.8 μm, which is related to OH^- groups trapped in the crystals during growth, the absorption is less than 0.6 % cm^{-1}. At longer wavelengths, however, the absorption increases considerably and above 4 μm the transmission decreases rapidly to zero. For KTA and RTA the highly transmitting region is extended to 3.6 μm as can be seen in Fig. 4.7 for RTA.

	d_{15} [pm/V]	d_{24} [pm/V]	d_{31} [pm/V]	d_{32} [pm/V]	d_{33} [pm/V]
KTP	1.9	3.6	2.5	4.4	16.9
RTP	-	-	3.3	4.1	17.1

Table 4.3. The nonlinear coefficients for KTP and RTP.

One of the main reasons to choose members from the KTP family in nonlinear experiments, is their advantageous nonlinear properties. As KTP belongs to the mm2 point group the only nonzero nonlinear coefficients are d_{15}, d_{24}, d_{31}, d_{32} and d_{33}. The values are presented in Table 4.3.[44] Here it can be seen that the most favourable nonlinear coefficient for both KTP and RTP is d_{33}, meaning that the most efficient conversion is achieved, if all radiation fields are polarised along the *z*-direction.

4.4 Comparison between $KTiOPO_4$ and other Nonlinear Crystals

Among the first nonlinear materials, which were used in frequency conversion processes, were potassium dihydrogen phosphate (KDP) and ammonium dihydrogen phosphate (ADP). These crystals were well known, since they had previously been employed in piezoelectric applications. They can easily be grown in large sizes and have very large damage thresholds. Some disadvantages are, however, their small nonlinear coefficients, their limited

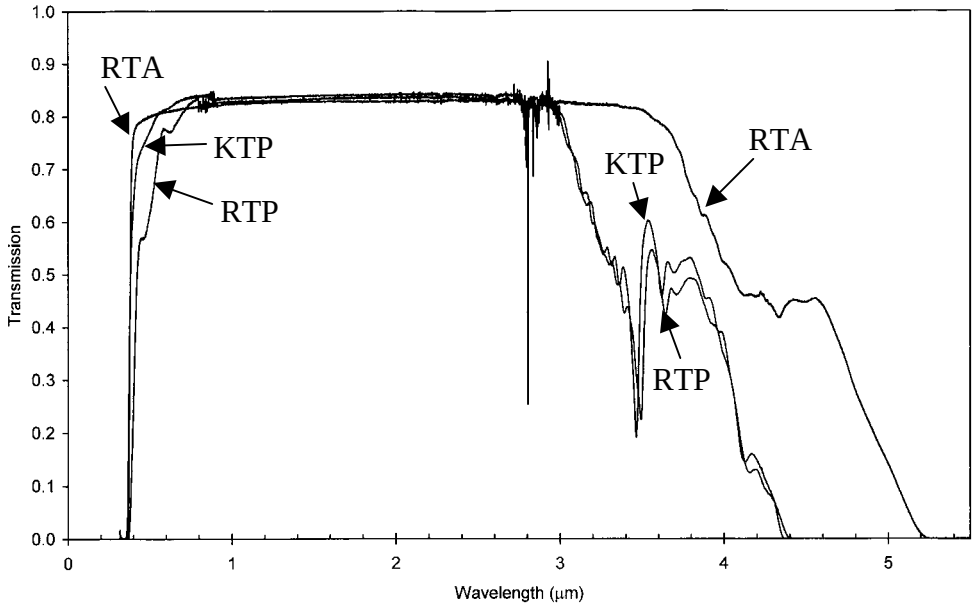

Figure 4.7. Transmission of KTP, RTP and RTA as a function of wavelength.[19]

transparency range in the IR and that they are hygroscopic. Two other materials, which also have large damage thresholds but comparably small nonlinear coefficients, are Beta-Barium Borate, β-BaB_2O_4 (BBO), and Lithium Triborate, LiB_3O_5 (LBO). They were developed during the last three decades and have a wider transparency range in the IR region than KDP and ADP. A more recently developed material for nonlinear processes is BiB_3O_6 (BIBO). Most of its properties are similar to BBO and LBO, it has, however, larger nonlinear coefficients.[45] Since these five nonlinear materials are highly birefringent they are all suitable for birefringence phasematching. It is however believed that they are not ferroelectric, which excludes them from being periodically poled. Hence walk-off effects have to be considered, which limit the length of the crystals.

The most commonly used crystal for QPM processes is so far congruent $LiNbO_3$ (CLN). CLN is a very mature nonlinear material that offers slightly better transmission in the infrared region compared to KTP and has the advantage of possessing a larger nonlinear d_{33} coefficient. Thus, the figure of merit, which commonly is defined by $d_{eff}^2/(n_1 n_2 n_3)$, and describes a material's ability to efficiently convert power, is smaller for KTP compared to CLN.

However, several reasons exist to favour KTP isomorphs for certain applications. One of the most important motivations to choose members from the KTP family instead of CLN is that the magnitude of the coercive field only is approximately one-tenth for KTP compared to CLN. This facilitates the production of thick periodically poled crystals, which are needed for high power applications.[46]

Another advantage of the KTP isomorphs is their high resistance to optical damage. Photorefractive damage can occur when optically excited free carriers get trapped in crystal regions not exposed to the beam. These carriers can create an internal field that distorts the beam via the electro-optic effect. KTP offers a several orders of magnitude higher resistance

to photorefraction than CLN due to its higher conductivity. To prevent damage in CLN, these crystals have to be operated above 100 °C. Further, the use of KTP allows larger optical peak intensities, since it is less sensitive to material breakdown caused by strains that are induced by local temperature increases.

During the last decade some new materials, e.g. stoichiometric $LiNbO_3$ (SLN) and $LiTaO_3$ (SLT), have appeared. These materials are, however, more expensive than the congruent ones and their growth technology still has to be improved considerably to achieve homogeneous crystals. An important advantage compared to their congruent siblings is their reduced coercive field, which for SLT is reported to be comparable to that of KTP.[47] By doping these crystals with MgO during growth, the conductivity is increased, which makes them more resistant to optical damage. Despite this improvement, operation above room temperature might still be needed to further reduce the photorefraction and achieve efficient energy conversion.[48]

All in all, there are several candidates, which can perform as the gain material in a nonlinear process and the choice of the best one depends on the specific application. The wavelength, the pulse duration, the input and the output power levels are only some of the properties that have to be taken into consideration when choosing the most suitable material. However, in general KTP is an attractive material, since it offers an excellent combination of the most important properties: large nonlinear coefficients, large damage threshold and wide transparency range.

Chapter 5

Electric Field Poling

It is not straightforward to implement a periodic structure inside a crystal, where every domain has an opposite spontaneous polarisation to its neighbours, in order to achieve quasi-phasematching. Different techniques have been proposed and tested.

One method is to cut a single domain crystal into thin slices, rotate every second slice, and stack them back together again.[8] The first quasi-phasematched crystal was constructed in this way and it is still sometimes used for creating quasi-phasematched semiconductors.[49] However, since this technique is complicated and expensive it is less attractive for any practical applications in ferroelectric crystals. Another method is the realisation of a periodic polarisation structure during the crystal growth, by for example passing currents through the crystal or employing temperature fluctuations.[50,51] This is a complex procedure, prolonging the growth time, changing the optimised growth conditions and resulting in crystals, which all have the same period.

Inverted domains can also be achieved by periodically altering the surface structure of already grown crystals. Webjörn *et al*.[52] and Lim *et al*.[53] were the first to demonstrate efficient second harmonic generation employing periodically domain-inverted waveguides in $LiNbO_3$. Later QPM KTP waveguides were obtained by immersing samples, which were Ti masked on their c^- side, in a $RbNO_3$: $Ba(NO_3)_2$ molten salt bath.[54,55] Ion exchange occurs in the unmasked areas, where Rb^+ ions diffuse into the sample and replace K^+ ions. At the same time the exchange causes domain inversion on the original c^- side of the sample and shallow QPM structures are produced. This is a very versatile technique, since the structure in the material is solely determined by the mask, which easily can be produced with the required dimensions. Although the limited thickness of these diffused layers prevent this application for bulk crystals, it can be useful for waveguides, where efficient conversion can be achieved due to the tight confinement of the radiation.

Nowadays, the technique mostly employed for achieving QPM, is periodic electric field poling. This method was used to fabricate all the QPM crystals employed during this work and was originally demonstrated in CLN in 1993.[56] Although electric field poling is only possible for ferroelectric material, the further development of this technique was very important to increase the availability of phasematched crystals for a variety of different applications. The production of QPM crystals became easier and hence more widespread.

Even though much progress has been achieved, resulting in a better understanding of the processes taking place while poling, it should be noted that electric field poling is still a complex process. After all it means switching several hundred well-defined structures with a few µm length over a distance of 5 mm and a depth of 1 mm in a controlled manner from one stable configuration to another.

5.1 Preparation for Poling

The first step in the preparation of new wafers for poling is to examine their structure. This means determining, whether they are single-domain or have small substructures (micro-domains). This is done by monitoring the piezoelectric response of the wafers. An inhomogeneous wafer should be pre-poled in order to ensure that the crystal is single domain before the periodic poling, however most wafers in this work were single-domain from the beginning.

The second step is to cut the wafers into smaller pieces, which have sizes that are appropriate for the specific purpose, typically resulting in $10\ \text{mm} \times 5\ \text{mm} \times 1\ \text{mm}$ crystals. As the light will be propagating along the *x* axis after the crystal has been poled, the *x*-surfaces are polished.

After having thoroughly cleaned the sample, an approximately 2 µm thick layer of photoresist S1818 is spun on one of the polar surfaces and the crystal is baked on a hot plate. Afterwards, a periodic pattern of the photoresist is achieved by using a finger mask in a mask aligner. The parts of the photoresist lying underneath the mask's metal stripes, are protected from being exposed to the mask aligner's UV light. During the development step only those parts of the positive photoresist, which had been exposed to the UV light, are washed away by the developer, whereas the unexposed stripes remain on the crystal.

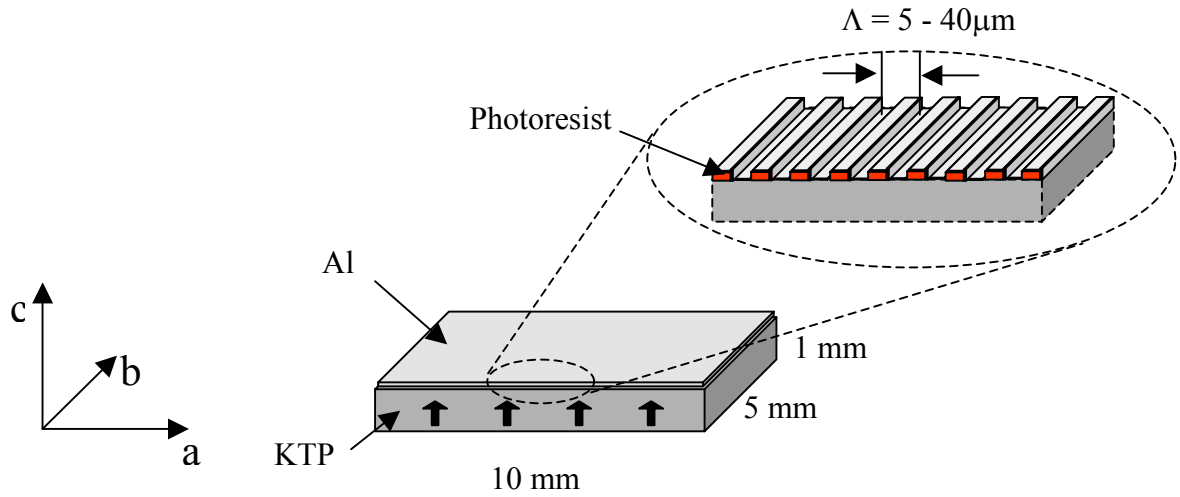

Figure 5.1. The crystal just before poling.

The final step before poling is the evaporation of a thin (50-100 nm) metal film on the patterned surface. Both Ti and Al films have been tested, but the latter was used more frequently, because its removal after the poling process is easier. The stripes of photoresist, which are underneath the metal, have an insulating function during the poling process, because no current can flow through the resist at the voltages required for poling. The structure of the sample, before it is inserted into the poling setup, is shown in Fig. 5.1.

5.2 Electric Field Poling

In order to achieve antiparallel domains, the crystal structure of the KTP sample is changed from one stable state to the other during the poling process. Stolzenberger *et al*. proposed that the domain inversion takes place by shifting the K^+ ions in the c-direction, i.e. the nine-coordinated cations become eight-coordinated and vice versa.[57] At the same time the TiO_6/PO_4 framework is forced to adjust. The short Ti-O bonds turn into long bonds and vice versa, while the PO_4 tetrahedra and the TiO_6 octahedra undergo slight rotation.[58] The reversal of the crystal orientation requires compensation by transferring a charge $Q = 2P_sA$ to the sample, where A is the area of the reversed domains.

The poling of KTP crystals is assumed to be similar to poling of $LiNbO_3$.[59] It preferentially starts by the growth of domains at the surface, which has the periodic pattern. Most likely, the inversion starts by nucleation of needle-like domains at the edge of the metal electrodes, which quickly grow along the *c* axis to the opposite side of the crystal. Afterwards the domains widen in the *a*- and *b*-directions by collapsing under the electrodes.

During the poling procedure the patterned crystal is positioned in a holder, which enables both the *c*-surfaces to be in contact with liquid electrodes. The electrolyte, which is a nearly saturated solution of KCl, is used to apply kV pulses over the crystal. The whole poling setup can be seen in Fig. 5.2 and consists of a pulse generator, an amplifier and a monitoring part. The pulse generator is set to produce square pulses having a duration of 6 ms and a fall time of additionally 1 ms. The output voltage is limited to 10 V, but since KTP and RTP demand kV pulses to reverse the polarisation, a power amplifier is needed.

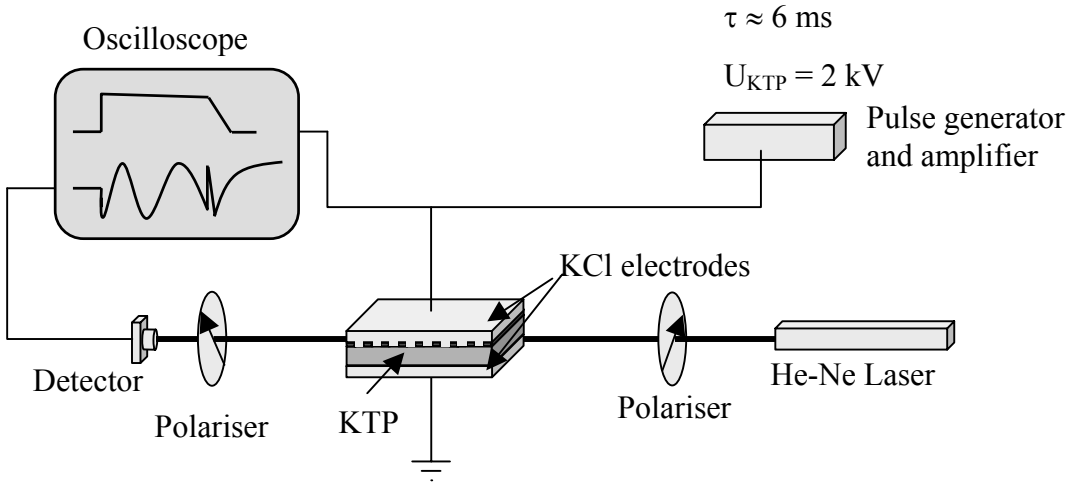

Figure 5.2. The electric field poling setup.

Most KTP crystals were typically poled at a voltage of 2 kV, whereas the RTP crystals studied here needed a slightly higher voltage to reverse their polarisation. All crystals were poled by applying several pulses at slowly increasing voltages.

As mentioned in the introduction, electric field poling was first demonstrated for CLN. For this and other low-conductive materials the poling process can be observed by detecting the flow of compensation charges. Apart from this current caused by charge movement when domains change their spontaneous polarisation, an ionic current is present as well. This contribution originates from the sample's conductivity and can be very large for high-conductive material like KTP. For RTP the ionic current is small enough to enable the measurement of the compensation current, in KTP, on the other hand, this current is almost completely concealed by the strong ionic current.

Thus, an alternative method had to be developed to monitor the poling in KTP, which was done by Karlsson *et al.*[32] A He-Ne laser beam passes through a polariser, which is set at an angle of 45° to the *z* axis, resulting in a *y*- and a *z*-component, which both have the same magnitude, see Fig. 5.2 When voltage is applied to the crystal and the beam propagates along the *x*-direction through the crystal, the electro-optic effect causes the *y*- and *z*-components to be phase shifted in relation to each other. The size of the shift can be determined by letting the beam pass through a second polariser, that is rotated 90° in relation to the first one. The photodetector situated behind the last polariser couples the signal to an oscilloscope, visualising the phase shifts.

During the rise and fall time of the voltage the electro-optic effect will cause a phase shift between the components. When the voltage is constant and lower than the coercive field, the phase shift is constant too, leading to a horizontal line on the oscilloscope. On the other hand, if the sample is starting to reverse its spontaneous polarisation, the phase shift will vary even when the voltage is constant. Thus depending on the electro-optic response the voltage is increased until poling is observed. The poling process can be considered to be finished, when the phase shift does not change during the rise and fall of the voltage.

Another method for observing the poling progress is to measure the intensity of the SH generated in the crystal when it is irradiated with a laser beam.[60] A cw Ti:sapphire laser is loosely focussed into the crystal and tuned to a wavelength, which will generate a higher order SH for the specific period of the pattern. Once the electric voltage starts to invert domains in the crystal, a weak SH spot will become visible. The more domains have become reversed and the closer the duty cycle is to 50 %, the stronger will the intensity of the SH become.

When a sample is poled, it is basically a matter of combining these different techniques to obtain a high-quality crystal, by ensuring that the process is neither stopped too early nor too late.

One problem with periodic poling is that the domains can be inhomogeneous over the depth of the crystal. If the poling process was stopped too early, the domains have not grown through the crystal to the opposite side. If the poling on the other hand proceeded too long, the domains have started merging on the patterned side whereas the structure on the opposite side might still have a duty cycle of 50%-50%. However, the high anisotropy of the KTP isomorphs seems to limit the domain wall propagation perpendicular to the *c*-axis, resulting in samples with high quality periodic domains. A recent study on the growth of domains has

been published by Canalias *et al*., showing that the domains grow ~30 times faster in the *b*-direction than in the *a*-direction.[28] This difference can be explained by the anisotropy of the crystal's structure. Since domain walls parallel with the (100) planes do not cut through the helical chains, these directions are the most favourable. The velocity along the polar axis is at least two orders of magnitude larger than in the *a*-*b* plane.

5.3 Evaluation of the Poled Crystals

It is important that the duty cycle of the periodicity for QPM crystals is 50%-50%, because the conversion efficiency of the crystal decreases due to phase mismatching, if the domains have different sizes.[20] Another essential factor that affects the quality of a QPM sample is the homogeneity of the structure along the *c* axis. Therefore, it is essential to examine the quality of the crystals' periodicity after the poling process.

The quickest and easiest technique to examine the duty cycle on the former c^+ and c^- sides is by chemical etching of the crystal. The sample is placed in a warm (80 °C) solution consisting of water, KNO_3 and KOH for approximately 20 min.[61] The hydroxide in the mixture attacks the negative c^- domains of the crystal, whereas the positive c^+ domains are left relatively untouched. Afterwards, the duty cycle of a poled crystal can be determined by inspecting the surfaces in a microscope. Although this technique is very useful for characterising the *c*-sides, it cannot be employed to visualise the domain structure on the crystal's *a*- or *b*-sides, since they remain uncharged. Another disadvantage of this method is that it is destructive for the sample's *c*-faces.

In any case, the most important test for QPM crystals is to insert them into the parametric process that they were made for. All PPKTP crystals which were fabricated during this work, were first analysed in an OPO setup. Measuring the threshold is a good indication of the poling quality.

An alternative method, which was recently developed by Wittborn *et al*.[62], is to analyse the crystal in a slightly modified atomic force microscope (AFM). This technique allowed high-resolution imaging of the domains and the domain walls on the polar c-faces. An important result was the deduction that the domain wall width in PPKTP is approximately 20-80 nm. Later Canalias *et al.* [A1] used the same approach to determine the domain structure not only on the polar surfaces, but also through the whole depth of the crystal.

An external electric field is applied to the y-face, which results in an in-plane movement due to the piezoelectric coefficient d_{24}. This movement causes the AFM's cantilever to be deflected, which can either be in phase or out of phase with the applied voltage depending on the direction of the domain's polarisation. The deflection is determined by using a lock-in amplifier and a resulting picture can be seen in Fig. 5.3. The analysed crystal had a low second harmonic conversion efficiency, which indicated that the poling was not homogeneous and that the duty cycle differed from 50%-50%.

This new method of domain imaging allows the characterisation of the domain morphology and the duty cycle. Additionally, this could give some more insight into their dependence on the poling conditions, leading to a better understanding of the domain reversal

processes. Since the evaluation of the domain structure employing this method is time consuming, it was not used for evaluation of ordinary OPA crystals.

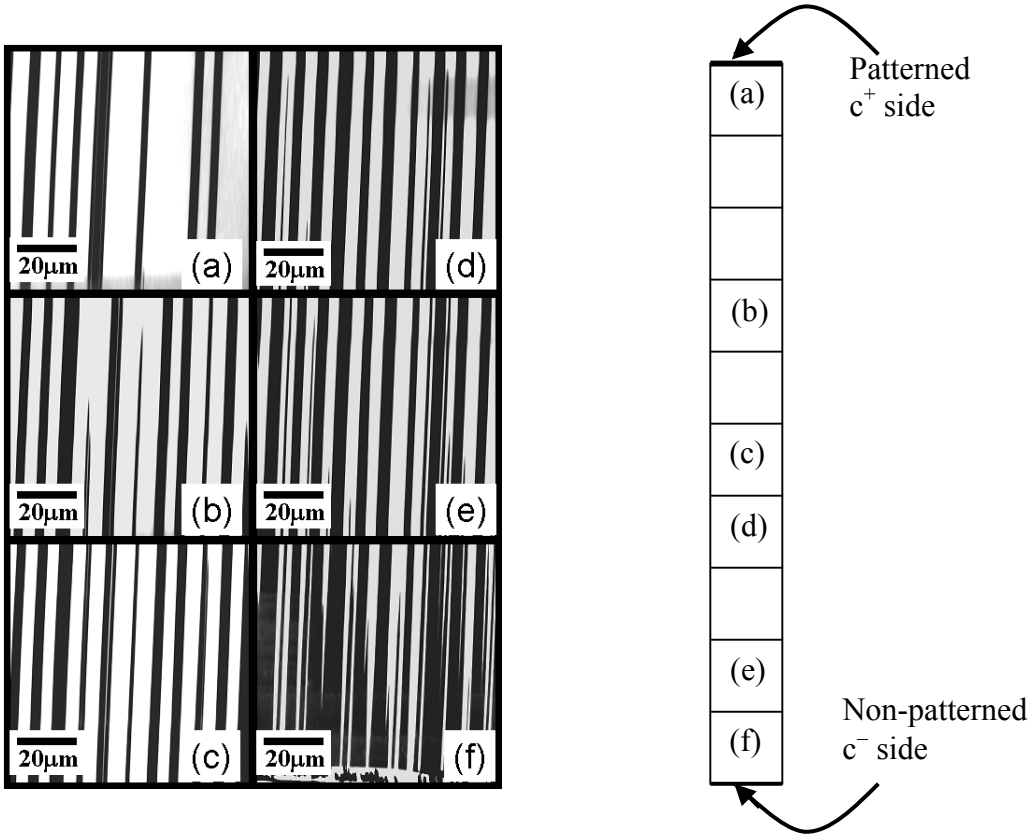

Figure 5.3. Inverse piezoresponse AFM pictures (100 μm × 100 μm) showing the growth procedure of some domains. (a) is directly below the patterned c^+ side. (b) 200 μm below (a), (c) 100 μm below (b), (d) directly below (c), (e) 100 μm below (d), (f) at the c^- side. [A1]

5.4 Nonlinearities in Domain Wall Regions

A completely different evaluation of some periodically poled crystals was done in Paper [IV]. Although the experiment also illustrated the crystals' periodic structures, it was mainly performed to give some more information on the not yet fully understood regions close to the domain walls. When irradiating the samples with both *x*- and *y*-polarised radiation along the *z* axis, intense SH light emerged from the crystals as two separate beams on each side of the transmitted fundamental beam, see Fig. 5.4. The beams were symmetrically positioned at two different external angles and were all polarised parallel to the *x* axis. The internal angles between the SH and the fundamental beam corresponded to the Čerenkov angles θ_x and θ_y, given by:

$$\cos\theta_{x,y} = \frac{n_{x,y}^{F}}{n_{x}^{SH}} \tag{5.1}$$

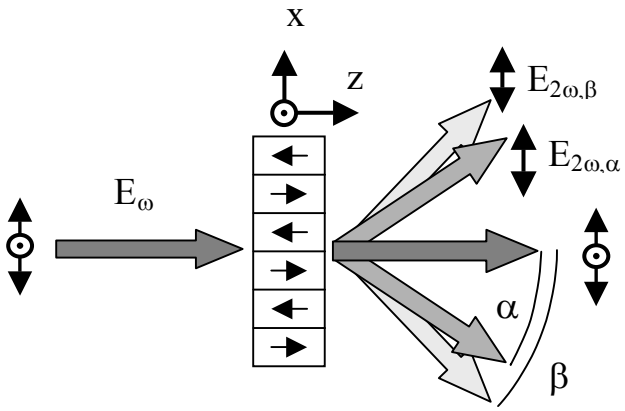

Figure 5.4. Two pairs of SH beams are generated in the Čerenkov directions. The incident fundamental beam has an *x*- and a *y*-component, whereas all SH beams are polarised parallel to the *x* axis.

Here the superscript *F* and *SH* denote the fundamental and the second harmonic, respectively, and the subscripts *x* and *y* the direction of the polarisation. Similar results were previously obtained employing waveguides.[63,64] Those experiments showed that discontinuities in the nonlinear coefficient, which can be achieved by domain-inverted channels, will enhance the generation of the second harmonic in the Čerenkov directions.

To investigate the origin of the nonlinear process a high-resolution scan along one crystal's *x* axis was performed. A beam, generated by a mode-locked Ti:sapphire, was focussed to a diameter of 1 μm, which was considerably smaller than the period of the domains. This measurement clearly showed that SH was only generated at the domain walls and in the regions adjacent to them and not in the centre of a domain, see Fig. 5.5.

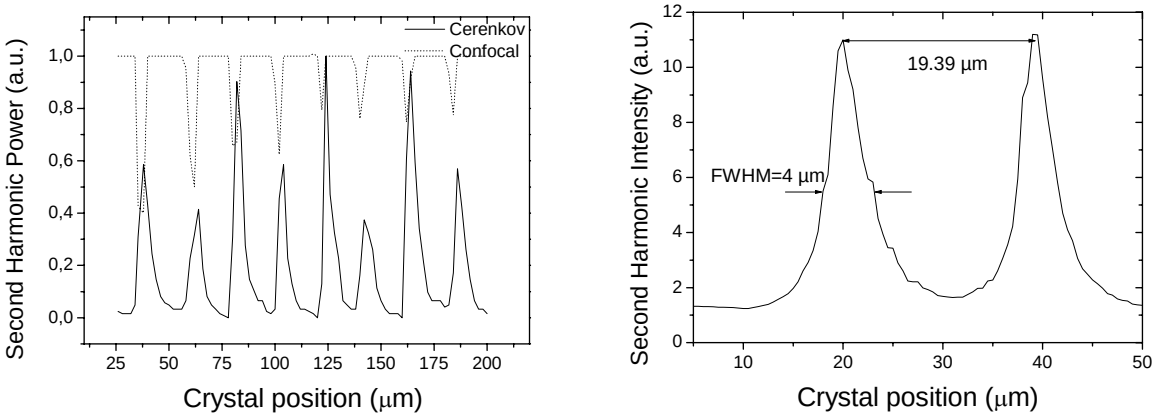

(a) (b)

Figure 5.5. (a) The power of the second harmonic in the collinear and the Čerenkov directions as a function of the position in the crystal. (b) A high resolution scan of the second harmonic across two domain walls.

The conversion from an *x*- or a *y*-polarised fundamental beam to an *x*-polarised SH can only be attributed to the nonlinear coefficients d_{11} and d_{12}, respectively. These coefficients are equal to zero in KTP, but close to domain walls they are apparently nonzero, giving rise to the SHG. The appearance of these nonlinearities is attributed to strains at the domain walls, which are caused by the atomic reorientation occurring during the poling process. These strains lead to dc piezoelectric fields $E_{dc,x}$, which by third order nonlinear processes result in dc-induced second harmonic generation according to

$$P_x(\omega_{SH}) \propto \chi^{(3)}_{xxxx}(-\omega_{SH};0,\omega_F,\omega_F)E_{dc,x}(0)E_x(\omega_F)E_x(\omega_F) \tag{5.2}$$

and

$$P_x(\omega_{SH}) \propto \chi^{(3)}_{xxyy}(-\omega_{SH};0,\omega_F,\omega_F)E_{dc,x}(0)E_y(\omega_F)E_y(\omega_F) \tag{5.3}$$

Formally this interaction could also be regarded as a second order nonlinear process, if the following substitution is made: $d_{11} = 3/2\chi^{(3)}_{xxxx}E_{dc,x}$ and $d_{12} = 3/2\chi^{(3)}_{xxyy}E_{dc,x}$. Approximate values for these coefficients were derived to be $d_{11} \approx 0.45$ pm/V and $d_{12} \approx 0.56$ pm/V. It could further be deduced that the direction of these nonlinearities are opposite to each other on either side of the domain wall.

Chapter 6

Optical Parametric Amplification

Already in 1962, very quickly after the demonstration of the first laser, the possibility of parametric amplification of light waves was suggested for the first time [8,65,66]. The basic idea of parametric amplification, however, actually existed before the laser was invented. Already in the late 50s microwave parametric amplifiers were demonstrated, but not even then the principle of employing a nonlinear material to amplify a weak field at a certain frequency with a strong field at a different frequency was new, since this technique previously had been demonstrated in electrical circuits.[67,68]

The first experimental observation of optical parametric amplification was made three years after the original suggestion. Wang and Racette[69] employed KDP to amplify a HeNe laser. Due to the low pump power and the small nonlinearity of the gain material the amplification did not reach more than 4.5 dB although the crystal was 8 cm long. Since this pioneering experiment the principle of optical parametric amplification has developed into an important and valuable technique, although the progress was initially slowed down by the limited availability of suitable nonlinear material and suitable pump lasers. However, during the last two decades the discovery of new gain material with larger nonlinearities combined with the development of the quasi-phasematching technique have assisted the spreading of OPAs into new fields.

Nowadays, OPAs are commonly employed to amplify both narrowband and broadband radiation in an enormous wavelength region spanning from the UV to the far-IR. Amplification of pulses with durations ranging from several nanoseconds to a few femtoseconds can be achieved, reaching TW power levels for femtosecond OPAs.

6.1 Amplification of Lasers

The main task of an amplifier is obviously to increase the energy of the weak seed beam. It is, however, also important that this process does not change any other properties of the incident wave. Thus, after having passed through an ideal amplifier, all the spatial and spectral features of the output should be identical to those of the input. Another advantageous feature would be

if the amplification process does not have to rely on good spectral and spatial properties of the powerful pump source, since this would allow the use of simple and inexpensive pump lasers.

One candidate that can fulfil these criterions is the optical parametric amplifier. However, although parametric amplification was one of the first techniques suggested and demonstrated to amplify lasers, it is not the only method. The most intuitive technique to construct an amplifier for a laser would be to employ the very same material that generates the radiation to also amplify this radiation in a second stage. Two important but completely different methods exist, namely the regenerative and the multipass amplifier. In both systems the amplifying medium is a laser crystal and the beam to be amplified has to pass through this crystal several times, since the single pass gain generally is less than 10 dB.[70] In the multipass architecture high gain is accomplished by up to ten consecutive passes through the same tightly focussed spot in the gain material, which leads to stability problems and a complex design. The regenerative setup employs the build-up of a pulse inside a cavity, which results in those problems involved with constructing and maintaining a laser cavity. When the pulse energy has grown to a considerable high value, the pulse is dumped from the cavity. The outcoupling is accomplished by switching an electro-optic Pockels cell, which demands very precise timing and therefore complicates the setup.

A commonly used material in lasers and in laser amplifiers is Ti:sapphire.[71] The Ti:sapphire laser is one of the most important lasers, since this material has a very broad gain bandwidth, which makes it suitable both as a tuneable laser and for short pulse generation.[72] Laser materials have however two potential drawbacks, which have to be taken care of, when they are used in high power amplifiers. The first problem is the generation of noise due to amplified spontaneous emission (ASE) and the second is the heating effects during operation due to the quantum defect. This temperature increase can have serious consequences, since thermal stress can create cracks in the crystal. Cooling the laser crystal is therefore crucial, but the maximum achievable energies and repetition rates are still limited by the heat dissipation.

One way of facilitating the cooling of the gain material is to employ fibre amplifiers. Another advantage of fibres is that even a material with a small gain can accomplish large amplification if the interaction length is long. Rare-earth doped fibre amplifiers were demonstrated for the first time in 1964[73] and especially the Erbium-doped fibre amplifier (EDFA) has attracted much attention because it operates near 1.55 µm where fibre losses are minimised. By employing different rare-earth ions as dopants, fibre amplifiers that operate in different wavelength regions can be constructed. One example is the Yb doped fibre amplifier operating in the region from ~975 to ~1200 nm, which can achieve more powerful pulses than EDFAs, since this material has a smaller quantum defect. Fibre amplifiers are mainly used for applications where peak powers are kept low, e.g. for cw applications, since large peak powers lead to the occurrence of nonlinearities, which can change the beam's spectral and temporal properties.

Basically, a variety of different techniques exist to amplify a weak laser beam with a powerful pump and all methods have advantages and limitations. The different fields of applications are primarily determined by the wavelength and the pulse duration of the signal that should be amplified and the desired output intensity. However, in general optical parametric amplifiers are very attractive devices, since they can operate in very wide spectral regions and at the same time provide large single pass gains.

6.2 Basic Principles of Optical Parametric Amplification

As mentioned in the introduction to OPAs in Chapter 2, an OPA consists of three basic elements: a powerful pump laser, a seed source and a nonlinear gain material. When the nonlinear crystal is placed in the pump beam and is simultaneously seeded by a weak beam at a different wavelength, it will exhibit optical gain at the idler wavelength through the generated nonlinear polarisation at this wavelength. At the same time the idler wave will couple with the pump wave to generate polarisation at the signal wavelength, which will amplify the seed. This coupling between the waves will lead to the simultaneous amplification of both signal and idler and can result in single pass gains of up to 55 dB [III]. In general, the generation of the idler beam can be regarded as the introduction of a loss, however in some applications a second intense beam at a different wavelength can be useful.

One important feature of OPAs is their ability to maintain the phase of the seed throughout the amplification stage. The optical parametric amplification process takes place when a constant phase, φ, is maintained between the interacting waves:

$$\varphi = \varphi_p - \varphi_s - \varphi_i = const \tag{6.1}$$

Here φ_p, φ_s and φ_i are the phases of the pump, signal and idler pulse. Since the phases of the pump and the seed are given by the incident waves, the phase of the idler will adjust itself to fulfil the phase condition for amplification. This also means that any random phase shifts between the pump and the seed pulses will be eliminated by the generation of an idler that compensates this difference to yield the constant phase.[74] Moreover, if the phase of the seed is modulated, so will the amplified signal's phase be.

Since the OPA process will amplify the seed coherently, all the seed's properties will remain unchanged in the amplified signal. Apart from the phase also the wavelength and the spatial beam quality will be preserved. Thus, even if the pump beam has a large M^2 value, the signal can still retain the intensity and spatial phase distribution as long as the pump is not depleted, since the spatial properties of the pump will be converted to the idler instead. The spatial characteristics of the signal beam can be very important for certain applications, especially when the beam is supposed to propagate over long distances, as e.g. in LIDAR (light detection and ranging) measurements.

Contrary to a laser amplifier, OPA is an instantaneous process and no energy can be stored in the nonlinear crystal. Since energy conversion can only occur between temporally and spatially overlapping pulses, the duration of the signal is determined by the shortest of the interacting pulses. Further, tough requirements would be placed on the synchronisation, if both the pump and the seed source emitted very short pulses. Since any timing jitter between the pump and the seed pulses would lead to an unsatisfactory amplification, it is common to employ schemes, where one of the pulses is longer than the other. By, for example, pumping an OPA with a powerful femtosecond pulse and seeding with a nanosecond pulse at a different wavelength, the critical synchronisation is removed, permitting the generation of a powerful femtosecond signal.[75] Another strategy to simplify the synchronisation is employed in OPCPAs. Here the femtosecond seed pulse is temporally stretched to a picosecond pulse, before it interacts with the pump pulse, which has typical durations of more than ~100 ps.

6.3 Optical Parametric Amplification with Periodically Poled $KTiOPO_4$

The main reason for employing PPKTP as the nonlinear crystal in OPAs is that these samples combine several features, which are valuable for parametric processes. The large nonlinearity and damage threshold of KTP, combined with the ability to achieve noncritical phasematching in a wide spectral region using the QPM technique, result in a very useful gain material.

The first OPAs that were constructed used KDP and ADP as the nonlinear crystals. These materials were well known, since they had previously been employed in piezoelectric applications. One important drawback of KDP and ADP was, however, their small nonlinear coefficients, which demanded high pump intensities to achieve efficient power conversion from the pump to the seed. Hence, these OPAs had to be pumped with mode-locked picosecond lasers, which complicated the setups.

The first OPAs based on KTP were also birefringence phasematched. Since they employed the comparably small nonlinear coefficients d_{24} and d_{32}, they had to be pumped with mode-locked lasers, too. Pumping at 532 nm with picosecond pulses at intensities of up to 10 GW/cm^2 was reported without damaging the KTP crystals[27], which illuminates the large damage threshold of KTP. In these early experiments also large tuneability was demonstrated in a variety of wavelength regions by angle rotation of the crystals.[76,77,78] However, the generated energies were strongly dependent on the wavelength, because the nonlinear coefficient is a function of the phase-matching angle for BPM. Further walk-off effects had to be taken care of by using several, comparably short crystals.

When QPM crystals, due to the development of electric field poling, became available, the largest noncollinear coefficient of KTP, d_{33}, could be employed. This reduced the pump intensity that was necessary for achieving large gains in OPAs. Even pumping with less complex sources in the nanosecond regime resulted in considerable amplification of a weak seed beam. In Paper [III] we demonstrated small signal gains of up to 75 dB employing one PPKTP crystal by pumping with a commercially available, nanosecond Nd:YAG laser. Pulse energies of more than 1 mJ were generated at 1535 nm, but due to the QPM technique basically any wavelength within the material's transparency range can easily be amplified.

By employing QPM crystals in OPAs, the whole system becomes more flexible, since both the seed and pump wavelength can be chosen freely. Further, walk-off effects are avoided, because noncritical phasematching can be achieved for any process by choosing the proper QPM period. Thus, longer crystals can be employed in OPAs, which results in considerable gain even for smaller pumping intensities. Since the damage threshold is reduced to a typical value of 900 MW/cm^2 for nanosecond pulses in the IR region, the reduction of the necessary pump intensities is very helpful. Even though the damage threshold is considerably smaller for nanosecond than for picosecond pulses, it is still larger than for many other materials, e.g. CLN.

The remaining disadvantage with OPAs based on PPKTP is the limited aperture of periodically poled samples. Since thin crystals restrict the peak powers of the pump pulses, these periodically poled samples are mainly employed in intermediate power regimes. Even though this leads to a certain limitation, preventing PPKTP to be used for extremely high power applications aiming for TW output powers, PPKTP is an ideal candidate for compact and tuneable amplifier systems.

6.4 Description of a Typical Optical Parametric Amplification Setup

All the experiments performed in this work, employed PPKTP crystals as the gain medium. The samples were prepared according to the electric field poling technique described in Chapter 5 and had QPM periods that were most suitable for the specific frequency conversion. For OPAs pumped with 1064 nm the crystal periods were ~ 35 μm, whereas pumping at 532 nm required shorter periods of ~ 9 μm. This possibility of choosing the QPM period of a crystal depending on the wavelength of the pump laser partially illustrates the large flexibility of employing QPM crystals in OPAs. Since the refractive index of KTP is ~1.8, each surface of the crystal results in power losses of ~ 8 % due to reflections. AR coatings can be applied to the sample to prevent the attenuation of the beams. However, most of the crystals were left uncoated, since previous experiments have shown that the coatings are damaged at pump intensities considerably lower than the damage threshold of the crystal itself.

Apart from the Nd:YVO_4 seeded Nd:YAG regenerative amplifier employed in Paper [VI], all OPA experiments were pumped by the same actively Q-switched Nd:YAG laser. When the laser was run at 1064 nm, 20 mJ pulses with durations of approximately 5 ns were emitted at a maximum repetition rate of 20 Hz. Further, the bandwidth of the laser was $\Delta\nu \approx 40$ GHz and the generated beam was non-diffraction limited with a quality factor of $M^2 = 7$. If the frequency doubling crystal was inserted in the laser, 7 mJ pulses at 532 nm were generated instead.

While the pump source and the gain medium for all the experiments were very similar - if not the same - the seed sources varied tremendously: a spectrally broadened OPO signal [I], a gain-switched laser diode [II], an Er-Yb:glass laser[79] [III] and an Er-fiber laser [VI] were employed during this work. All these sources were emitting pulses, which obviously varied in energy, duration and wavelength and each of these seeds had to be amplified efficiently, which can be achieved by employing QPM KTP.

The wide spread of the seed's pulse durations – from nanoseconds over picoseconds to femtoseconds – illustrates the wide exploitability of OPAs. Although the spectral range of the seed sources (975 nm and 1500-1700 nm) is not as large as the temporal spread, it can nevertheless highlight the large adjustability of OPAs. Basically, almost any source can be amplified using OPAs.

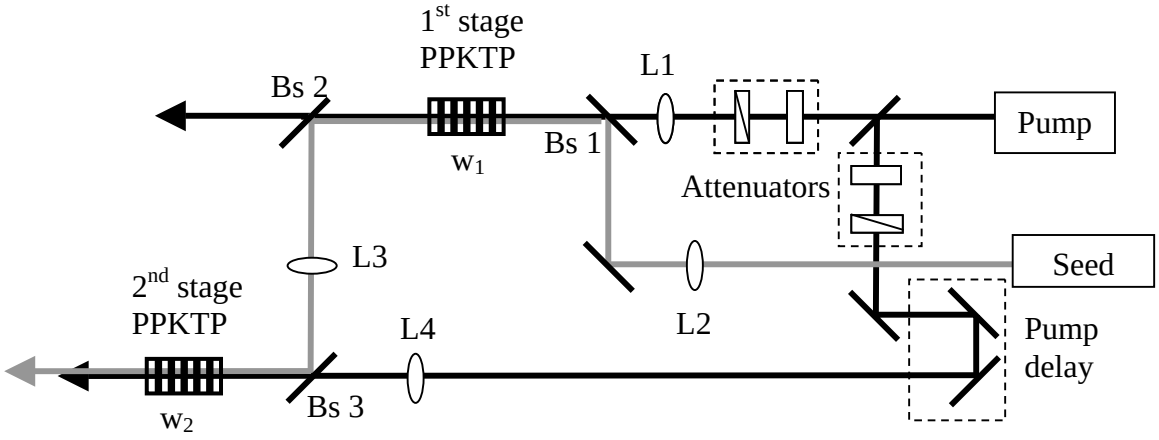

Figure 6.1. A typical two-stage OPA setup, where $w_1 < w_2$; Bs: Beamsplitter, L:Lens

Three of the four constructed OPA arrangements consisted of two amplifying stages to maximise the power converted from the pump laser to the signal beam. This technique was especially employed to achieve large amplification of comparably weak seed sources. By splitting the amplifier into two stages, each stage can focus on a separate task to optimise the overall performance. In general, the first stage performs as a pre-amplifier with a large gain and the second stage is operating as a power converter at a lower gain.

Fig. 6.1 shows a schematic design of a double stage OPA. It has most resemblance with the setups used in Paper [II] and [III], but it has also several basic concepts in common with the other two OPA designs. In the employed double stage setups the pump beam is first split into two separate beams by a partially reflecting mirror. This arrangement allows each stage to be pumped by an individual beam, instead of using the remainder of the first stage to pump the second stage. In each path an adjustable attenuator consisting of one half-wave plate and one polariser enables the independent regulation of the pulse energy. The spatial overlap between the seed and the pump beam in the first gain material is achieved by using beamsplitter Bs 1, which is a dichroic mirror being AR coated for the pump wavelength and highly reflective at the seed wavelength. The radius of the beams, w_1, inside the crystal can be regulated by the position and strength of lenses L1 and L2. The temporal synchronisation of the seed and pump pulses is achieved with a delay generator, which e.g. triggers the Q-switches of the lasers.

Each PPKTP crystal is placed on a temperature-controlled cube made of copper, which itself is situated on the top of a tower consisting of several translation and rotation stages. This arrangement permits the fine-tuning of the crystal's position and temperature. After the first amplification stage beamsplitter Bs 2 separates the signal from the pump. Also the idler is coupled out at this point. This helps to avoid back-conversion in the second stage, which can lead to deterioration of the signal's beam quality.[80] Lens L3 focuses the signal to a radius w_2 inside the second PPKTP crystal, where it will perform as the seed. The pump for the second stage was previously rerouted through a delay line after Bs 1 and is now focused with L4 into the PPKTP sample, where it coincides with the seed with the help of Bs 3.

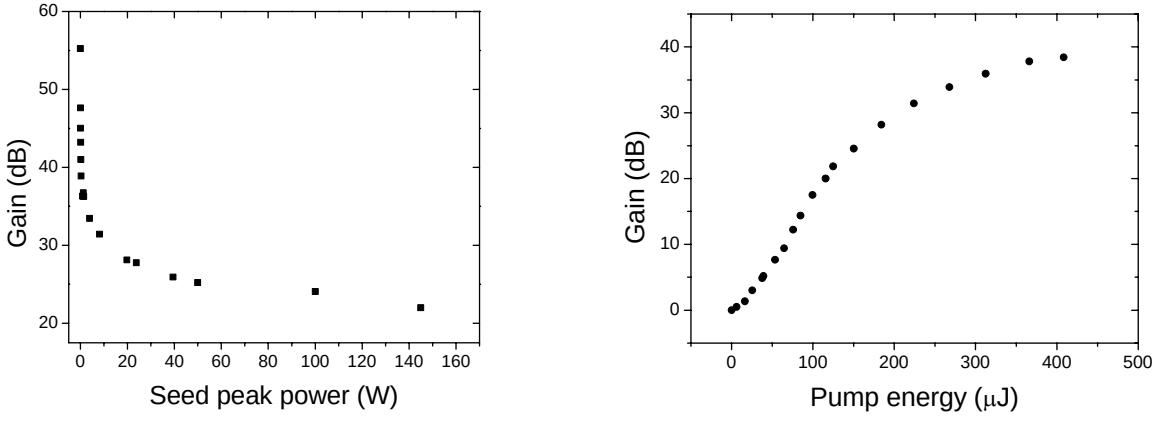

Figure 6.2. The large gains achievable in the first amplification stage: (a) The graph is taken from Paper [III] and shows the signal gain as a function of the seed peak power at a constant pump energy. (b) This diagram describes the signal gain as a function of the pump energy at a constant seed energy and is a result from Paper [II].

If the seed energy is very small, i.e. has a typical energy of a few pJ, and therefore is many orders of magnitude weaker that the pump, the seed beam has to be focused to a relatively tight spot. This leads to an increase in intensity and helps to discriminate against spontaneous fluorescence generated in this amplification stage. Quantum noise, which is equivalent to half a photon per mode, has an approximate intensity of 1 μW/(cm^2).[81]

It is further important to avoid that the pump beam is considerably larger than the seed, since parametric superfluorescence could easily be generated in these regions. On the other hand employing a small pump beam also means restricting the pump power and thereby limiting the maximum achievable signal power. Two graphs are shown in Fig 6.2 illustrating the large gains, which we have achieved in the first stages in Paper [II] and [III].

The main power conversion from the pump to the signal is instead obtained in the second stage, which is generally operating at a comparably low gain of ~ 10 - 20 dB, see Fig. 6.3. (a). Usually this stage is driven close to saturation, which will lead to high pulse stability, since the amplified energy is less sensitive to seed fluctuations in this regime. In this OPA the seed energy is generally only a few orders of magnitude smaller than the pump energy, so that the signal power will be boosted by efficiently extracting energy from the pump.

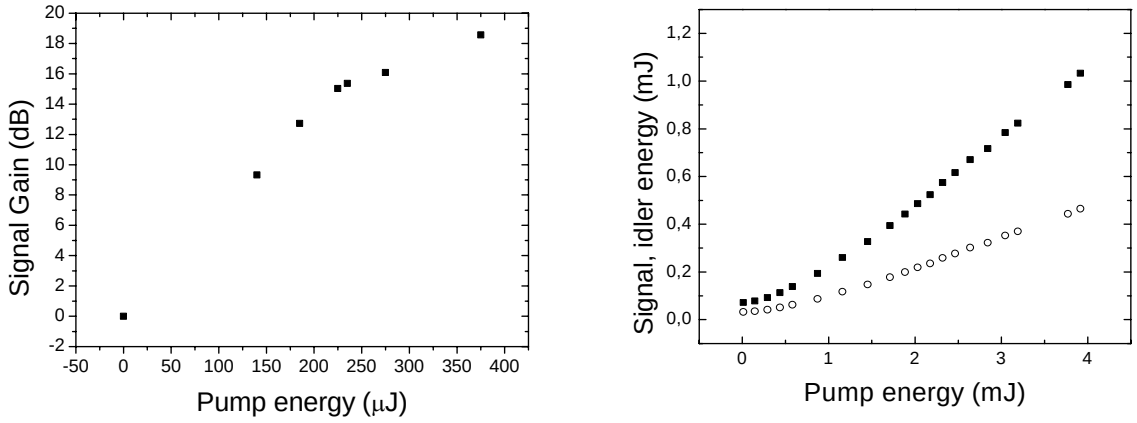

(a) (b)

Figure 6.3. Illustration of the second stage, which typically operates at a comparably low gain and results in large conversion efficiencies. In (a) the signal gain is plotted as a function of the pump energy and is a result from Paper [II]. (b) The graph is taken from Paper [III] and shows the signal and idler energies versus the pump energy.

After this second amplification stage the signal energies have usually grown to values that are comparable to the pump energies. This leads to large conversion efficiencies, which can be seen in Fig. 6.3 (b), where we achieved values as high as 37 %. Of course it is always possible to add further amplification stages to reach even higher energies. This, however, increases the size and complexity of the setup, and was not done in our experiments, since the prospect of adding only a few dB to the signal energy was a too weak motive.

6.5 Optical Parametric Generation - a Competing Process

The general goal of an OPA is to increase the energy of the seed, but at the same time leave the other seed properties, like spectral and spatial beam characteristics, unchanged. At relatively moderate pump intensities this is not a problem. However, the situation changes significantly when the threshold for OPG is reached. As mentioned in Chapter 2 OPG starts from quantum fluctuations, which can also be denoted as noise. When these fluctuations interact with the pump field, a nonlinear polarisation is produced that attempts to generate radiation at all frequencies and in all directions. Of course this process does not occur completely at random, since energy conservation needs to be fulfilled. Apart from this constraint the growth of radiation is favoured at wavelengths and in directions, which approximately satisfy the phasematching condition. If the pump intensity is sufficiently high and the interaction length is long enough, the noise will be amplified to a level that is detectable. The bandwidth of an OPG signal is basically only limited by the crystal's bandwidth, which will be discussed in Chapter 7. Further, the spatial beam quality of the generated signal and idler beams are generally very poor.[82] Adding a spatial filter after the OPG can ensure reasonable beam qualities, but leads instead to substantial losses. One way to take advantage of this spontaneous process is to construct an OPG-OPA tandem.[77] Here the spatially filtered and therefore attenuated OPG signal reaches the OPA stage as the seed and can experience considerable gain.

Due to the OPG's poor characteristics, operating an OPA above the OPG threshold can result in a degradation of the amplified signal. However, in Paper [II] and [III] we could observe that the threshold for OPG is increased when a seed is present. This leads to a suppression of superfluorescence, which will be more closely discussed in section 6.7. Obviously, this suppression can only occur when the pump and seed overlap. Therefore OPG is a larger problem when the pump has a significantly longer pulse duration than the seed, since superfluorescence can be generated during those pump intervals when no seed pulse is available. Further, superfluorescence can easily be generated in certain regions within the crystal where the pump but no seed is present. Hence, the spatial overlap between the seed and the pump has to be optimised to avoid considerably larger radii for the pump than for the seed.

6.6 Nanosecond Optical Parametric Amplification

The first double stage OPA based on PPKTP was demonstrated in Paper [III], where the main motivation for constructing this setup was to investigate the possibility of scaling PPKTP OPAs to the millijoule level. Here, the challenge was to design a high gain configuration, which could generate a diffraction limited signal beam that was neither spectrally nor spatially broadened by parametric superfluorescence. The strategy of employing two consecutive stages where each one operates in a different amplification mode was presented in subchapter 6.4. In this section a short overview of the experiment is presented, summarising the most important results.

The experiment was operating in the IR region ~ 1550 nm, which is called "eye-safe", because the human eye is less sensitive to these wavelengths than other IR regions. If such a

laser beam is incident on an eye, these wavelengths will mainly be absorbed in the front part of the eye, so that little or no damage is done to the very sensible and irreparable retina. Powerful nanosecond pulses in the infrared are desirable for many different applications, such as LIDAR, medicine, spectroscopy and range finding. Due to the high absorption of tissue at 1550 nm this wavelength could also be useful for surgery.

A home built, actively Q-switched Er-Yb:glass laser[79] was used to seed the OPA. It generated 6 μJ pulses at 1535 nm having a duration of 36 ns in a nearly diffraction limited beam (M^2 = 1.1). The Er-Yb:glass laser could be run at repetition rates of up to several kHz without changing its properties significantly. However, during this experiment the seed was synchronized with the Nd:YAG pump laser, which had a limited repetition rate of 20 Hz.

Both the seed and the pump beams were focused into a periodically poled KTP sample, which had a period of 35.4 μm. The pump power was set to a value where no superfluorescence was generated in the crystal, but at the same time an amplification of 55 dB to 22 dB could be achieved depending on the seed energy. After the crystal the signal was separated from the pump and idler and used to seed the second stage, which was pumped by the larger part of the Nd:YAG beam that had been redirected before the first stage. Before this second pass through the same PPKTP sample, but in the opposite direction, the beam radii were increased to allow stronger pumping. The second stage added between 10 and 20 dB to the total gain, reaching maximum total values of 75 dB. Pumping this stage with 4 mJ pulses, the conversion efficiency from the pump to the signal and idler achieved 37 % and the overall conversion efficiency for both stages was close to 30 %.

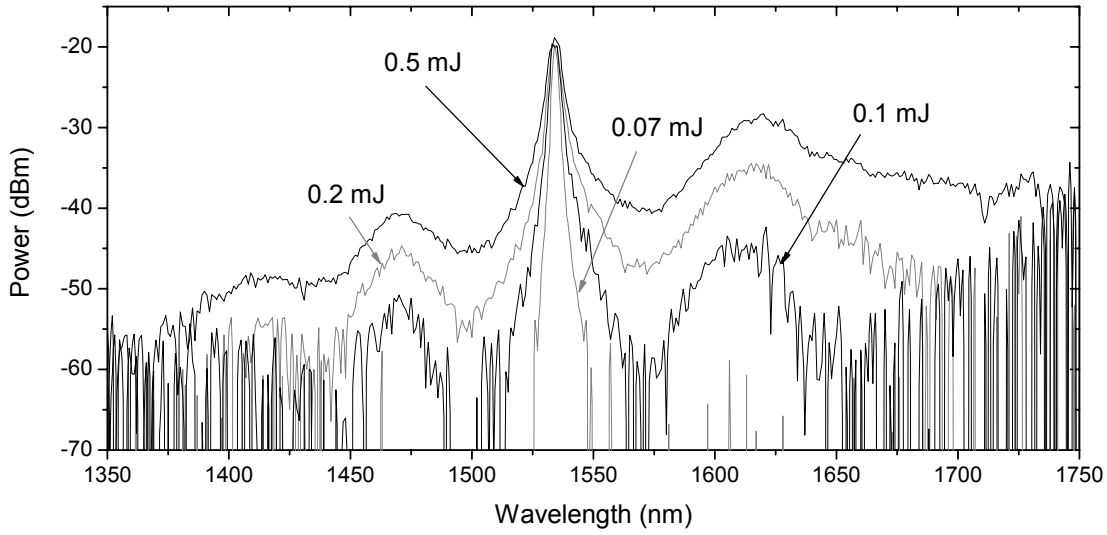

Figure 6.4. The signal's spectrum after propagation through a 5 m long single-mode, dispersion-flattened fibre for different signal energies.

All in all, this setup generated an almost diffraction limited beam, consisting of pulses with durations of 5 ns having energies of 1 mJ, see Fig. 6.3 (b). Comparison of the seed's and the amplified signal's spectrum confirmed that no spectral broadening due to superfluorescence occurred.

Although it is for most applications beneficial to use beams with narrow bandwidths, some situations exist, where broadband operation is needed instead. This was the motivation to examine the possibility of easily broadening the signal's narrow spectrum. One method is to employ the nonlinearities of a fibre. Therefore, the signal from the double pass OPA was coupled into various fibres and the spectra obtained after a 5 m long single-mode, dispersion-flattened fibre can be seen in Fig. 6.4. Mainly three different third order nonlinear processes were assumed to be responsible for the broadening: self-phase modulation, stimulated Raman scattering and four-wave mixing. If even broader spectra are required, photonic crystal fibres could be employed.

6.7 Picosecond Optical Parametric Amplification

Inspired by the construction of the reliable and well-performing nanosecond optical parametric amplifier, another goal was to design and build a compact device emitting powerful picosecond pulses, which also are needed for certain applications, as for example in nonlinear microscopy. The most commonly used technique to generate pulses with picosecond durations is to employ mode-locked solid-state lasers. These devices can readily generate pulse energies in the sub-nJ regime, however, in order to increase the output energy to microjoule levels, the setup has to be modified significantly by increasing the cavity length[83] or by adding a cavity dumping arrangement[84]. An alternative approach is to gain-switch a laser diode, which can produce pulses with picosecond to nanosecond durations depending on the diode structure and the electrical feeding characteristics. Since the pulse energy is comparably small (~ pJ) considerable, subsequent amplification is needed. Compared to the previously demonstrated techniques to increase the energy of gain-switched diodes, e.g. regenerative[85] and fibre[86] amplifiers, OPAs offer several advantages. Mainly the setup is simplified significantly, since large gains can be achieved in single pass configurations and no additional components are needed for in- and outcoupling of the seed and signal beams or to prevent the build-up of noise.

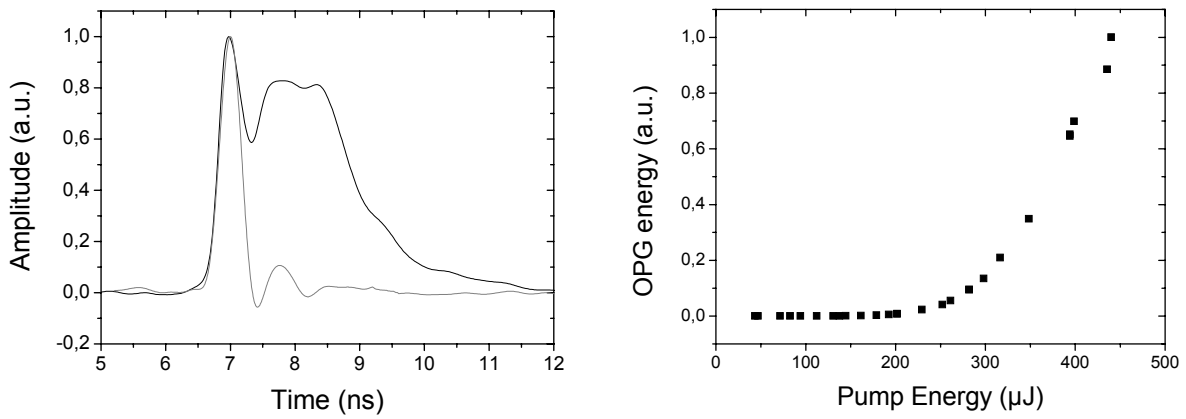

(a) (b)

Figure 6.5. (a) The oscilloscope traces of the picosecond and nanosecond seed pulses. (b) The amplitude of the unseeded OPG as a function of pump energy.

A setup was constructed, where an OPA was seeded by a long gain-channel laser diode emitting linearly polarised radiation at 972 nm and pumped by a frequency doubled Nd:YAG laser that emitted 5 ns long pulses. In order to amplify the pulses to the microjoule level without adding any superfluorescence, a double stage setup consisting of two PPKTP crystals was built.

By feeding the laser diode with adjustable electric pulses generated by a high-speed current switch, we could tune the pulse length of the emitted radiation from 20 ps to 2 ns. The temporal traces of these two extreme pulse lengths can be seen in Fig. 6.5 (a), where the duration of the short pulse was increased by the limited bandwidth of the detector and oscilloscope.

The first stage of the OPA could be operated at high gain, reaching approximately 40 dB for both the short and the long seed pulse, see Fig. 6.2 (b). Comparison of the amplification behaviour for the picosecond and the nanosecond pulses showed, however, significant differences in the onset of parasitic superfluorescence. When no seed was incident on the PPKTP crystal, the pump power was still efficiently converted to the signal and idler wavelength by the OPG process, which can be seen in Fig. 6.5 (b). To get a feeling for the substantial power conversion of this process, the ratio between the amplitude of the unseeded OPG and the amplitude of the seeded OPA is plotted versus the pump energy in Fig 6.6 (a). In the presence of the nanosecond seed, the optical parametric amplification process, however, suppressed the generation of concurrent superfluorescence. This effect is illustrated in Fig. 6.6 (b) where a comparison of the spectra for the unseeded OPG and the seeded OPA is shown.

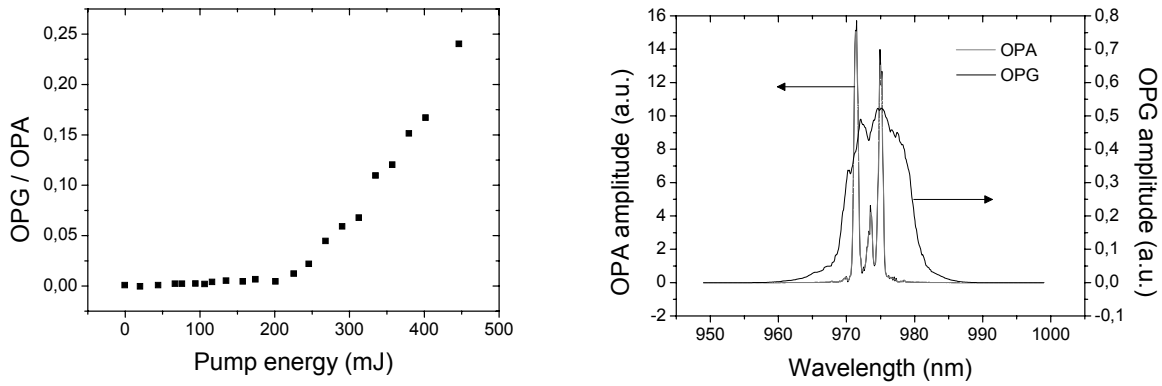

(a) (b)

Figure 6.6. (a) The ratio between the amplitudes of the unseeded OPG and the seeded OPA (b) Suppression of the superfluorescence while seeding the OPA. The grey curve is the spectrum of the seeded OPA, whereas the black curve shows the spectrum of the unseeded OPG.

The situation was slightly different for the picosecond seeded OPA. One problem occurring when the pump is significantly longer than the seed is that superfluorescence is not suppressed, but instead easily generated in the pump intervals where no seed is present. Hence, the pump energy for the first stage was limited to a lower value for the picosecond seed than for the nanosecond seed.

Since the beam radii were increased in the second stage, this OPA could be pumped harder, and resulted in an additional gain of 15 dB for the picosecond seeded OPA and 12 dB for the nanosecond seeded OPA. Hence, a total gain of ~50 dB was achieved, which allowed the amplification of both pulses to the microjoule level. At the same time, pulses with only slightly less energy were emitted at the idler wavelength 1175 nm.

Probably even larger amplification and energies can be achieved for the picosecond seeded OPA by employing a different pump laser. If the duration of the pump pulses is comparable to the seed pulses, stronger pumping and a subsequently larger gain would be possible without risking spectral or spatial distortion of the signal by the generation of superfluorescence.

The pulse length of the picosecond signal was determined by a noncollinear autocorrelation measurement. A PPKTP crystal generating the SH was pumped with the OPA signal and the pulse duration was derived to be approximately 20 ps, see Fig. 6.7.

To conclude, diode seeded OPAs could potentially be an alternative to mode-locked lasers in the picosecond regime. Since the pulse duration and the repetition rate of the diode are easily controlled by the applied current, synchronisation to other equipment is simplified. OPAs can further achieve considerable amplification and are very stable arrangements. Once the OPA setup was optimised, it operated for several weeks without requiring any realignment.

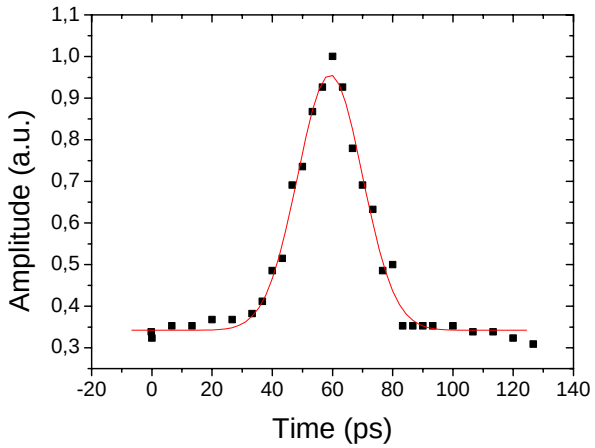

Figure 6.7. The autocorrelation trace of the amplified picosecond signal with a fitted Gaussian approximation.

Chapter 7

Broadband Optical Parametric Amplification

When a weak laser beam is amplified it is essential to maintain its spectral shape throughout the amplification stage and neither broaden nor narrow down the bandwidth. Apart from parasitic effects, like superfluorescence, the bandwidth of a signal that has been amplified by an OPA depends on mainly two factors: the bandwidth of the seed and the bandwidth of the gain medium. If the spectral width of the seed is considerably smaller than the gain bandwidth of the nonlinear crystal, the spectrum will basically remain unchanged by the amplification stage. This was the case for most of the OPAs constructed in this work. However, in the case of the other extreme – a spectrally very broad seed amplified by a crystal with a narrow gain bandwidth – the signal's spectrum will be distorted and narrowed down to the crystal's bandwidth. This is a major problem when amplifying pulses with durations of less than 1 ps. A gaussian, transform limited 100 fs pulse has, for example, a bandwidth of more than 4 THz. An amplification stage with a smaller gain bandwidth would lead to spectral narrowing and subsequently an increase of the amplified signal's pulse duration, which has to be avoided.

7.1 Broadband Techniques

One way of achieving large bandwidths in nonlinear crystals is to use short samples. Since a non-zero Δk cannot grow to a large phase mismatch, $\Delta k \cdot L$, if only L is small enough, the amplification bandwidth increases for short crystals and vice versa. However, employing short crystals obviously limits the conversion efficiency of the OPA and stands in clear contrast to the main motive of phasematched interactions.

Some significantly more constructive techniques, which manage to maintain a seed's large bandwidth but still achieve considerable gain, exist as well. One method is to employ crystals, which, instead of being periodically poled, have inverted domains with increasing lengths, see Fig. 7.1. (a). These so called "chirped" or "aperiodic" crystals amplify different wavelengths in different regions of the gain material. This technique was originally suggested for compressing pulses while generating the SH[87]. It was later also employed in OPOs to give

few-cycle femtosecond pulses[88] and has been suggested for OPAs as well[89]. One disadvantage is that the crystals have to be longer to allow considerable amplification of all wavelengths. Additionally any irregularities in the domain-inversion quality will lead to a spectral modulation of the amplified signal.

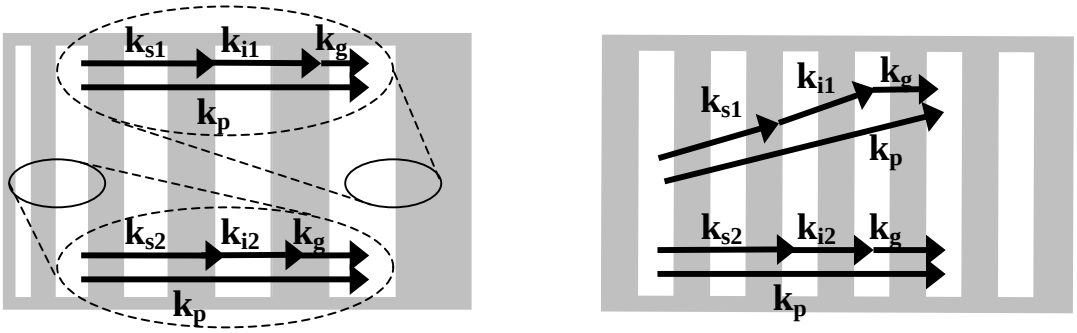

(a) (b)

Figure 7.1. Two quasi-phasematching techniques, which result in broadband amplification: (a) In an aperiodically QPM crystal different signal wavelengths will be amplified in different parts of the sample, because the magnitude of k_g changes depending on the domains lengths. (b) In achromatic phasematching the different signal wavelengths are amplified at different angles.

Another method employs a similar strategy in the sense that different wavelengths require different QPM periods. In achromatic phasematching, the seed is first angularly dispersed, so that different wavelengths can propagate at different angles through the periodically poled sample. The directions for the different wavelengths are chosen such that the phasematching condition is fulfilled for all wavelengths at the same time, see Fig. 7.1. (b). After the nonlinear process the signal beam has to be collimated again by cancelling the angular dispersion employing for example another grating or prism. This strategy was originally suggested for SHG of broadband, femtosecond pulses, where the different wavelengths travelled at different angles to achieve phasematching in the crystal.[90] It has recently also been employed for broadband optical parametric amplification in BPM crystals.[91]

A different approach where extremely large bandwidths can be reached, is to operate close to degeneracy or in retracing regions (i.e. turning of the phasematching curve).[92,93] This method is however relatively inflexible, since these large bandwidths can only be found in certain spectral regions, which depend on the gain material and require pump lasers that operate at the specifically needed wavelength.

A more adaptable technique, which does not have to rely on specific material properties, is to let the interacting beams propagate noncollinearly through the amplifying crystal. The first time efficient noncollinear parametric processes were predicted in nonlinear material was in 1967 by two independent groups.[94,95] Shortly afterwards noncollinear OPG was observed in ADP by Magde *et al.*[96] It took, however, almost 30 years until noncollinear OPGs [97,98] and OPOs [99] were employed with the goal to achieve broad bandwidths and large tuning ranges. The first noncollinear OPA, which afterwards became known as NOPA, was demonstrated soon afterwards. A white-light continuum seeded BBO crystal was combined with a prism compressor to render 16 fs long visible pulses.[100]

7.2 Wavelength Tuning of a Noncollinear Optical Parametric Amplifier with a Periodically Poled Crystal

A schematic picture of the wave vectors involved in a noncollinear OPA is plotted in Fig. 7.2. The phasematching conditions along the *x* axis and along the *y* axis are given by

$$\Delta k_x = k_p \cos\alpha_p - k_s \cos\alpha_s - k_i \cos\alpha_i - k_g = 0 \tag{7.1}$$

$$\Delta k_y = k_p \sin\alpha_p - k_s \sin\alpha_s - k_i \sin\alpha_i = 0 \tag{7.2}$$

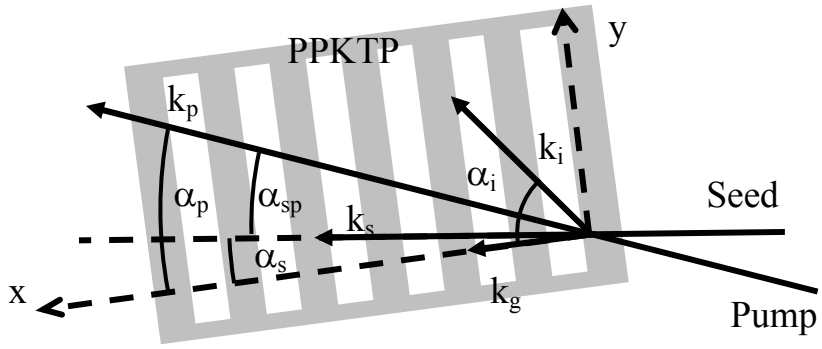

Figure 7.2. A schematic of the wave vectors and angles involved in a noncollinear QPM OPA.

Here all the angles α_s, α_i and α_p are defined towards the grating wave vector, k_g. Further, the angle between the pump and the seed is denoted by α_{sp} and describes the noncollinearity of the process.

If the angles of incidence for the seed, α_s, and the pump beam, α_p, are varied, the signal

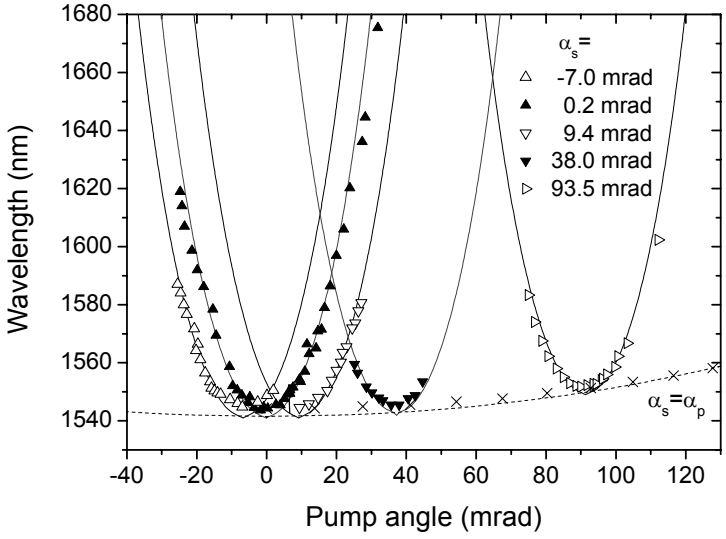

Figure 7.3. Wavelength tuning of a noncollinear OPA. By adjusting the pump and seed angles the signal and idler wavelength can be tuned continuously. Triangles and crosses are experimental values, whereas the curves are theoretical derivations.

and idler wavelengths, which fulfil the phasematching conditions, will change. A graph demonstrating this possibility of tuning the wavelength is shown in Fig 7.3, which is a result from Paper [I]. Here the crosses and the dotted curve represent the case when the pump and signal are collinear, $\alpha_{sp} = 0$, and the crystal is rotated around its polar axis. The moderate slope of this curve illustrates the limited tuning ability for collinear interaction. Significantly larger tuning ranges are, however, achieved if the pump and seed beams are interacting noncollinearly, which means $\alpha_{sp} \neq 0$. Several curves representing different noncollinear seed and pump configurations illustrate the increased tuning capacity in Fig.7.3.

7.3 Theoretical Derivation of an Optical Parametric Amplifier's Bandwidth

Employing the FWHM definition, the bandwidth of an optical parametric process is described by the points where the intensity has decreased to half of its maximum value. In order to derive the bandwidth of an OPA, equation (2.14) can be employed. The phase mismatch, Δk, has to be expanded in a Taylor series and for a collinear BPM OPA the bandwidth is given by:[101]

$$\Delta\nu_L \approx \frac{2(\ln 2)^{1/2}}{\pi}\sqrt{\frac{g}{L}}|v_{si}| \qquad \text{for } v_s \neq v_i \tag{7.3}$$

$$\Delta\nu_L \approx \frac{2(\ln 2)^{1/4}}{\pi}\left(\frac{g}{L}\right)^{1/4}\frac{1}{\sqrt{|g_s + g_i|}} \qquad \text{for } v_s = v_i \tag{7.4}$$

Here g is the gain coefficient given by (2.15) and $1/v_{si} = 1/v_s - 1/v_i$ describes the mismatch between the group velocities of the signal, v_s, and the idler, v_i. The group velocity dispersion of the signal and the idler are denoted g_s and g_i, respectively. Generally, large bandwidths can be expected close to degeneracy, where $v_s \approx v_i$.

For the noncollinear case the phase mismatch, Δk, is according to (7.1) and (7.2) a function of both wavelength and angles. Therefore (2.14) turns into a complex equation when the Taylor expansion of Δk is inserted. Hongjun *et al*. derived a solution for this equation for a BPM OPA.[102] Their solution was more complex than (7.3) but had still the same general characteristics, showing the close dependency between the bandwidth and the group velocity mismatch. Since the addition of the grating wave vector for a QPM OPA complicates the situation further, basically the only way to derive bandwidths is by numerical simulations coupled with approximations.

An alternative approach to derive an expression for the bandwidth of an OPA is to employ the angular dispersion, $\partial\alpha_s/\partial\omega_s$. For the angular dispersion an analytic expression can be derived and since the bandwidth is closely related to the inverse of the angular dispersion, significant insight into the bandwidth can be gained by examining this expression.

Starting with the phase matching equations (7.1) and (7.2), the signal's angular dispersion for the general case of noncollinear interaction ($\alpha_i \neq \alpha_s$) is given by:

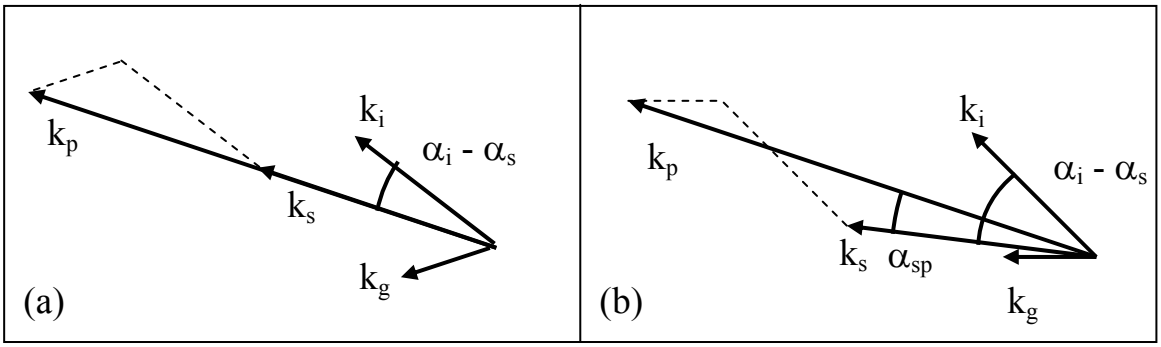

Figure 7.4. (a) Illustration of the phasematching for collinear signal and pump propagation. (b) Phasematching condition for the same wave vectors as in (a) but for noncollinear signal and pump configuration.

$$\frac{\partial \alpha_s}{\partial \omega_s} = \frac{1}{k_s \sin(\alpha_i - \alpha_s)}\left[\frac{1}{v_i} - \frac{\cos(\alpha_i - \alpha_s)}{v_s}\right] \tag{7.5}$$

Since $v_s > v_i$ for KTP in the IR region, the bracket in (7.5) will only approach zero for collinear interaction at the degeneracy point. The largest bandwidths for nondegenerate cases are instead achieved at the angles α_i and α_s that minimise the angular dispersion. Examining first Fig 7.4 (a) for collinear signal and pump interaction, it can be seen that the angle α_i - α_s is positive, but comparably small. Due to the dominating sine term in (7.5), this leads to a rather large angular dispersion. A comparison with the noncollinear signal and pump interaction in Fig. 7.4 (b), shows that the angle between the signal and the idler increases for increasing noncollinearity, α_{sp}. This immediately leads to a decreasing angular dispersion according to (7.5) and hence a larger bandwidth.

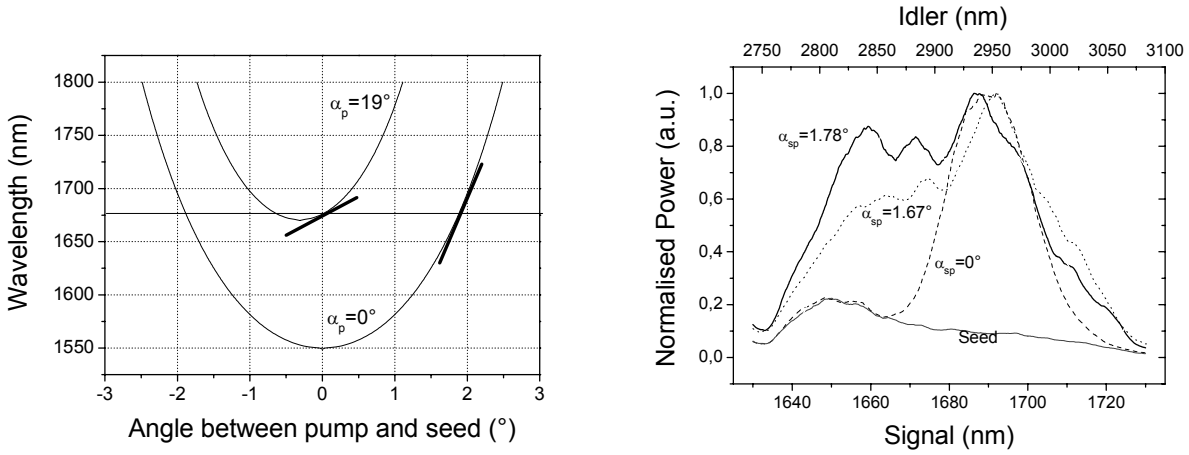

(a) (b)

Figure 7.5. The dependence of the signal bandwidth on the noncollinearity: In (a) the signal wavelength is plotted as a function of the noncollinear angle, α_{sp}, with the pump angle as a parameter. The graph in (b) shows the experimental signal bandwidth achieved for different noncollinear angles.

An idea about the large bandwidth difference for collinear and noncollinear pump and signal propagation can also be achieved, when examining Fig. 7.5 (a). Here the signal wavelength is plotted as a function of the angle between the pump and the signal, for two different pump angles. Examining both curves at e.g. 1680 nm shows that the slope is considerably steeper for noncollinear interaction than for collinear signal and pump propagation. The moderate slope for the collinear case shows clearly that a larger spread in the pump-signal angle is needed to achieve a certain bandwidth, than what is the case for noncollinear propagation.

7.4 Experimental Bandwidth of a Noncollinear Optical Parametric Amplifier

To confirm the trend of increasing bandwidths for increasing noncollinearity experimentally, a noncollinear OPA was designed and constructed. The broadband seed, which is required for examination of the OPA's bandwidth, was obtained by spectrally broadening a signal generated by an OPO. By coupling these intense signal pulses, which had a wavelength of 1550 nm, into a single-mode fibre, various third order nonlinear effects broadened the spectrum. Hence a continuum, covering the spectral region from 1500 to 1750 nm, was emitted, which could be employed for amplification in a noncollinear OPA. The PPKTP sample had a period of 35.6 μm and rotation about its polar *z* axis allowed the tuning of the seed angle versus the grating vector, α_s. A Nd:YAG laser operating at 1064 nm was used to pump the OPA and its angle versus the seed, α_{sp}, could be adjusted separately. A significantly larger pump than seed radius ensured spatial overlap for noncollinear interaction. The change in the signal bandwidth was measured at a central wavelength of 1680 nm and in Fig. 7.5 (b) the amplified spectra for collinear and for two noncollinear seed and pump configurations are shown. When adjusting α_{sp} from 0 to 31 mrad (1.78 °) the bandwidth increased from 2.4 to 6.9 THz, which is large enough to accommodate sub 100 fs pulses. If even larger bandwidths are required, larger noncollinear angles are needed, which a crystal with a shorter period can provide. It should however be noted that the angular dispersion given by (7.5) will saturate, which limits the bandwidth increase for a QPM crystal with a single period.

7.5 Femtosecond Optical Parametric Amplification

Apart from powerful nanosecond and picosecond pulses, also powerful femtosecond pulses are desirable, e.g. for ultrafast, time resolved spectroscopy on biological and chemical samples. Other possible areas of interest are surgery, high-precision material processing with both industrial and medical applications and imaging by for example two-photon absorption. The main technique for amplifying femtosecond pulses has so far been to utilise solid-state laser amplifiers. Apart from the disadvantages mentioned in Chapter 6, another major drawback with utilising laser crystals is the generally narrow bandwidth of the gain material, which can lead to spectral narrowing and subsequent pulse broadening.

An alternative approach is to use optical parametric amplifiers to generate femtosecond pulses with high energies. This technique has the advantage that the crystals typically used in OPAs, such as KTP, are less susceptible to thermal effects at high powers than laser crystals,

because the material is not heated up during the amplification process. Other important benefits are the possibility to choose the spectral range of the phasematching crystal by adjusting the period of the QPM structure and the reasonable simplicity of the setup.

One major problem with all types of femtosecond amplifiers is the high peak power inside the amplifying medium due to the short pulse duration. Most crystals cannot withstand these powers and risk catastrophic optical breakdown because of lensing effects. Thus, a common method employed for femtosecond amplifiers is chirped pulse amplification (CPA), which was first demonstrated by Strickland and Mourou in 1985.[103] In the original experiment picosecond pulses emitted by a mode-locked Nd:YAG laser were coupled into a single mode fibre, where they were chirped and therefore stretched. After amplification in a Nd:YAG regenerative amplifier, the pulses were sent to a grating compressor, which rendered energetic and compressed pulses. Since the seed pulses are chirped, the technique is nowadays called chirped pulse amplification. Actually, the idea of amplifying stretched pulses to avoid high peak powers was not entirely new when Strickland and Mourou suggested this approach for intense light pulses. This technique had already been developed for radar systems where short, yet energetic pulses were needed as well.

Nowadays, it is more common that both the stretcher and the compressor consist of gratings to introduce a wavelength dependent delay. If the amplification does not affect the chirp linearity, the pulses can be fully recompressed to their original lengths. Otherwise the grating in the compressor should be optimised to cancel both the stretcher and any chirp introduced by the rest of the setup as efficiently as possible. Employing this method not only limits lensing effects, but also other intensity dependent processes, such as Raman scattering and SPM, which can change the characteristics of the beams.

For femtosecond OPAs additional reasons exists to stretch the pulses, for example facilitating the synchronisation of the pump and the seed and increasing the conversion efficiency. Since parametric amplification is an instantaneous process, the pulse length difference between an inexpensive nanosecond pump and a femtosecond seed would be very detrimental to the conversion efficiency. Analogous to CPA, this technique is called optical parametric chirped pulse amplification (OPCPA) and was demonstrated for the first time by Dubietis *et al*.[104]

A recently published article summarises the progress in OPCPA and points out that three different trends can be observed.[105] One group is aiming for pulses with extremely high powers by pumping with 532 nm or 527 nm and operating close to degeneracy. LBO, BBO and KDP crystals, which have the highest damage thresholds, are used as the amplifying material and the highest power achieved so far is ~16 TW.[106] This does however not stop groups from aiming at still higher powers. For example exawatt (10^{18}) and zettawatt (10^{21}) powers would permit the acceleration of electrons to extremely high energies opening up fundamentally new domains of physics.[107] The second trend focuses on the generation of extremely short pulses and makes use of noncollinear parametric amplification. The shortest pulses obtained by this method had durations of 4 fs.[108]

The last group strives for developing reliable and compact systems with powers and pulse durations in the intermediate range. These schemes were initially intended to be alternatives to the commercially available Ti:sapphire based regenerative amplifiers with the additional advantage of wavelength flexibility. The predominantly used crystals are periodically poled ferroelectrics like PPKTP and PPLN. Due to their large nonlinearity they improve the parametric gain, however their small apertures limit the maximum peak powers.

The wish to extend the possible applications of the third group and to further improve the already achieved results, were the main motivations for performing the OPCPA experiment leading to Paper [VI].

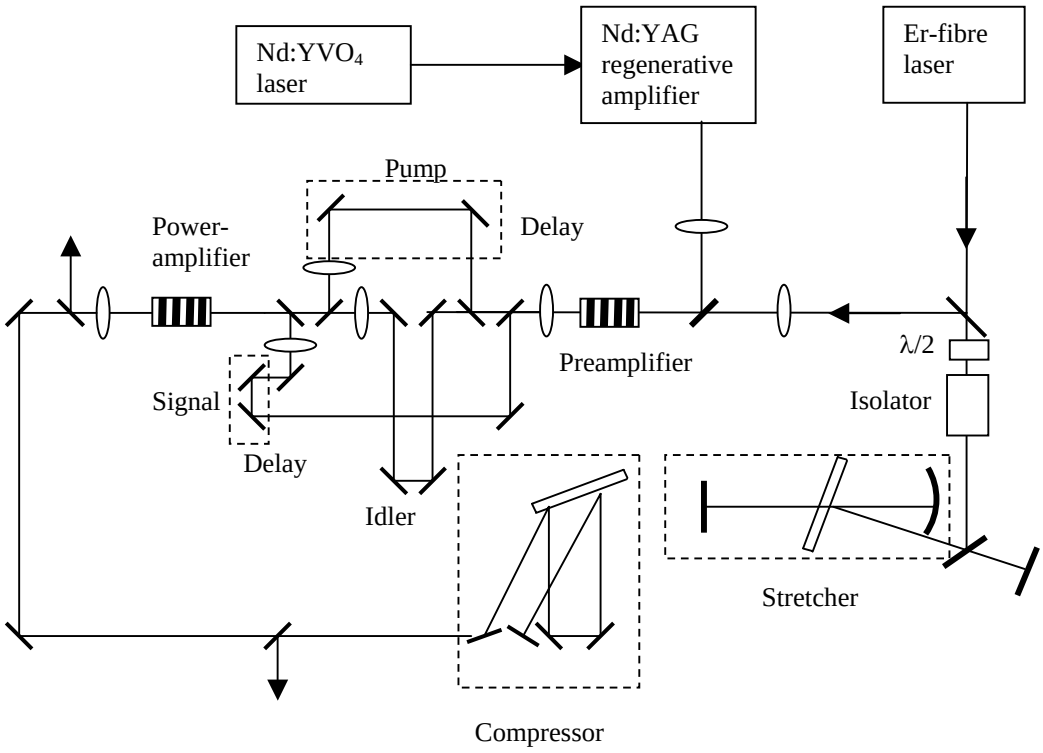

Figure 7.6. The experimental setup of the double stage optical parametric chirped pulse amplifier.

Rotermund *et al*. were the first to employ PPKTP as the gain material in an OPCPA rendering 20 μJ pulses with durations of 320 fs at 1.5 μm.[109] They used a single crystal with a length of 12 mm, which limited the pump power and hence the largest achievable amplification.

The new experiment performed shortly afterwards, aimed at obtaining more energetic pulses with better temporal and spectral characteristics. By constructing the experimental setup shown in Fig. 7.6, a total gain of 60 dB was achieved in Paper [VI]. The seed was provided by a diode-pumped Er-fiber laser, which generated 55 fs pulses. Employing a grating stretcher, the pulse duration was increased to 250 ps. Each pulse had an energy of 60 pJ, when it reached the OPA, where it was preamplified in a PPKTP sample with a QPM period of 36 μm. The pump was provided by a regenerative amplifier, which was seeded by a Nd:YVO_4 laser, and generated 1 mJ pulses having a duration of 1 ns.

After the first stage the signal's energy had increased by more than 40 dB to 3 μJ. Before reaching the second PPKTP crystal, all beams were separated from each other. They were rerouted through three different delay lines with individual focusing, which allowed precise temporal and spatial adjustment for the second stage of the OPA. After the power amplifier stage the signal energy reached 85 μJ, resulting in a total gain of more than 60 dB. For the

second stage this resulted in a power conversion from the pump to both signal and idler of 20 %. If both stages are considered the efficiency reached 12.5%.

The successive recompression led to an amplified signal having a bandwidth of 21 nm and a pulse duration of 270 fs. The spectrum and the autocorrelation trace can be seen in Fig. 7.7. The main reason for the increase of the pulse duration is the narrow gain bandwidth of the PPKTP crystals employed in the experiment. Utilising e.g. the noncollinear optical parametric amplification approach discussed in earlier sections could potentially decrease the pulse duration of the amplified signal considerably.

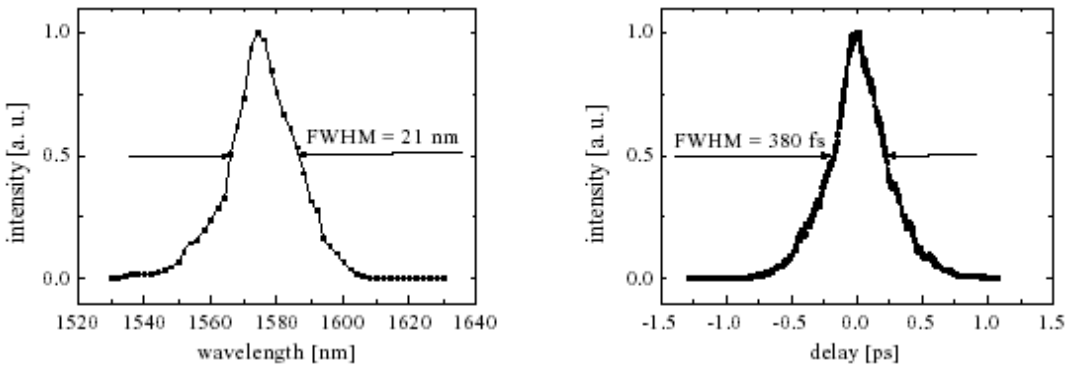

(a) (b)

Figure 7.7. (a) The spectrum of the amplified signal. (b) The autocorrelation trace of the compressed signal.

If significantly larger signal energies or peak powers are needed, the strategies of the first group have to be employed. Birefringent phasematched crystals have to be used instead of periodically poled crystals, which have limited apertures and do therefore not permit the substantially higher pump powers that are required. The largest energies and peak powers in the 1.5 µm region were reported by Rudd *et al.*[110] Four KTA and four RTP samples were used in a far from trivial setup to amplify 260 fs pulses to 30 mJ, thus reaching peak powers of 100 GW.

However, as stated earlier, PPKTP samples are very attractive nonlinear crystals for compact and wavelength flexible amplifiers, emitting e.g. femtosecond pulses at 1575 nm with energies as large as 85 µJ.

Chapter 8

Conclusion

This thesis demonstrates that it is advantageous to use periodically poled crystals from the KTP family for efficient and compact OPA applications, which can be pumped by low- to mid-power lasers. By performing a systematic investigation of various OPAs, the amplification of pulses extending from the nanosecond to the femtosecond regime in a wide spectral range was explored. Further, some material properties of periodically poled crystals from the KTP family were studied and derived to facilitate the future use.

During the course of this work four different OPA setups were constructed to allow the investigation of this technique's advantages and limitations. While the pump laser and the gain material were very similar in all these experiments, the sources generating the seed beam differed considerably. This illustrated the adaptability of OPAs based on periodically poled KTP crystals. They can be used to amplify radiation in both a wide spectral range and temporal regime. Several experimental setups showed that small signal gains of 60 to 75 dB could be achieved for double stage arrangements using one or two PPKTP crystals. To avoid degradation of the signal quality during the amplification process, the OPAs were optimised to avoid parasitic effects like superfluorescence. This allowed the spectral and spatial properties of the pulses emitted by these amplifiers to be solely determined by the seed lasers. Due to the large conversion efficiencies achieved for these setups, the energies of the amplified signals, however, approached the level of the pump pulses. Hence, powerful pulses were emitted in diffraction-limited beams at various wavelengths and with a variety of different durations.

In one experiment a setup was constructed which generated nanosecond pulses at 1535 nm with energies reaching the millijoule level. A single PPKTP crystal was employed in a double pass setup. Further, a comparably simple and reliable OPA was demonstrated which amplified picosecond pulses emitted by a gain-switched laser diode. This possible alternative for mode-locked lasers generated microjoule pulses with durations adjustable from 20 ps to 2 ns at 973 nm.

It was further investigated, if broadband amplification could be achieved for nondegenerate signal and idler wavelengths. This study was motivated by a femtosecond OPA experiment,

where spectral narrowing during the amplification process caused an increase of the amplified pulse's length. Different techniques were investigated and an increase of the bandwidth by a factor of almost three was demonstrated by letting the seed and the pump interact noncollinearly in a PPKTP crystal with a single QPM period. This would allow the amplification of pulses with sub 100 fs durations at any wavelength, without having to rely on specific advantageous material properties.

Several investigations of material properties were performed as well. They resulted in more insight in the characteristics of periodically poled crystals from the KTP family. By employing nonlinear devices based on PPRTP we were able to derive two new sets of coefficients for the accurate determination of the refractive index and its temperature dispersion. This will facilitate the future use of this material in nonlinear processes.

Another experiment focused on the yet not fully understood areas close to domain walls in periodically poled materials. Efficient second harmonic generation, which was caused by two nonlinear coefficients that are zero in single domain material, was observed in these regions. It was found that the poling process causes strains in the material, which leads to the appearance of these nonlinearities.

All in all, periodically poled crystals from the KTP family are found to perform well and efficiently in several nonlinear devices. Especially OPAs based on PPKTP achieved excellent results, making them attractive and valuable candidates for amplification of radiation in a wide spectral and temporal range.

Chapter 9

Description of the Included Papers and Contributions by the Candidate

Paper I:

Broadband nondegenerate optical parametric amplification in the mid infrared with periodically poled $KTiOPO_4$
A. Fragemann, V. Pasiskevicius, and F. Laurell
Opt. Lett. **30**, 2296 (2005).

Broadband optical parametric amplification was demonstrated by employing noncollinear seed and pump configurations in periodically poled KTP. A broadband seed was generated, by coupling the spectrally narrow signal emitted by an OPO into a single mode fibre. Third order nonlinear effects in the fibre broadened the signal and resulted in the emission of a continuum, which was used to seed the amplification stage. An analysis of the OPA's tuning ability indicated an increase of the amplification bandwidth for noncollinear seed and pump interaction. To confirm this behaviour, the bandwidth of the amplification stage was examined for various noncollinear configurations and compared to the theoretically derived results. Employing noncollinear interaction for a nondegenerate signal at 1680 nm enabled the amplification of 6.9 THz broad signals with small signal gains of 22 dB.

Contributions by the author: I designed the experimental setup, poled the crystals and had the main responsibility for all the experiments. The candidate and V. Pasiskevicius derived the theory and wrote the paper.

Paper II:

Optical parametric amplification of a gain-switched picosecond laser diode
A. Fragemann, V. Pasiskevicius, and F. Laurell
Opt. Expr. **13**, 6482 (2005).

A gain-switched laser diode, emitting pulses with variable durations at 973 nm, was used to seed an optical parametric amplifier pumped by a frequency doubled nanosecond Nd:YAG laser. By applying current pulses to the laser diode, it emitted picojoule pulses with controllable durations between 20 ps and 2 ns. These pulses were amplified in a two stage OPA employing two PPKTP crystals and reached pulse energies of 1 μJ and 20 μJ for the short and the long pulses, respectively. A total amplification of up to 50 dB was achieved for both pulses. Further, suppression of superfluorescence could be observed for the long pulses, which emphasises the need of both temporal and spatial overlap between the seed and the pump pulses to achieve the largest possible amplification. The duration of the short pulses was determined by employing a noncollinear autocorrelation setup based on a second harmonic generating PPKTP crystal.

Contributions by the author: The candidate had the main responsibility for the design of the setup and the experiment. V. Pasiskevicius helped with the electric control of the laser diode and participated in the experiments. The paper was written by the candidate and V. Pasiskevicius.

Paper III:

High-peak power nanosecond optical parametric amplifier with periodically poled $KTiOPO_4$
A. Fragemann, V. Pasiskevicius, G. Karlsson, and F. Laurell
Opt. Expr. ***11****, 1297, (2003).*

The first double pass optical parametric amplifier based on a single PPKTP crystal was designed and constructed, with the aim to explore the scalability of PPKTP OPAs. A homebuilt Er-Yb:glass laser, operating as the seed, was amplified by interacting with a Nd:YAG laser, which was performing as the pump, in the nonlinear sample. By allowing two passes through the crystal a maximum small signal gain of 75 dB was achieved. We thoroughly investigated the performance of the two stages and optimised their individual operation to yield the best total amplification. The setup generated 1 mJ pulses with a duration of 5 ns in a diffraction limited beam at 1535 nm. Spectral and spatial broadening of the signal was prevented by avoiding the occurrence of superfluorescence. By coupling the signal into a single mode, dispersion-flattened fibre, the signal's narrow bandwidth could be broadened.

Contributions by the author: The candidate had the overall responsibility of the experiment, which included poling the crystal, designing and building the setup and performing the experiment itself. G. Karlsson designed and built the Er-Yb:glass laser. The candidate and V. Pasiskevicius wrote the paper.

Paper IV:

Second-order nonlinearities in the domain walls of periodically poled $KTiOPO_4$
A. Fragemann, V. Pasiskevicius, and F. Laurell
Appl. Phys. Lett. **85**, 375 (2004).

The origin of phase-matched second harmonic generation, which was generated in PPKTP when irradiated along the polar *c* axis, was investigated. The SH was emitted in directions corresponding to the Čerenkov angles and occurred only when the fundamental beam was focused on a domain wall and not if the beam was centred in the middle of a domain. Analysis of the beams' polarisation resulted in the conclusion that the SHG has to be attributed to the nonlinear coefficients d_{11} and d_{12}, which are not present in single domain KTP. The poling process is, however, assumed to cause strains close to the domain walls, which result in dc piezoelectric fields. These fields can by third order nonlinear processes cause dc-induced second harmonic generation. The approximate magnitudes of these nonlinear coefficients were derived to be $d_{11} \approx 0.45$ pm/V and $d_{12} \approx 0.56$ pm/V.

Contributions by the author: The candidate and V. Pasiskevicius designed and performed all the experiments, discussed the theory and wrote the article.

Paper V:

Frequency converters from visible to mid-infrared with periodically poled $RbTiOPO_4$
A. Fragemann, V. Pasiskevicius, J. Nordborg, J. Hellström, H. Karlsson, and F. Laurell
Appl. Phys. Lett. ***83****, 3090, (2003).*

Several PPRTP crystals for optical parametric oscillation and second harmonic generation were examined. Analysis of the generated wavelengths' dependency on the grating period resulted in the derivation of a new set of Sellmeier coefficients, which in the future will allow the accurate determination of phasematching periods. Conversion efficiencies in the OPOs of 40% resulted in the emission of pulses having energies just below 1 mJ. The OPOs were temperature tuned, which led to the generation of radiation covering almost the complete range between 1.55 μm and 3.4 μm. Using this data, the temperature dispersion of the refractive index was determined, permitting precise control of the wavelength's tuning ability in PPRTP. In general, the performance of the PPRTP crystals in SHGs and OPOs was comparable to operating these devices with PPKTP.

Contributions by the author: The candidate performed the experiment and the simulations needed to derive the new Sellmeier equations together with V. Pasiskevicius. The samples used in the experiment were poled by the candidate, J. Nordberg, J. Hellström and H. Karlsson. V. Pasiskevicius and the candidate wrote the paper.

Paper VI:

Efficient All-Diode-Pumped Double Stage Femtosecond Optical Parametric Chirped Pulse Amplification at 1-kHz with Periodically Poled $KTiOPO_4$

V. Petrov, F. Noack, F. Rotermund, V. Pasiskevicius, A. Fragemann, F. Laurell, H. Hundertmark, P. Adel, and C. Fallnich

Jpn. J. Appl. Phys. ***42****, L 1327, (2003).*

Femtosecond pulses were stretched and subsequently amplified in a two-stage optical parametric chirped pulse amplifier employing two periodically poled $KTiOPO_4$ crystals. A grating stretcher was employed to stretch the 55 fs seed pulses generated by an Er-fibre laser at 1.57 μm. This resulted in chirped pulses with durations of 250 ps and energies of 60 pJ. While passing through the two PPKTP crystals the seed was amplified with a signal gain of 60 dB resulting in 85 μJ pulses. Simultaneously an idler was generated at 3.3 μm. The amplified signal had a bandwidth of 21 nm and after the recompression a pulse duration of 270 fs was achieved. The increase in the pulse length was mainly caused by the narrow gain bandwidth of the crystals and could be improved by employing noncollinear seed and pump interaction.

Contributions by the author: I poled the crystals used in the experiment and made an initial evaluation of them. The candidate also participated to some extent in the experiment, which was set in Berlin. V. Pasiskevicius and V. Petrov wrote the article.

Paper VII:

Enhanced stimulated Raman scattering in optical parametric oscillators from periodically poled $KTiOPO_4$

V. Pasiskevicius, A. Fragemann, F. Laurell, R. Butkus, V. Smilgevicius, and A. Piskarskas

Appl. Phys. Lett. ***82****, 325, (2003).*

Six periodically poled KTP crystals were examined for the possibility to achieve Raman oscillation concurrent to optical parametric oscillation. If the OPO generated idlers in the wavelength region of KTP's absorption band, efficient Raman oscillation was observed. The absorbed idler is assumed to drive phonons, which enhance the creation of coherent Stokes photons. Conversion efficiencies from the signal to the Stokes wave of 17 % were achieved. An increase of the threshold for Raman oscillation was observed when the crystals were heated above 80 °C. This effect was attributed to the thermal generation of incoherent phonons, which cause dephasing.

Contributions by the author: V. Pasiskevicius had the overall responsibility for the experiment and wrote the article. The candidate poled some of the crystals and participated in some parts of the experiment. I was also involved in the discussions of the theory.

References

[1] T. H. Maiman, *Nature* **187**, 493 (1960).

[2] P. A. Franken, A. E. Hill, C. W. Peters, and G. Weinreich, *Phys. Rev. Lett.* **7**, 118 (1961).

[3] A. Yariv, *"Quantum Electronics"*, John Wiley & Sons, New York (1989).

[4] P.N. Butcher and D. Cotter, *"The Elements of Nonlinear Optics"*, Cambridge University Press, (1990).

[5] R. L. Sutherland, "*Handbook of nonlinear optics*", Optical Engineering, Marcel Dekker, Inc, New York, (1996).

[6] Y. R. Shen, *"The principles of nonlinear Optics"*, New York: Wiley-Interscience. (1984).

[7] G. D. Boyd and D. A. Kleinman, *J. Appl. Phys.* **39**, 3597 (1968).

[8] J. A. Armstrong , N. Bloembergen, J. Ducuing, and P. S. Pershan, *Phys. Rev*. **127**, 1918 (1962).

[9] S. E. Harris, M. K. Oshman, and R. L. Byer, *Phys. Rev. Lett.* **18**, 732 (1967).

[10] W. H. Louisell, A. Yariv, and A. E. Siegman, *Phys. Rev.* **124**, 1646 (1961).

[11] J. P. Gordon, W. H. Louisell, and L.R. Walker, *Phys. Rev.* **129**, 481 (1963).

[12] W. G. Wagner and R. W. Hellwarth, *Phys. Rev.* **133**, A915 (1964).

[13] J. A. Giordmaine and R. C. Miller, *Phys. Rev. Lett.* **14**, 973 (1965).

[14] J. M. Manley and H. E. Rowe, *Proc. IRE* **44,** 904 (1956).

[15] R. A. Baumgartner and R. L. Byer, *IEEE J. Quant. Elec.* **15**, 432, (1979).

[16] J. A. Giordmaine, *Phys. Rev. Lett.* **8**, 19 (1962).

[17] P. D. Maker, R. W. Terhune, M. Nisenoff, and C. M. Savage, *Phys. Rev. Lett.* **8**, 21 (1962).

[18] P. A. Franken and J. F. Ward, *Rev. Mod. Phys.* **35**, 23 (1963).

[19] H. Karlsson, "*Fabrication of periodically poled crystals from the KTP family and their applications in nonlinear optics*" PhD-thesis, ISSN 0280-316X, Royal Institute of Technology (1999).

[20] M. M. Fejer, G. A. Magel, D. H. Jundt, and R. L. Byer, *IEEE J. Quant. Electr.* **28**, 2631 (1992).

[21] P. A. Čerenkov, *Dokl. Akad. Nauk SSSR* **2**, 451 (1934).

[22] A. Zembrod, H. Puell, and J. A. Giordmaine, *J. Opto- Electron.* **1**, 64 (1969).

[23] P. K. Tien, R. Ulrich, and R. J. Martin, *Appl. Phys. Lett.* **17**, 447 (1970).

[24] L Ouvrad, M. Troost, *Compt. Rend.* **121**, 117 (1890).

[25] I. Tordjman, R. Masse, and J. C. Guitel, *Zeitschrift für Kristallographie* **139**, 103 (1974).

[26] F. C. Zumsteg, J. D. Bierlein, and T. E. Gier, *J. Appl. Phys*. **47**, 4980 (1976).

[27] J. D. Bierlein, and H. Vanherzeele, *J. Opt. Soc. Am. B* **6**, 622 (1989).

[28] C. Canalias, J. Hirohashi, V. Pasiskevicius, and F. Laurell, *J. Appl. Phys.* **97**, 124105-1 (2005).

[29] G. E. Kugel, F. Brehat, B. Wyncke, M. D. Fontana, G. Marnier, C. Carabatos-Nedelec, and J. Mangin, *J. Phys. C* **21**, 5565 (1988).

[30] D. Xue, and S. Zhang, *Appl. Phys. Lett*. **70**, 943 (1997).

[31] V. Pasiskevicius, C. Canalias, and F. Laurell, "Highly efficient stimulated Raman scattering of picosecond pulses in $KTiOPO_4$" submitted to *Appl. Phys. Lett.* (2005)

[32] H. Karlsson, F. Laurell, and L. K. Cheng, *Appl. Phys. Lett*. **74**, 1519 (1999).

[33] P. A. Morris, *J. Crystal Growth* **106**, 76 (1990).

[34] M. N. Satyanarayan, A. Deepthy, and H. L. Bhat, *Critical Reviews in Solid State and Material Science* **24**, 103 (1999).

[35] J. Nordborg, "*Non-linear Optical Titanyl Arsenates, crystal growth and properties*", ISBN 91-7197-882-8, PhD-thesis, Chalmers University of Technology (2000).

[36] Y. V. Shaldin and R. Poprawski, *J. Phys. Chem. Solids* **51**, 101 (1990).

[37] K. Kato and E. Takaoka, *Appl. Opt.* **41**, 5040 (2002).

[38] K. Fradkin, A. Arie, A. Skliar, and G. Rosenman, *Appl. Phys. Lett*. **74**, 94 (1999).

[39] T.Y. Fan, C. E. Huang, B. Q. Hu, R. C. Eckardt, Y. X. Fan, R.L. Byer, and R. S. Feigelson, *Appl. Opt*. **26**, 2390 (1987).

[40] V.G. Dmitriev, G.G. Gurzadyan, D.N. Nikogosyan, "*Handbook of Nonlinear Optical Crystals*" Ed: A.E. Siegman, Springer series in optical science, Vol 64, Springer-Verlag, Berlin Heidelberg, 1991.

[41] Y. Guillien, B. Menaert, J. P. Feve, P. Segonds, J. Douady, B. Boulanger, O. Pacaud, *Optical Materials* **22**, 155 (2003).

[42] W. Wiechmann, S. Kubota, T. Fukui, and H. Masuda, *Opt. Lett.* **18**, 1208 (1993).

[43] G. Hansson, H. Karlsson, S. Wang, and F. Laurell, *Appl. Opt*. **39**, 5058 (2000).

[44] L. K. Cheng, L. T. Cheng, J. Galperin, P. A. Morris Hotsenpiller, J. D. Bierlein, *J. Cryst. Growth* **137**, 107 (1994).

[45] M. Ghotbi and M. Ebrahim-Zadeh, *Opt. Expr.* **12**, 6002 (2004).

[46] J. Hellström, V. Pasiskevicius, H. Karlsson, and F. Laurell, *Opt. Lett.* **25**, 174 (2000).

[47] T. Hatanaka, K. Nakamura, T. Taniuchi, H. Ito, Y. Furukawa, and K. Kitamura, *Opt. Lett.* **25**, 651 (2000).

[48] N. E. Yu, S. Kurimura, Y. Nomura, M. Nakamura, K. Kitamura, J. Sakuma, Y. Otani, and A. Shiratori, *Appl. Phys. Lett.* **84**, 1662 (2004).

[49] E. Lallier, L. Brevignon, and J. Lehoux, *Opt. Lett.* **23**, 1511 (1998).

[50] R. L. Byer, *Nonlinear Optics* **7**, 235 (1994).

[51] D. Feng, N. B. Ming, J. F. Hong, Y. S. Yang, J. S. Zhu, Z. Yang, and Y. N. Wang, *Appl. Phys. Lett.* **37**, 607 (1980).

[52] J. Webjörn, F. Laurell, G. Arvidsson, *J. Lightwave Technol.* **7**, 1597 (1989).

[53] E. J. Lim, M. M. Fejer, R. L. Byer, and W. J. Kozlovsky, *Electron. Lett.* **25**, 731 (1989).

[54] J. D. Bierlein, D. B. Laubacher, J. B. Brown, and C. J. van der Poel, *Appl. Phys. Lett.* **56**, 1725 (1990).

[55] C. J. van der Poel, J. D. Bierlein, J. B. Brown, and S. Colak, *Appl. Phys. Lett.* **57**, 2074 (1990).

[56] M. Yamada, N. Nada, M. Saitoh, and K. Watanabe, *Appl. Phys. Lett.* **62**, 435 (1993).

[57] R. Stolzenberger and M. Scripsick, *SPIE* **3610**, 23 (1999).

[58] J. D. Bierlein and F. Ahmed, *Appl. Phys. Lett.* **51**, 1322 (1987).

[59] L. E. Myers, R. C. Eckardt, M. M. Fejer, R. L. Byer, W. R. Bosenberg, J. W. Pierce, *J. Opt. Soc. Am. B* **12**, 2102 (1995).

[60] S. Wang, V. Pasiskevicius, and F. Laurell, "Highly efficient periodically poled Rb-doped $KTiOPO_4$ using in-situ monitoring", submitted to *J. Appl. Phys.* (2005).

[61] F. Laurell, M. G. Roelofs, W. Bindloss, H. Hsiung, A. Suna, and J. D. Bierlein, *J. Appl. Phys.* **71**, 10 (1992).

[62] J. Wittborn, C. Canalias, K. V. Rao, R. Clemens, H. Karlsson, and F. Laurell, *Appl. Phys. Lett.* **80**, 1622 (2002).

[63] K. Hayata, K. Yanagawa, and M. Koshiba, *Appl. Phys. Lett.* **56**, 206 (1990).

[64] M. J. Li, M. De Micheli, Q. He, and D. B. Ostrowsky, *IEEE J. Quant. Electr.* **26**, 1384 (1990).

[65] N. M. Kroll, *Phys. Rev.* **127**, 1207 (1962).

[66] S. A. Akhmanov and R. V. Khokhlov, *Zh. Ekxperim. I Teor. Fiz.* **43**, 351 (1962). English Translation: *Soviet Phys.-JETP* **17**, 252 (1963).

[67] W. E. Danielson, *J. Appl. Phys.* **30**, 8 (1959).

[68] I. P. Kaminov, *IEEE Spectrum*, 35 (1965).

[69] C. C. Wang and G. W. Racette, *Appl. Phys. Lett.* **6**, 169 (1965).

[70] A. Galvanauskas, A. Hariharan, D. Harter, M. A. Arbone, and M. M. Fejer, *Opt. Lett.* **23**, 210, (1998).

[71] P. F. Moulton, *J. Opt. Soc. Am. B* **3**, 125 (1986).

[72] J. Seres, A. Müller, E. Seres, K. O'Keeffe, M. Lenner, R. F. Herzog, D. Kaplan, C. Spielmann, F. Krausz, *Opt. Lett.* **28**, 1832 (2003).

[73] C. J. Koester and E. Snitzer, *Appl. Opt.* **3**, 1182 (1964).

[74] A. Dubietis, R. Danielius, G. Tamosauskas, and A. Piskarskas, *J. Opt. Soc. Am. B* **15**, 1135 (1998).

[75] F. Rotermund, V. Petrov, F. Novack, V. Pasiskevicius, J. Hellström, and F. Laurell, *Opt. Lett.* **24**, 1874 (1999).

[76] D. E. Gragson, D. S. Alavi, and G. L. Richmond, *Opt. Lett.* **20**, 1991 (1995).

[77] L. Carrion and J. P. Girardeau-Montaut, Opt. Commun. **152**, 347 (1998).

[78] K. Finsterbusch, R. Urschel, and H. Zacharias, *Appl. Phys. B* **74**, 319 (2002).

[79] G. Karlsson, V. Pasiskevicius, F. Laurell, and J. A. Tellefsen, *Opt. Commun.* **217**, 317 (2003).

[80] G. Arisholm, Ö. Nordseth, and G. Rustad, *Opt. Expr.* **12**, 4189 (2004).

[81] P.N. Butcher and D. Cotter, *"The Elements of Nonlinear Optics"*, Cambridge University Press, p 228 (1990).

[82] P. E. Powers, P. K. Bojja, R. Alkuwari, E. Vershure, and K. L. Schepler, *J. Opt. Soc. Am. B* **22**, 2169 (2005).

[83] S. H. Cho, F. X. Kärtner, U. Morgner, E. P. Ippen, J. G. Fujimoto, J. E. Cunningham, and W. H. Knox, *Opt. Lett.* **26**, 560 (2001).

[84] M. S. Pshenichnikov, W. P De Boeij, and D. A. Wiersma, *Opt. Lett.* **19**, 572 (1994).

[85] F. Balembois, M. Gaignet, P. Georges, A. Brunn, N. Stelmakh, and J. M. Louritoiz, *Appl. Opt.* **37**, 4876 (1998).

[86] C. C. Renaud, H. L. Offerhaus, J. A. Alvarez-Chavez, J. Nilsson, W. A. Clarkson, P. W. Turner, D. J. Richardson, and A. B. Grundinin, *IEEE J. Quantum Electron.* **37**, 199 (2001).

[87] M. A. Arborne, O. Marco, and M. M. Fejer, *Opt. Lett.* **22**, 865 (1997).

[88] T. Beddard, M. Ebrahimzadeh, T. R. Reid, and W. Sibbett, *Opt. Lett.* **25**, 1052 (2000).

[89] D. Artigas, D. T. Reid, M. M. Fejer, and L. Torner, *Opt. Lett.* **27**, 442 (2002).

[90] O. E. Martinez, *IEEE J. Quantum Electron.* **25**, 2464 (1989).

[91] A. Shirakawa, I. Sakane, M. Takasaka, and T. Kobayashi, *Appl. Opt. Lett.* **74**, 2268 (1999).

[92] C.-W. Hsu and C. C. Yang, *Opt. Lett.* **26**, 1412 (2001).

[93] C.-W. Hsu, C.-T. Chen, and C.-C. Yang, *J. Opt. Soc. Am. B* **19**, 1150 (2002).

[94] D. N. Klyshko, *Zh. Ekxperim. i Teor. Fiz. Pis'ma v Redaktsiyu* **6**, 490 (1967). English Translation: *Soviet Phys.-JETP Letters* **6**, 23 (1967).

[95] T. G. Giallorenzi and C. L. Tang, *Phys. Rev.* **166**, 225 (1968).

[96] D. Magde, R. Scarlet, and H. Mahr, *Appl. Phys. Lett.* **11**, 381 (1967).

[97] V. Krylov, A. Kalintsev, A. Rebane, D. Erni, and U. P. Wild, *Opt. Lett.* **20**, 151 (1995).

[98] P. D. Trapani, A. Andreoni, C. Solcia, P. Foggi, R. Danielius, A. Dubietis, and A. Piskarskas, *J. Opt. Soc. Am. B* **12**, 2237 (1995).

[99] G. M. Gale, M. Cavallari, T. J. Driscoll, and F. Hache, *Opt. Lett.* **20**, 1562 (1995).

[100] T. Wilhelm, J. Piel, and E. Riedle, *Opt. Lett.* **22**, 1494 (1997).

[101] R. Danielius, A. Piskarskas, A. Stabinis, G. P. Banfi, P. Di Trapani, and R. Righini, *J. Opt. Soc. Am. B* **10**, 2222 (1993).

[102] L. Hongjun, Z. Wei, C. Guofu, W. Yishan, C. Zhao, R. Chi, *Appl. Phys. B* **79**, 569 (2004).

[103] D. Strickland and G. Mourou, *Opt. Commun.* **56**, 219 (1985).

[104] A. Dubietis, G. Jonusauskas, and A. Piskarskas, *Opt. Commun*. **88**, 437, (1991).

[105] R. Butkus, R. Danielius, A. Dubietis, A. Piskarskas, and A. Stabinis, *Appl. Phys. B* **79**, 693 (2004).

[106] Y. Leng: in *Tech. Dig. Conf. Lasers & Electro-Optics, Baltimore, Maryland, 2003* (Optical Society of America, Washington, DC 2003) p. 169

[107] T. Tajima and G. Mourou, *Phys. Rev. Spec. Top.* **5**, 031301 (2002).

[108] A. Baltuska, T. Fuji, T. Kobayashi, *Opt. Lett.* **27**, 306 (2002).

[109] F. Rotermund, V. Petrov, F. Noack, V. Pasiskevicius, J. Hellström, F. Laurell, H. Hundertmark, P. Adel, and C. Fallnich, *Electron. Lett.* **38**, 561 (2002).

[110] J. V. Rudd, R. J. Law, T. S. Luk, and S. M. Cameron, *Opt. Lett.* **30**, 1974 (2005).